FACILITY FORM 602
N71-38692
(ACCESSION NUMBER)
(THRU)
(PAGES)
(CODE)
(NASA CR OR TMX OR AD NUMBER)
(CATEGORY)

ADVANCED TECHN

RADIATION AND METEOROID SATELLITE

FINAL REPORT

CONTRACT NAS9-9195

ATC Report No. B-95000/1CR-11

MARCH, 1971

CASE FILE
COPY

The Research Center of LTV Aerospace Corporation and LTV Electrosystems, Inc.

CR-115206

RADIATION AND METEOROID SATELLITE

FINAL REPORT

CONTRACT NAS9-9195

ATC Report No. B-95000/1CR-11

MARCH, 1971

Prepared for

NATIONAL AERONAUTICS AND SPACE ADMINISTRATION
MANNED SPACECRAFT CENTER
HOUSTON, TEXAS

Prepared by

J. H. Johnson

B. J. Farmer

R. G. Bagwell

B. R. King

ADVANCED TECHNOLOGY CENTER, INC.
BOX 6144
DALLAS, TEXAS 75222

TABLE OF CONTENTS

		Page
1.0	INTRODUCTION	1
2.0	MISSION OBJECTIVES	3
2.1	RADIATION EXPERIMENT	3
2.2	METEOROID EXPERIMENT	4
3.0	MISSION SUMMARY	5
4.0	MISSION ANOMALIES	8
4.1	BEFORE LAUNCH ANOMALIES	8
4.2	LAUNCH ANOMALIES	8
4.3	ORBITAL ANOMALIES	9
5.0	RADIATION EXPERIMENT	13
5.1	INTRODUCTION	13
5.2	NASA IONIZATION CHAMBER DOSIMETER SYSTEM	14
5.2.1	IONIZATION CHAMBER	17
5.2.2	DOSIMETER ELECTRONICS MODULE	17
5.3	ELECTRON-PROTON SPECTROMETER	19
5.3.1	SPECTROMETER TELESCOPE	19
5.3.2	SPECTROMETER ELECTRONICS	21
5.4	SPECTRUM-TO-DOSE SYSTEM	29
5.4.1	THEORY	29
5.4.2	SPECTRUM-TO-DOSE ELECTRONICS	30
5.5	CALIBRATION	32
5.5.1	SPECTROMETER CALIBRATION	33
5.5.2	IONIZATION CHAMBER CALIBRATION	37
5.5.3	DETERMINATION OF PULSE-HEIGHT SPECTRUM-TO-DOSE CONVERSION FUNCTIONS	41
5.5.4	GSFC DATA REDUCTION	49
5.6	PRELIMINARY DATA ANALYSIS	49
5.7	CONCLUSIONS	56
6.0	METEOROID EXPERIMENT	58
6.1	INTRODUCTION	58
6.2	METEOROID DETECTION INSTRUMENT	59

6.2.1 THIN-FILM METEOROID SENSORS 61
6.2.2 ROW AND COLUMN ISOLATION. 64
6.2.3 AMPLIFIERS. 64
6.2.4 DATA FORMATION AND ENCODING 64
6.2.5 MEASUREMENT OF SENSOR LEAKAGE CURRENT 66

6.3 TESTING AND CALIBRATION. 66

6.4 PRELAUNCH OPERATIONS 70

6.5 ORBITAL OPERATIONS AND DATA ACQUISITION. . . 72

6.6 PRELIMINARY DATA ANALYSIS. 75

6.6.1 SENSOR LIFETIME 75
6.6.2 METEOROID VELOCITY MEASUREMENTS . . 81
6.6.3 MEASUREMENT OF METEOROID FLUX . . . 82

6.7 CONCLUSIONS. 83

7.0 SPACECRAFT 84

7.1 STRUCTURE. 84

7.2 DYNAMICS 89

7.3 ELECTRONICS. 94

7.3.1 COMMAND SYSTEM. 94
7.3.2 TELEMETRY SYSTEM. 97
7.3.3 DATA PROCESSING 101
7.3.4 POWER SYSTEM. 105

7.4 GROUND SUPPORT EQUIPMENT 107

7.5 THERMAL ANALYSIS 109

8.0 CONCLUSIONS. 110

9.0 REFERENCES 111

10.0 BIBLIOGRAPHY 112

LIST OF FIGURES

Figure No.	Title	Page
5-1	Radiation Data Run Sequences	15
5-2	NASA Ionization Chamber Dosimeter	16
5-3	Block Diagram of the RMS Radiation Dosimeter	18
5-4	Spectrometer Telescope	20
5-5	Electron-Proton Spectrometer Calibration Curves	22
5-6	Amplifier System	24
5-7	De/DX vs. Total Energy Curves	25
5-8	A.D.C. Approximation Sequence	27
5-9	Radiation Experiment	31
5-10	Typical Angular Efficiencies of the Electron-Proton Spectrometer	34
5-11	Omnidirectional Efficiency of the Electron-Proton Spectrometer for Protons	35
5-12	Omnidirectional Efficiency of the Electron-Proton Spectrometer for Electrons	36
5-13	Response of the Electron-Proton Spectrometer to 2-MeV Electrons with Normal Incidence	38
5-14	Response of Electron-Proton Spectrometer to Protons in the Proton II Region	39
5-15	Ionization Chamber Calibration Curves	42
5-16	Angular Response of Unshielded Ionization Chamber for 1 MeV Electrons	43
5-17	Response of the Unshielded Ionization Chamber to Omnidirection Electrons	44
5-18	Response of Unshielded Ionization Chamber to Protons at Normal Incidence and Omnidirection	45
5-19	Response of the Thin-Shielded Ionization Chamber to Protons at Normal Incidence and Omni-direction	46

Figure No.	Title	Page
5-20	Response of Thick Shielded Ionization Chamber to Protons at Normal Incidence and Omni-direction	47
5-21	Electron Pulse-Height Spectrum-to-Dose Conversion Function using Unshielded Ion Chamber Response	48
5-22	Proton Pulse-Height Spectrum-to-Dose Function Using Unshielded Ion Chamber Response	50
5-23	Proton Pulse-Height Spectrum-to-Dose Function using Thin Shielded Ion Chamber Response	51
5-24	Proton Pulse-Height Spectrum-to-Dose Function using Thick Shielded Ion Chamber Response	52
5-25	Comparison of RMS Electron and Vette Model for Similar Anomaly Passes	54
5-26	Comparison of RMS Proton Spectrum and Vette Model for Similar Anomaly Passes	55
6-1	Meteoroid Detectors	60
6-2	Thin-Film Meteoroid Sensor having a Solar Filter	63
6-3	Meteoroid Experiment Electronics	65
6-4	Meteoroid Time to Voltage Conversion	67
6-5	Conversion of Column Leakage Current to ADC BIN Number	68
6-6	Leakage Current for the Outer Plane of Meteoroid Detector Box 1	76
6-7	Leakage Current for the Inner Plane of Meteoroid Detector Box 1	77
6-8	Leakage Current for the Outer Plane of Meteoroid Detector Box 2	78
6-9	Leakage Current for the Inner Plane of Meteoroid Detector Box 2	79
7-1	FW-4S Scout Interface	85
7-2	RMS Structural Arrangement	86
7-3	"E" Section Modifications	87
7-4	RMS Package Arrangements	88

Figure No.	Title	Page
7-5	Radiation and Meteoroid Satellite	90
7-6	RMS/OFO at Spin Balance	91
7-7	RMS/OFO with Scout Heat Shield Partially in Place	92
7-8	RMS/OFO Dynamics	95
7-9	Command System	96
7-10	Tone Acceptance Windows	98
7-11	Telemetry System	99
7-12	Meteoroid Experiment Data Processing	102
7-13	Radiation Experiment Data Processing	103
7-14	Power System	106
7-15	RMS Ground Support	108

LIST OF TABLES

Table No.	Title	Page
5-1	Energy Channel Boundaries for the Electron-Proton Spectrometer	40
7-1	RMS Weight Summary	93

1.0 INTRODUCTION

This report is submitted in accordance with the terms of Contract NAS9-9195, Contract Schedule, Article IV and constitutes the final report for the contract.

The Radiation and Meteoroid Satellite Program was carried out by the Advanced Technology Center, Inc. (formerly the LTV Research Center) with the support of the Vought Missiles and Space Company (formerly the Missiles and Space Division of the LTV Aerospace Corporation) under the direction of the Earth Orbital Missions Office and the Space Physics Division of the Manned Spacecraft Center, Houston, Texas. A preliminary design phase of the program was completed in November 1968 under Contract NAS9-8841. This study resulted in the definition of the basic experimental packages and satellite structure as described in the final report (LTV Report No. 0-71100/8R-15, dated 12 November 1968).[1] The Interface Definition Document (LTV Report No. 0-71100/8R-17, dated 8 November 1968)[2] was also prepared during the preliminary design.

This report covers all phases of NAS9-9195. These include design, fabrication, test and launch, and post launch support. During the design phase, the electronic and mechanical aspects of the satellite were defined and fully integrated. A structural test model of the satellite was constructed and utilized in vibration tests to facilitate final mechanical design of the electronic packages and their mounting. Following the design phase, a single satellite was fabricated for launch after being subjected to environmental and flight acceptance tests at the Vought Missiles and Space Company and at the Manned Spacecraft Center in Houston. The launch operation was successfully completed on 9 November 1970. Post launch operations were initiated immediately and continued under contract through 31 December 1970. The report covers the total mission until the reentry of the satellite on 7 February 1971.

This report covers the basic aspects of the RMS program. The mission objectives are discussed along with the degree to which each item was fulfilled. A mission summary is presented which gives a brief chronology of the pre- and post-launch operations. The major difficulties which arose during the mission are discussed with particular emphasis on the problem associated with the separation of the two payloads after injection into orbit. A complete description

of the experiment packages - their design, fabrication, and calibration - is given. A less detailed discussion of engineering aspects of the satellite and its various subsystems is included. In conclusion, a summation of the mission is given with a brief description of the recommended approach to the analysis of the data.

2.0 MISSION OBJECTIVES

The RMS mission was an earth orbital flight research program consisting of two scientific experiments to measure radiation and meteoroid parameters. The Radiation and Meteoroid Satellite was placed in orbit by an LTV Scout Launch Vehicle in conjunction with the Orbiting Frog Otolith (OFO) Satellite. The dual satellite launching was made possible when the OFO, originally planned for an Apollo flight, was rescheduled for a Scout launch. The projected OFO weight of approximately 300 pounds, compared to the lifting capability of Scout and a requirement that launch accelerations on the biological specimens be limited to a maximum of 10 G's, left approximately 50 pounds available for additional experiments. A joint proposal by the LTV Research Center and the Manned Spacecraft Center to the OFO Program Office was approved to utilize the available weight. A number of constraints was imposed on RMS in order to insure that it would not compromise the OFO mission. These will be evident in later sections, but did include a weight limit of 46 pounds. It was determined that a minimum mission lifetime of 90 days was necessary to properly test the meteoroid instrumentation. The specific mission objectives listed in the Experiment Implementation Plan (Revision B)[3] were given in two parts and are reiterated below.

2.1 RADIATION EXPERIMENT

The primary objective of the radiation experiment was to demonstrate the feasibility and accuracy of the spectrum-to-dose conversion concept and instrumentation in a real-time mode in actual space radiation environment. Pulse-height distributions of electrons and protons were to be converted to dose rates which were then to be compared in real time to dose rates measured by NASA furnished dosimetry systems.

The first objective was met when the electron dose obtained from the spectral measurements of RMS and subsequent dose computations were within experimental error of the electron dose obtained from the thin-walled ionization chamber.

As a secondary objective, the experiment was to provide data to develop maps of the radiation belts. Both electron and proton flux and dose determinations were made. From the spectrometer aboard RMS, electron spectra

and spatial distributions were obtained. Using data from both the spectrometer and ionization chambers, proton spatial distributions and crude spectra were obtained. Preliminary comparisons of these measurements with the Vette models are favorable.

2.2 METEOROID EXPERIMENT

The meteoroid experiment was designed to flight qualify materials and instrumentation to be used on large-area, long-duration meteoroid flight experiments for future study of the meteoroid population of the solar system. It was to measure intercept velocities of 10^{-12} gm meteoroids and larger and to count impacting meteoroid flux of 10^{-14} gm and larger.

The meteoroid experiment on RMS successfully demonstrated that thin film capacitor type meteoroid sensors can be successfully flown in the space environment, survive the launch and measure meteoroid flux and velocity. Two velocity measurements were made and correlated with periods of known high meteoroid intensity. An upper limit for flux of particles with mass greater than about 10^{-14} gm will be determined from a detailed analysis of the data and further, the increased flux during the Ursids meteor shower is very prominent in the data and should result in an excellent opportunity to analyze its effect on small particle flux near the earth. This data should have a significant impact on theories concerning the incidence of lunar ejecta from primary meteoroids.

3.0 MISSION SUMMARY

The Radiation and Meteoroid Satellite Program was an unusual one. Not only was the spacecraft launched into space "piggyback" and was conceived and launched in a little over two years, but also was designed and fabricated for NASA under a firm, fixed-price contract. The magnitude of this undertaking will become clear in later sections, which describe the complex experiments and spacecraft that make up the Radiation and Meteoroid Satellite. The following list provides a summary of events significant to the RMS mission.

1. Preliminary Design Contract, NAS9-8841, September 9, 1968.
2. Preliminary Design Review meeting, October 23, 1968.
3. Contract for completion of RMS through launch, NAS9-9195, April 1, 1969.
4. Critical Design Review July 31, 1969.

The spacecraft was essentially completed in June 1970. The following qualification tests were performed prior to final acceptance at Wallops Island, Virginia.

1. STADAN Compatibility Test #1 at Goddard Space Flight Center, Greenbelt, Maryland, February 1970.
2. Orbital Solar Vacuum Test at NASA Manned Spacecraft Center, Houston, Texas, June 8 through 12, 1970.
3. Vibration and Shock Tests on Solar Panels at Vought Missiles and Space Company, Dallas, Texas on May 22, 1970.
4. Vibration and Shock Tests on the basic satellite structure at Vought Missiles and Space Company, July 1-2, 1970.
5. Preliminary Acceptance Test at Advanced Technology Center, Inc., Dallas, Texas, June 30, 1970.
6. STADAN Compatibility Test #2 at NASA Wallops Island, July 8, 1970.
7. Final Acceptance of the Spacecraft at Wallops Island on July 9 and 10, 1970.

After acceptance by NASA the spacecraft was subjected to the following events at Wallops Island.

1. Mating of RMS to the Scout "E" Seciton.
2. Mass Properties Testing on July 29, 1970.
3. Mating and Spin Balance of RMS and the fourth stage of Scout on August 3, 1970.

4. Mating and Spin Balance of RMS, OFO, and the fourth stage of Scout on Aug. 8, 1970.

After the mating of the spacecraft, the fourth stage was mated to the complete Scout for dress rehearsal and launch preparations. Four dress rehearsals and nine countdown attempts were performed. The launch attempts were made as follows:

Aug. 21, 1970	Launch countdown terminated due to high OFO payload water temperature caused by insufficient cooling capacity of ground cooling unit, ships in first stage impact area, and closing launch window.
Aug. 31, 1970	Launch date rescheduled because of Scout guidance problems associated with poppet valve electronics.
Sept. 10, 1970	Launch countdown terminated due to lack of OFO biological specimens due to massive infliction of "Red Leg" disease in frog colony in launch site OFO laboratory.
Oct. 21, 1970	Launch date rescheduled due to weather.
Oct. 22, 1970	Launch date rescheduled due to weather.
Oct. 23, 1970	Launch countdown terminated due to OFO spacecraft power subsystem malfunction.
Nov. 2, 1970	Launch countdown terminated due to weather.
Nov. 3, 1970	Launch countdown terminated due to a deteriorating OFO data channel.
Nov. 9, 1970	Launch countdown completed. Vehicle liftoff time was at 06:00:00.05 GMT.

The RMS spacecraft remained in orbit a total of 90 days and 4 hours. During this period the spacecraft accumulated data as follows:

1. Radiation data in the South Atlantic anomaly for the first two weeks of its lifetime.
2. Secured meteoroid sensor current leakage and count rate histories during this same two week period.

3. The spacecraft was put into meteoroid mode to conserve power and await anticipated meteoroid events. Two meteoroid velocity words were recorded during this two month period. Short memory-enabled calibration runs were made to check the validity of the measurements as soon as possible after each event.
4. The objectives of the mission were accomplished and the spacecraft conditions were reduced to an almost daily interrogation by the real-time routine.
5. Radiation runs and spacecraft systems checks were performed for the last two to three weeks of satellite lifetime.

The spacecraft re-entered the atmosphere at approximately 10:00 GMT on Feb. 7, 1971. The last real-time routine was commanded and secured three hours before re-entry.

4.0 MISSION ANOMALIES

Several problems were encountered before launch, during launch, and during orbital operations. Most of the problems were minor; however, some problems were encountered after launch that significantly affected performance. The major problems are discussed in the following paragraphs.

4.1 BEFORE LAUNCH ANOMALIES

After delivery and prior to launch two problems were encountered. The first failure before launch was a short in the back plane wiring of meteoroid box number 2. During the period between countdowns the unit was repaired with no loss in sensor area or delay of countdowns. The only other before launch failure was in the logic in the satellite control unit incrementing counter. A gate failed in module A3 causing an invalid carry to be propagated. The module was replaced by a spare unit that was available with no delays in the countdown starting time.

4.2 LAUNCH ANOMALIES

During the fourth stage boost phase of Scout several anomalies appeared in the data received from the OFO spacecraft. Since RMS had no devices capable of measuring these anomalies and only had a beacon switched on during this time, OFO data presented the only picture available of the sequence of events. This data was studied both by OFO and Scout personnel, resulting in the following inferred sequence:

1. Fourth stage ignition was normal.
2. Fourth stage was still thrusting at the time of Mormon clamp release.
3. RMS yo, which was controlled by the Scout timer, released before OFO was separated.
4. Separation occurred at burnout and normal OFO yo and boom deployment times were experienced with respect to separation, although higher spin rates and much greater coning angles than predicted were experienced.

From the data analysis by Space General in their Mission Performance Report Number 1333-032,[4] it was concluded that the two spacecraft definitely collided; however, Scout Final Flight Report S-174C concluded there was an interference

but no evidence of a collision. The presence of the great change of the OFO momentum vector would indicate that either a collision or a highly disturbed tip off occurred at separation.

A preliminary comparison of the early RMS proton spectra with the anticipated spectra of the Vette model indicated that the radiation experiment was not functioning properly. The nature of the malfunction is discussed in Section 5 of this report and is most probably due to the launch anomaly. The RMS spacecraft was extremely susceptible to any highly disturbed tip off, to rotation of one spacecraft with respect to the other while in contact, or to a collision of any part of the spacecraft structure. If any damage had occurred to the radiation experiment harness, which was particularly exposed, results such as the observed distorted proton spectra could be explained. In addition, any excessive shock in this area could also have relatively easily damaged the complex electronics in the experiment package or the external radiation heads. This experiment is the only area that observed anomalies could not be explained by simple logic problems.

4.3 ORBITAL ANOMALIES

After launch several problems were encountered. The initial beacon contact with the spacecraft was obtained but difficulty was experienced on the first command sequence. The telemetry transmitter could be switched on but the spacecraft would not respond to additional commands such as real-time data requests. The first real-time data was secured on orbit three but command problems were experienced until orbit ten. Commands were never consistent in acceptance by the spacecraft but became consistently workable after the first day in orbit. Occasional bad passes were experienced over the life-time but spacecraft controllers were able to work around these and secure the desired data.

The source of the command problems were, first of all, much more pronounced nulls in the antenna patterns than expected and secondly a rather pronounced blockage by the fourth stage Scout engine. The nulls coupled with the much faster than expected spin rate of the spacecraft probably caused significant perturbations to the spacecraft receiver A.G.C. causing signal loss during each command. As the spin resolved into a precess and then to a tumble in less than 15 days, the command acceptance by the spacecraft was

much more regular being interrupted only by the engine blockage which would block commands for a part of a pass. No command system difficulties could be attributed to anything other than these two problems.

Another problem that was noticed several days after launch during the radiation runs was a failure of the spacecraft to correctly perform the 6.4 and 10.67 minute time delays. The spacecraft accepted the command but entered the binary code for the 23.47 minute delay in place of the 6.4 minute delay and 27.75 minute delay in place of the 10.67 minute time delay. The failure of these delays was noticed quickly and command times were chosen to adequately work around these failures. This problem could not be attributed to any logic failure but only to a change in propagation delays in the logic either with time or temperature. However, the satellite control unit, which operated at about 50°F during the time of failure, was checked at room temperature before launch and at low temperature during satellite temperature testing and no similar problem was noticed. The fault was probably due to a slight change in the propagation delay of the preset input in a j-k flip-flop. Although the delay was probably still within specifications, the time entry design was marginal in its timing and as a result allowed any increase in delay of the toggle output from the preceeding flip-flop to override the time entry. During the latter orbits of the spacecraft, a test was conducted to prove the condition previously stated existed. A set of commands first set the incorrectly set flip-flop opposite to the desired condition, then the correct command was sent. The second entry caused the flip-flop to change to the correct state and the remaining flip-flops were set by the correct command entry. The test was a success and proved that the two failing delays could be entered with the addition of only one command to the sequence. However, since these delays were very seldom needed this procedure was never incorporated as a routine procedure.

From the early radiation data a problem was noticed with the spectrum-to-dose data. The electron dose determined on board the satellite was significantly higher than that calculated from the spectrum by the GSFC computer. The nature of the events was studied for both the electrons and protons. The results indicated the logic was incorrectly processing the random data acquired in space. A study of the electronic schematics revealed a termination drawn

to the wrong logic element. This incorrect connection caused a timing error that resulted in correct performance when a signal giving a repetitious address (constant amplitude) was presented by a pulser but random addresses caused erroneous inhibits and enables. It is unfortunate that the problem did not reveal itself during the thorough testing carried out before launch in which a pulser was used. The error actually had no effect on the mission. An inspection of a spectrum corresponding to a given spectrum-to-dose value proved that the satellite was computing in exactly the manner in which the wiring error would indicate. Also the GSFC was supplying the missing computation with the SDS computer which provided "quick look" data reduction. Thus, all comparisons were made as planned.

During early orbits it was noticed that the magnetic core memory was on an excessive amount of time. This was caused by a much higher breakdown count rate by the meteoroid sensors than anticipated, due to damage sustained on launch by the front plane sensors of both boxes. The rapid count rates were observed almost exclusively from box 2, and, as a result, it was cut off for most of the satellite's lifetime. Since the telemetry transmitter shared the same timer as the memory, the excessive count rate from the sensors also lengthened the telemetry transmitter automatic cut-off period in many instances. After box 2 was cut off this problem was eliminated and reliable automatic cut off was obtained when the transmitter was not manually cut off before LOS.

After fifteen days in orbit a heating problem was experienced in both the battery and the power-conversion units. This corresponded with the predicted time for the spacecraft to resolve from a random tumble to a pure tumble or flat spin along the long axis.[1] The heating problem was then related to the fact that the spacecraft was tumbling along the long axis with essentially one side facing the sun. The recorded temperatures indicated that the worst possible orientation had occurred, since the greatest heat producing units were facing the sun. Since the radiation experiment had been completed, the spacecraft was set to a minimum power condition with only the meteoroid experiment on and the memory disabled. The spacecraft operated in this condition for most of the remaining lifetime using the meteoroid standby storage registers for velocity data storage.

Only one electrical failure of any real significance was experienced during the lifetime. This happened approximately at orbit 810 when a cell in the battery failed. This coupled with the high temperature of the battery caused the battery voltage under load to drop below the low voltage protection circuit threshold point of 25V and cut off major spacecraft systems in the dark. If the battery had been on the cool side of the spacecraft, cell voltage would have been high enough to allow normal operation with the failed cell. However, the lower voltage produced by the high temperatures necessitated operation of the spacecraft experiments only during the sun parts of the orbits to maintain adequate voltage under load. Fortunately this failure occurred late enough in the mission that sufficient data had been accumulated from the high power consumption portions of the experiments and there was no effect upon the successful completion of the objectives of the mission. A post-mission internal examination of the back-up battery for RMS revealed the presence of corrosion and oxide accumulations on the individual cell cases, which may have been responsible for the difficulty.

5.0 RADIATION EXPERIMENT

5.1 INTRODUCTION

In 1958 a Geiger counter aboard Explorer I detected a region of high count rate starting at an altitude of about 1000 kilometers. This was unexpected and it was first suggested that the counter might have malfunctioned. However, this effect was verified when Explorer III showed the same results and Van Allen, who had conducted the experiments, suggested that the high count rates resulted from charged particles trapped in the geomagnetic field.

Space radiation dose measurements during Project Mercury clearly established the region of the South Atlantic magnetic anomaly as the principal source of ionizing radiation in low altitude non-polar orbits. This is shown in comparing the proton flux in the nuclear emulsions from the three orbit MA-7 mission, which did not traverse the anomaly, and the much higher proton flux recorded on the six orbits of the MA-8 mission.

Measurements have since been made by satellite and rocket-borne instrumentation which have provided additional information concerning the nature and characteristics of trapped radiation. Of particular interest are those made by MSC during the Mercury, Gemini, and Apollo missions. These measurements have shown that low-altitude, low-inclination, earth-orbital flights, and limited excursions to altitudes penetrating the trapped radiation belts are possible without overexposing spacecraft crew members.

The measurement of biological dose, however, as opposed to physical dose, is of much more significance as mission durations increase. Physical dose measuring devices, which have been flown in the past, cannot provide an accurate evaluation of the biological dose, since this dose is a function of particle type and energy distribution. The Radiation and Meteoroid Satellite has demonstrated that the spectrum-to-dose conversion system is not only feasible, but practical for determining the required dose parameters in real time or near real time for extended space missions.

The radiation experiment aboard RMS consisted of three basic systems: a proton-electron spectrometer, a pulse-height spectrum-to-dose conversion system and a triad of standard MSC ionization chambers. For the evaluation of the practicability of the spectrum-to-dose conversion system the ion

chambers were to form the baseline for comparison. The three ionization chambers, which were shielded by different amounts of material were carefully calibrated for electrons and protons. The resulting dose functions were then used to form the spectrum-to-dose conversion functions. This allowed immediate comparisons of the two systems to be made.

The pulse-height spectrum information was taken for short periods of time and the dose produced was integrated over the period. The ionization chambers' dose rates were read before and after the data period so that reasonable comparison with the integrated dose could be achieved. The four types of programmed radiation run sequences are shown in Figure 5-1. Two lengths of spectra data gathering periods (8 seconds and 31 seconds) and two selections of data density (high and low duty) combine to form these four data periods. Ionization chamber and spectrometer head count rates are stored before and after the spectra information is obtained in each period. In addition, the dose accumulated in the spectrum-to-dose converter over the spectra period is stored at the end of this period. A total of thirty such data periods are performed automatically when commanded and each period is sequentially stored in the memory for evaluation when the sequence has finished.

The following paragraphs give a basic description of the three systems comprising the RMS radiation experiment. In addition, the details of the calibration program are covered and a brief discussion of the preliminary data analysis is given.

5.2 NASA IONIZATION CHAMBER DOSIMETER SYSTEM

The ion chamber system consisted of three identical chambers, but with different amounts of shielding to provide different particle sensitivities. One chamber, a photograph of which is shown in Figure 5-2, was used with no additional shielding beyond that required to form the outer electrode of the ion chamber. This corresponded to a threshold for protons of approximately 10 MeV. The thin and thick shields for the other two chambers were made of brass and provided proton thresholds approximately 40 and 80 MeV, respectively.

Each dosimeter is made up of two basic units: an ionization chamber and an electronic module consisting of an electrometer, a linear-to-log converter network, and a postamplifier.

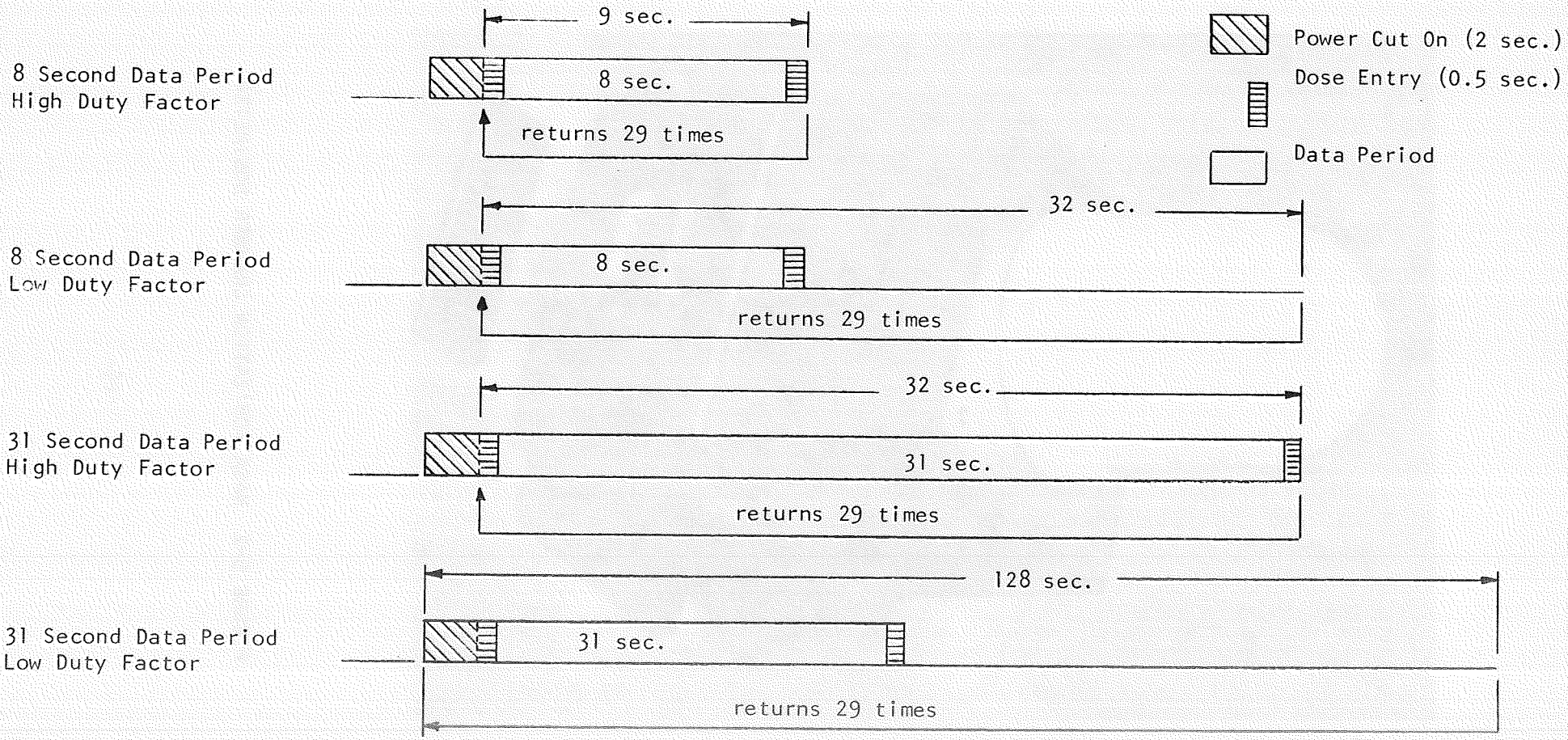


Figure 5-1 - Radiation Data
Run Sequences

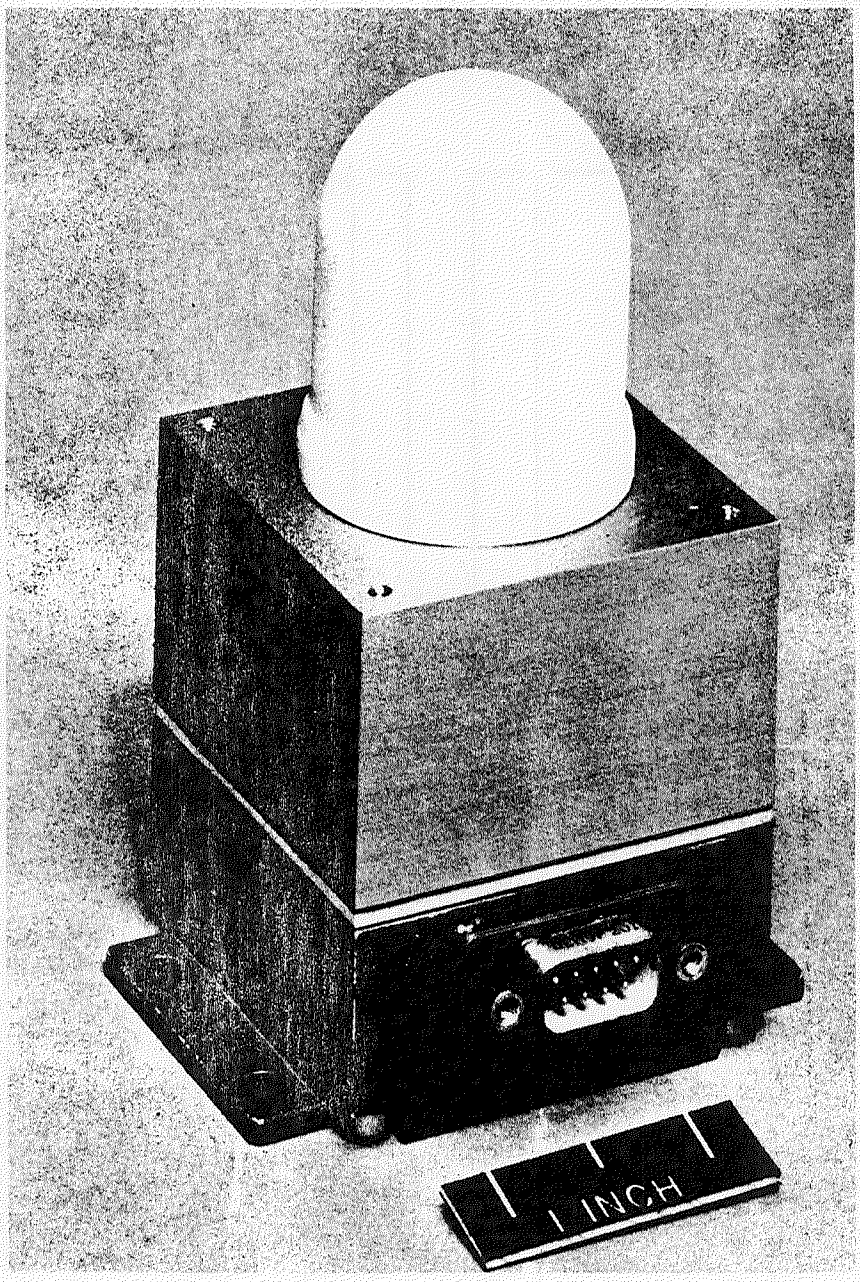


FIGURE 5-2 NASA IONIZATION CHAMBER DOSIMETER

5.2.1 IONIZATION CHAMBER

Radiation is detected in the ionization chamber, which delivers an output current that is proportional to the intensity of the ionizing radiation. The ion chambers are constructed of two hemispherical domes, separated by an 0.150 inch gap. These domes form the outer and inner electrodes. The outer electrode is 0.030 inches thick, and is biased at -15 VDC. The inner electrode is at zero potential and is the signal electrode. Both electrodes are made from delrin. The inner surface of the outer electrode is coated with aquadag. The inner electrode is solid, 0.685 inches in diameter at the base, and is also coated with aquadag. The outer cover is of 0.025-inch aluminum and is secured to the base by electron beam welding. Purging and filling of the ion chamber with a mixture of 90% ±5% argon and 10% ±5% helium to approximately 2.0 atmospheres is accomplished through a vent hole. When filling the ion chamber, the gas pressure is varied until an output current of 2.0×10^{-12} amps/rad/hour $\pm 0.2 \times 10^{-12}$ amps/rad/hour is reached. Volume of the ion chamber is approximately 10 cc.

Radiation penetration of the chamber ionizes the gas between the two electrodes causing a current to flow. The dynamic range at the output of the ion chamber is from 2×10^{-14} to 2×10^{-10} ampere. This corresponds to dose rates of from 0.01 rad/hour to 100 rad/hour, respectively.

5.2.2 DOSIMETER ELECTRONICS MODULE

The electronics module circuit block diagram is shown in Figure 5-3. This circuit consists of an electrometer amplifier, a linear-to-log converter network and a postamplifier.

The supply voltage to the electrometer amplifier is decoupled from the main supply voltage through a transistor series regulator. This decoupling isolates the electrometer from the power supply voltage variations and/or spurious signals riding on the main power supply.

The output current from the ion chamber as mentioned above, is very low. To meet this low current requirement, the input stage of the electrometer amplifier required a device with an input impedence of at least 10^{15} ohms, such as the MOSFET. Considering that the leakage current of

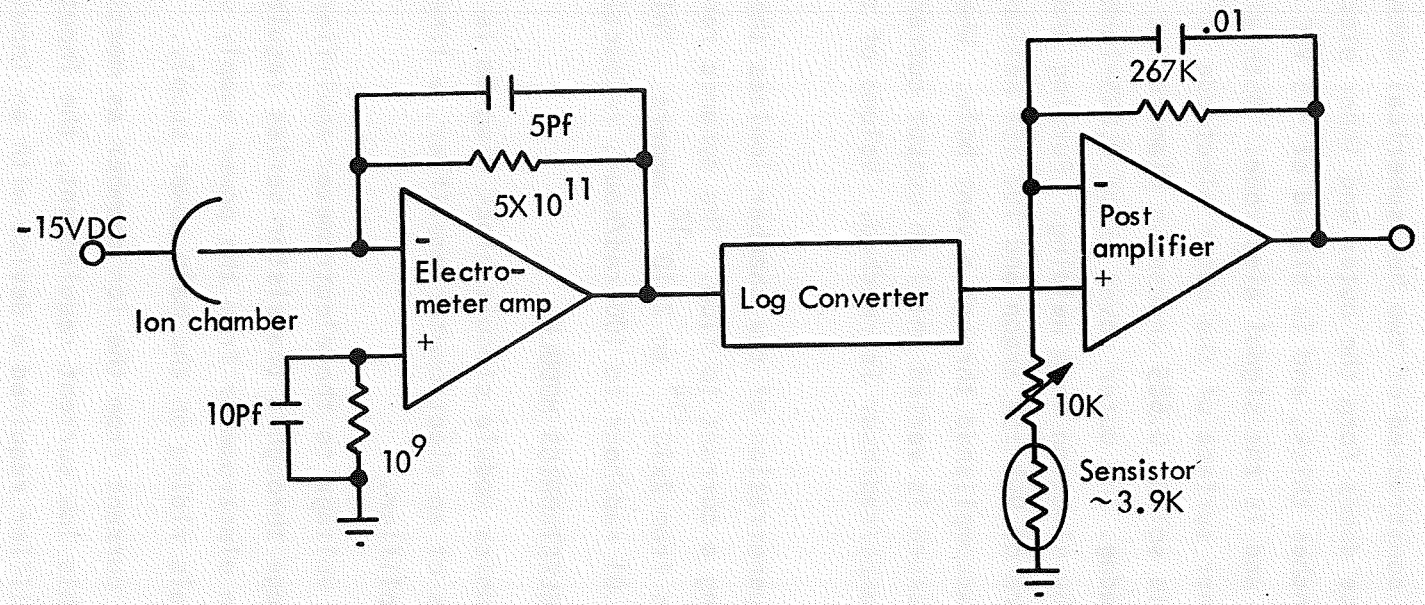


FIGURE 5-3 BLOCK DIAGRAM OF THE RMS RADIATION DOSIMETER

the MOSFET is much lower than the lowest value of ion chamber output current, then all current coming from the ion chamber will flow through the electrometer feedback resistor. Since the inverting input of the electrometer is at virtual signal ground, the voltage developed at the output is directly proportional to the incoming radiation detected in the ion chamber. Following the electrometer output is a linear-to-logarithmic converter active network for compressing the expected three decades dynamic range at the output of the electrometer. The low-level signals at the output of the linear-to-log converter are amplified to a higher level (0 to 5 vdc) by an FET input operational amplifier (post-amplifier) connected in the noninverting mode. The output of this amplifier is sampled by the spacecraft's commutated ADC.

5.3 ELECTRON-PROTON SPECTROMETER

5.3.1 SPECTROMETER TELESCOPE

After a series of designs was considered and in some cases tested in electron and proton beams, the spectrometer telescope configuration shown in Figure 5-4 was chosen. The 20 mil aluminum absorber is used to eliminate the very low energy electrons trapped in the geomagnetic field. These electrons would have overdriven the electronic circuit for the front detector. In addition, the entire head is encased in brass with a minimum thickness of 0.2 inches. The two thin surface barrier detectors at the front on the spectrometer serve two purposes. They form an active area collimator that sets the solid angle of the spectrometer. This was necessary to eliminate the bulk weight which would have been associated with a shielding type collimator system. Also, they are used as threshold detectors. Each detector has a 100 keV lower energy level discriminator and each of these must be exceeded before a count is registered. Also a 400-ns coincidence is required before any event is stored. This practically eliminates the possibility of an x ray or gamma ray being recorded. The geometry was such that the trajectory of unscattered particles which traversed the telescope would remain within a cone which was slightly smaller than the third detector of the total energy stack. The proton penetration detector was used to identify those particles which completely traversed the stack. To obtain maximum energy definition, the pulse heights of the first two detectors and that from the stack were summed after amplification. It is this signal which was then related to total energy lost in the head.

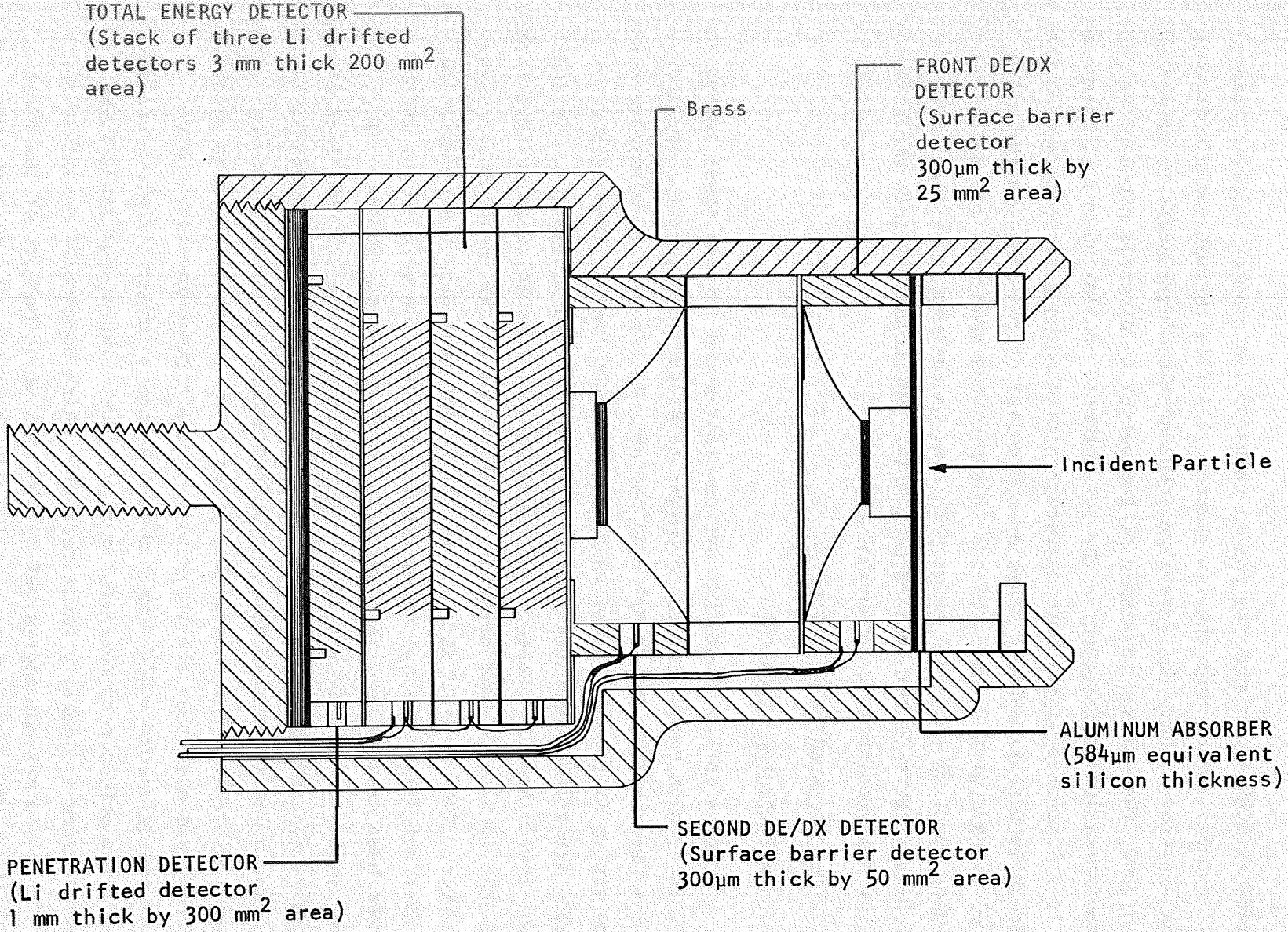


FIGURE 5-4 SPECTROMETER TELESCOPE

The manner in which this detector arrangement separates particle types and yields the individual spectra may be most easily described by referring to Figure 5-5. The points of the curves are the most probable energy losses taken from experimental calibrations to be discussed later. The solid lines are derived from calculated values. The curve labeled electrons shows that 600 keV electrons incident on the entrance aperture of the spectrometer will most probably lose 310 keV in the sensitive volume of the spectrometer. This is the lower energy of acceptance of the spectrometer. The electron curve extends up to an incident energy of 5 MeV which corresponds to a most probable energy loss of 4.8 MeV in the spectrometer. Electrons having incident energies below 5 MeV cannot penetrate the back detector. Thus,any energy loss below 5 MeV without a signal from the back penetration detector in the spectrometer will be interpreted as an electron. The region of the curve labeled Proton I signifies the protons which are totally stopped in the sensitive volume of the spectrometer. These will be protons with incident energies between 11.3 and 43 MeV. They will not produce a signal in the back detector. The region of the curve labeled Proton II represents the protons that penetrate the volume of the spectrometer and produce a signal in the back detector. This logic scheme reduces to insignificant levels any cross talk between protons and electrons.

Because of the limited solid angle of acceptance of particles by the telescope, three identical heads were used which were aligned along three orthogonal axes. In addition, the spacecraft was designed to attain a motion in orbit which would simulate a random tumble. Due to the interference at payload separation the desired motion was not achieved and little information could be inferred about the trajectories of the trapped particles. The effect of this on the mission success will be discussed later.

5.3.2 SPECTROMETER ELECTRONICS

In order to secure needed pulse-height and particle type information from the very small signals from the radiation heads, three entirely separate head amplifier systems were incorporated. Each system consisted of four doubly differentiating and singly integrating amplifiers for each detector group. The output of the front, coincidence, and stack detector systems were electronically summed to produce the total energy output. The pulse-height produced by this

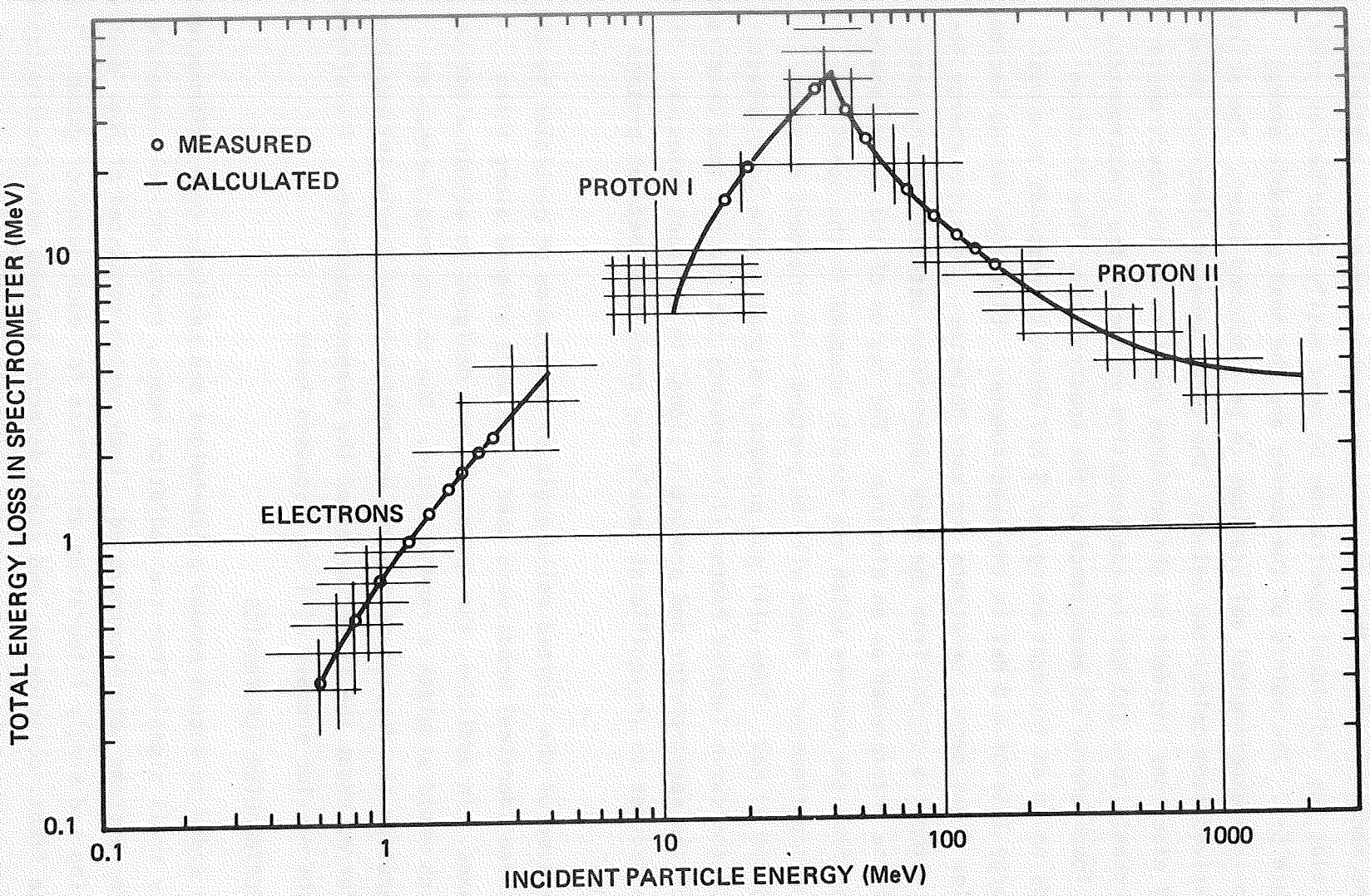


FIGURE 5-5 ELECTRON-PROTON SPECTROMETER CALIBRATION CURVES

output was held by the peak-retainers so that ADC might analyze the peak value. Level detectors from the front coincidence, and back detectors produced outputs when the energy levels previously discussed were exceeded. The coincidence of the output of the front and coincidence detector within a 400 ns period enabled the spectrometer logic to analyze the signal. The logic decided which head produced the signal, disabled the other two heads, determined the particle type, and then connected the appropriate peak retainer to the ADC for analysis. After analysis, the data was presented as a binary number that represented the pulse-height and particle type. The processing of signal from any head could be disabled by a logic control level from the command register that disabled the coincidence logic. The count rates in the first two detectors of each head were converted to an analog voltage level by integrating the pulses from a monostable multivibrator that was fired by an event in either front detector. This voltage was monitored by the data processing to determine if a head should be disabled.

In order to realize the basic concepts of the head system, an amplifier system that would produce summed signals for the total energy and separate outputs for the first two detectors was designed. Each detector group has a complete amplifier system as shown in Figure 5-6. A charge sensitive pre-amplifier is used to convert the very small charge increments produced by the detectors into a voltage output that is proportional to the energy absorbed in the detector. This output is differentiated and amplified in the next amplifier stage. At this point the outputs of the first two detector amplifiers are summed with the amplifier output of the thick stack to form the total energy output. The signal from the thick stack is amplified again and the peak value both before and after this last stage of amplification is retained by the peak-retainer for analysis by an analog-to-digital converter. This is done in order to obtain better resolution of the very wide dynamic range of total deposited energy. The outputs of all the systems then go to level detectors that produce logic outputs for a system of particle separation logic.

By relating the energy lost in the first detector (the dE/dx detector), which is proportional to the dE/dx of the particle, and the energy lost in the total stack, a pronounced separation of electrons from protons is possible. In addition, the influence of alpha and higher Z particles is eliminated. Figure 5-7 shows a group of levels that when combined with the level detector

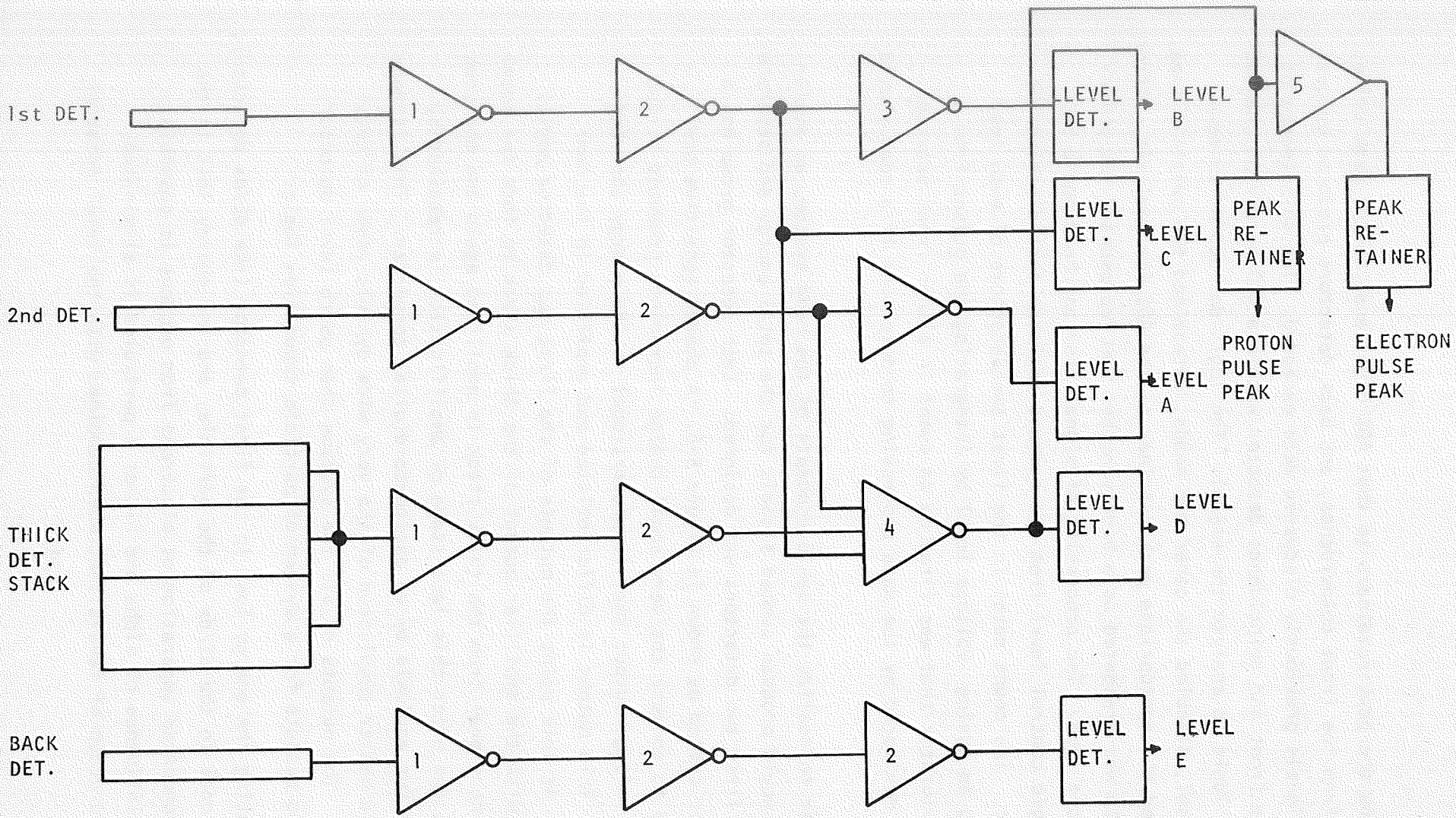


FIGURE 5-6 AMPLIFIER SYSTEM

1 - Charge Sensitive Preamp
2 - Differentiation Amplifier
3 - Differentiation - Integration Amplifier
4 - Sum - Differentiation - Integration Amplifier
5 - Non-Inverting Amp.

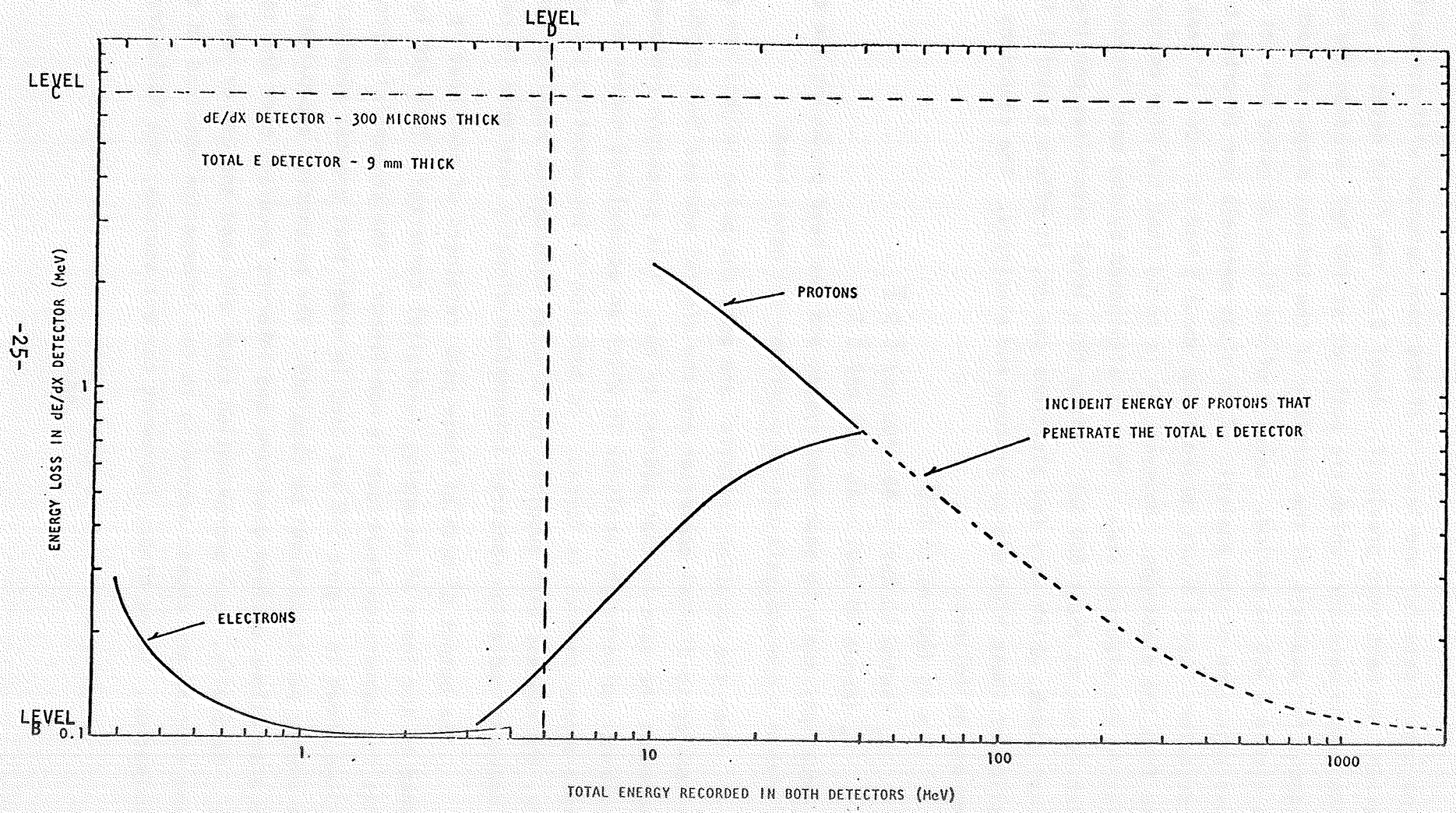


FIGURE 5-7 DE/DX VS. TOTAL ENERGY CURVES

A of the second detector and level E of the back detector will accomplish this separation. As mentioned previously, level B of the first detector and level A of the second detector, which are both set at 100 KeV, produce the needed requirement for analysis of the particle if the initial output of each detector occurs within a 400 ns period. Level C of the first detector was set at 7 MeV to cause rejection of the analysis if an alpha particle was absorbed by the front detector. Level D was chosen to be about 5 MeV in order to separate the protons from the electrons. However, it is noted that the high energy protons do exist in the electron area. This is eliminated by the back detector, level E, which is set at about 600 KeV. Since this level determines penetration of the total stack, which very few electrons can do, it offers a useful level for separation of these high energy protons and electrons. The equations thus derived are as follows,

$$E = AB\ (400\ ns)\ \overline{C}\ \overline{D}\ \overline{E}$$

$$P_1\ (\text{Below } 40\ MeV) = AB\ (400\ ns)\ \overline{C}\ D\ \overline{E}$$

$$P_2\ (\text{Above } 40\ MeV) = AB\ (400\ ns)\ \overline{C}\ E$$

These equations apply to each head system and the head producing the event AB first within a non-analysis period overrides all other heads.

When the equation criteria are met, the pulse heights are analyzed by the analog-to-digital converter and the digital address thus produced used to increment the data in that address by one. This procedure produces a multichannel pulse-height analyzer in which an accumulated number of counts for each energy channel is formed. In addition to incrementing the satellite memory, the address also supplies the digital information required for a system that converts radiation spectrum information directly into dose in real time.

The output of both of these peak retainers of each head is analog switched to the input of an analog-to-digital converter. This ADC is unique in that its conversion technique is non-linear. The sequential approximation technique shown in Figure 5-8 was used in order that greater resolution of the lower energy particles might be obtained. The sequential approximation technique also allows uniform dead-time and inherent accuracy over the temperature range. Basically, four approximation steps are used and one or more of five current sources are chosen according to the information obtained in the previous approximation. Using binary increment current sources, the following sources

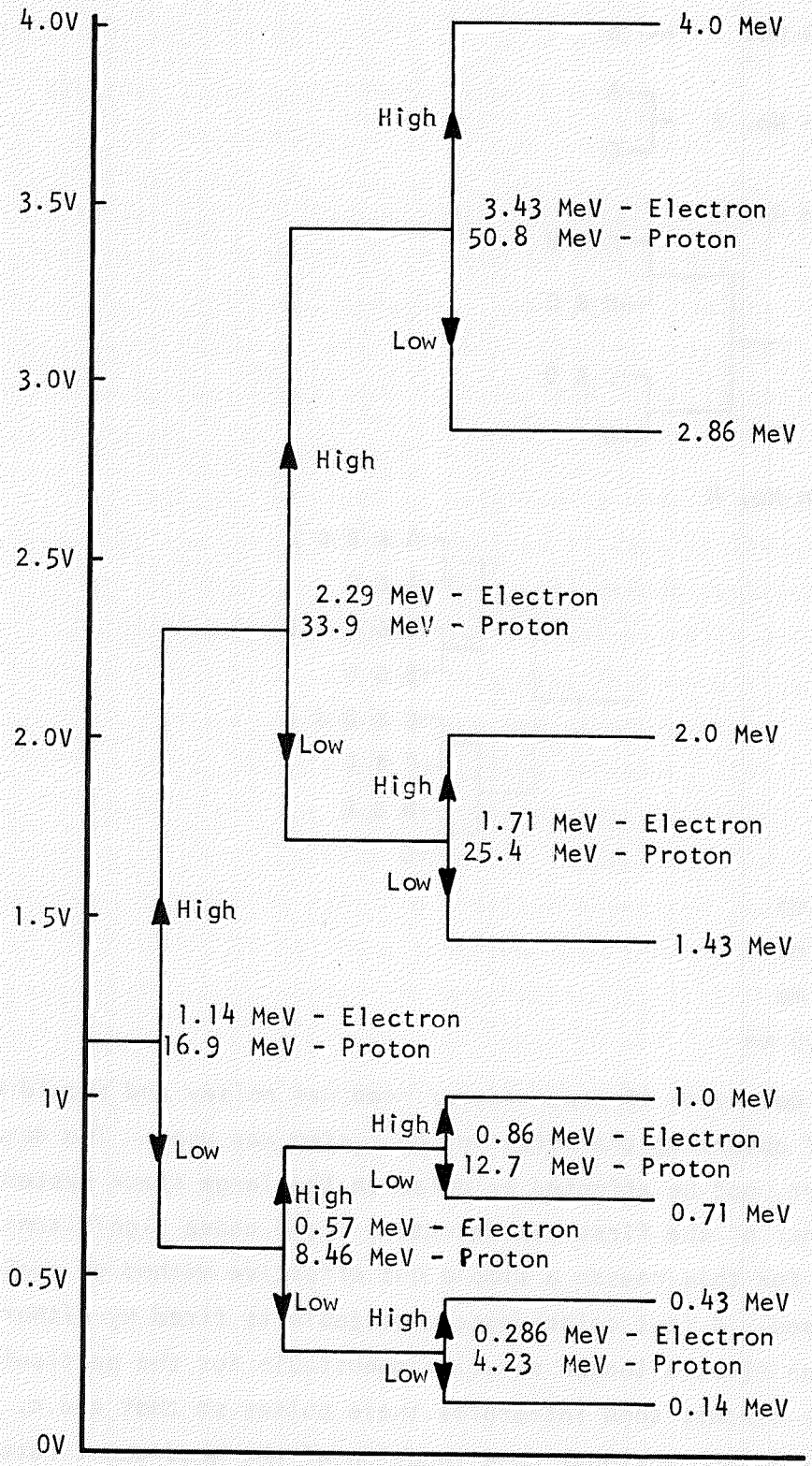


FIGURE 5-8 A.D.C. APPROXIMATION SEQUENCE

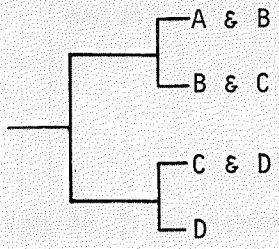
for each approximation may be derived from referencing Figure 5-8.

Approximation No. 1 — B

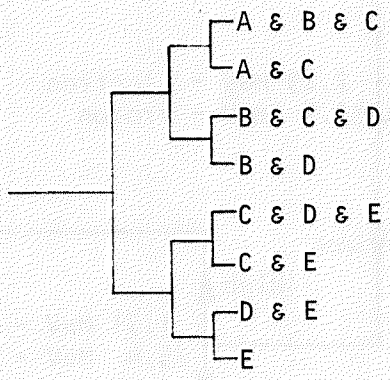
Approximation No. 2



Approximation No. 3



Approximation No. 4



where A = 4 ma
B = 2 ma
C = 1 ma
D = 0.5 ma

In order to determine if a particular head was noisey and should be inhibited, a method of observing the noise in the system was used. The data will, for the most part, not be affected by noise in the large stack system; however, noise in either of the first two detectors could cause significant changes in the data. For this reason a simple but effective method of monitoring these detectors was used. A fast coincidence monostable is fired by either level A or B which then fires a longer duration monostable for the particular head in question. The circuit then integrates these pulses so that a d.c. level is produced that is proportional to a function of the head count rate. This level is then monitored by satellite housekeeping and after calibration

of the system with a random source, represented the count rate of the front detectors of the particular head.

5.4 SPECTRUM-TO-DOSE SYSTEM

5.4.1 THEORY

A system was provided on board the satellite (physically located in the Satellite Control Unit) to convert to a dose, the information which is contained in the pulse-height spectra. The system involves the utilization of a set of weighting factors, referred to in the following analysis as F, which is the Spectrum-to-Dose Conversion Function and which is applied to the incoming data to obtain dose.

In a standard technique in determining dose from a spectrometer, far more calculations are made than are required if dose is the only parameter needed immediately, and quite often it is. The usual method requires that a complete instrument spectrum be accumulated which is statistically accurate. The instrument resolution is then removed from this distribution giving the true particle energy spectrum. This step requires the use of an inverted instrument resolution matrix or a more accurate but more time consuming iterative process. After this step is complete one has the particle distributions incident on the spectrometer, or in practice on a spaceship. A geometric matrix must then be applied which will give the particle spectrum a desired location inside the ship. The particle energy-to-dose function must then be applied to the last distribution to obtain the dose. An unnecessary utilization of expensive near real-time data reduction facilities is required and much information in the intermediate steps is generated which will never be required.

The simplified technique used here yields a result which is mathematically identical to the standard method while requiring no matrix manipulations or resolution matrix storage in the computer which is used for rapid mission data analysis. The simplified technique utilizes only a single function for each type dose required (e.g. physical dose, biological dose) and each geometric factor involved (e.g. surface skin dose at a specific location inside the ship). The functions for this test program were generated in advance of the mission using the same resolution functions, geometric factors and dose curves that would be used in the standard technique; however, the manipulations were

made only once for each function instead of each time a new instrument spectrum was received during the mission. Also the dose was calculated and accumulated while the data was being received, since it was not necessary to have a complete instrument spectrum before making a calculation.

The concept was described in references (1) and (2) and is briefly discussed here. The dose D is given by

$$D = CS \tag{1}$$

Where C is the particle energy-to-dose conversion function and S is the source system. The source spectrum is related to the pulse-height spectrum by the instrument resolution function R as follows:

$$P = RS \tag{2}$$

Solving for S gives

$$S = R^{-1}P \tag{3}$$

Substituting this into Equation (1) gives

$$D = C\ (R^{-1}P) \tag{4}$$

Inverting the order of matrix multiplication gives

$$D = (CR^{-1})P$$

or

$$D = F\ P$$

where

$$F \equiv CR^{-1}$$

where F is the pulse-height spectrum-to-dose conversion function mentioned above.

The functions F used in the RMS program were derived using the energy-to-dose conversion function C from the calibrated NASA ionization chambers. The derivation of these functions is discussed below in the calibration section.

5.4.2 SPECTRUM-TO-DOSE ELECTRONICS

A combination analog and digital system was used on the satellite because of its basic simplicity. The system shown in Figure 5-9 was designed for integrated dose but its application to dose rate, if required, can be seen readily. The logic and ADC outputs from the spectrometer were utilized in both the data processing and the spectrum-to-dose converter. The address produced by the spectrometer for multichannel pulse-height analysis also was used to locate the dose weighting value for that particular pulse-height

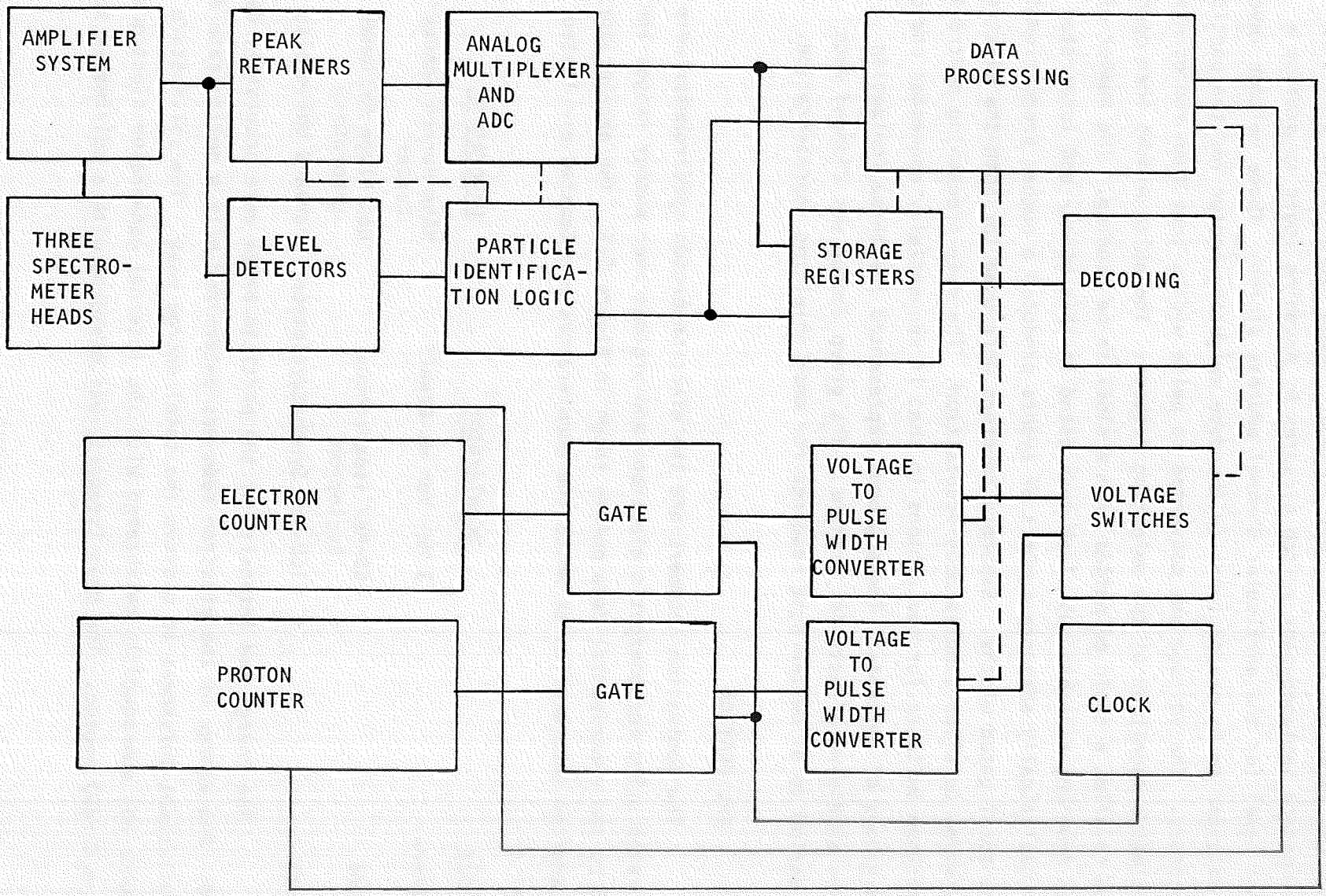


FIGURE 5-9 RADIATION EXPERIMENT

channel. In order to accomplish this, storage registers were used to store the address value for electrons and protons. These addresses were decoded into separate semiconductor switch closures by decoding logic to produce a voltage level for the particular channel address stored. These voltage levels were adjusted to be proportional to the dose weighting factor for the particular address. The voltage was converted to pulse widths that then represented the relative magnitude of the weighting factors. The pulse widths then opened a gate to allow a train of pulses from a clock to be counted. The number of pulses from the asynchronous clock when gated in this manner and integrated over statistically adequate numbers of events produced a number proportional to the total gated widths. Separate counters were used for both the electrons and protons to allow simultaneous acquisition. The data processing controlled the voltage switches for the protons in that it sequentially connected one of three groups of switches. These groups represented the three ionization chamber shielding effects for protons. The group chosen was changed each data period to allow ten dose readings for each shielding representation.

5.5 CALIBRATION

The ionization chambers and the electron-proton spectrometer were calibrated using monoenergetic electrons and protons over energy ranges indicated by the experimental data points shown in Figure 5-5. The accelerators used and the laboratories at which the accelerators are located are listed below:

Particle	Accelerator	Laboratory
Electrons	3-MeV Van de Graaff	NASA Manned Spacecraft Center
Protons	60-MeV Isochronous Cyclotron	Oak Ridge National Laboratory
Protons	160-MeV Synchrocyclotron	Harvard University

The energy and intensity of the particle beams were accurately determined. The energy of the electron beam was determined with a solid-state detector of sufficient thickness to observe the total energy peak. The solid-state detector was subsequently calibrated with the internal conversion electrons from a Bi-207 source. The beam intensity was measured with a collimated solid-

state detector for which the collimator area had been accurately measured. The energy calibration of the proton beams was obtained from data available at the accelerator facilities and was based on information taken from previous calibration experiments. The intensity of the beams was measured with a collimated solid-state detector and a transmission-ionization chamber for comparison purposes.

The cumulative errors in the energy and intensity calibration were less than ±10%. This is a conservative figure and is well within the value required for the overall experiment.

5.5.1 SPECTROMETER CALIBRATION

The complete calibration of the proton-electron spectrometer involved the determination of three basic parameters:

(a) the angular efficiency;

(b) the omnidirectional efficiency, and

(c) the response functions.

The angular efficiencies were measured directly for both electrons and protons at a number of energies. Typical results are shown in Figure 5-10. The angular distributions are seen to be quite different for the two types of particles. This results from the much larger scattering of electrons than protons in the 0.02-inch thick aluminum window and the 300 μm solid-state detector which forms the entrance aperture of the telescope. The proton distribution is rather constant over the energy range studied; however, that for electrons decreases in width slightly with increasing energy.

The efficiency of the spectrometer for an omnidirectional flux of particles was determined for each of the angular distribution measurements. In effect each of the distributions were multiplied by $2\pi \sin\theta \, d\theta$ (where θ is the angle of incidence) and integrated over θ to yield the efficiency per unit solid angle. The resulting values were then divided by 4π to obtain the omnidirectional efficiencies. These are shown in Figure 5-11 for protons and Figure 5-12 for electrons.

The response functions were measured by feeding the output of the spectrometer into a multichannel pulse-height analyzer which recorded the response to the incident electrons and protons. A typical response to electrons

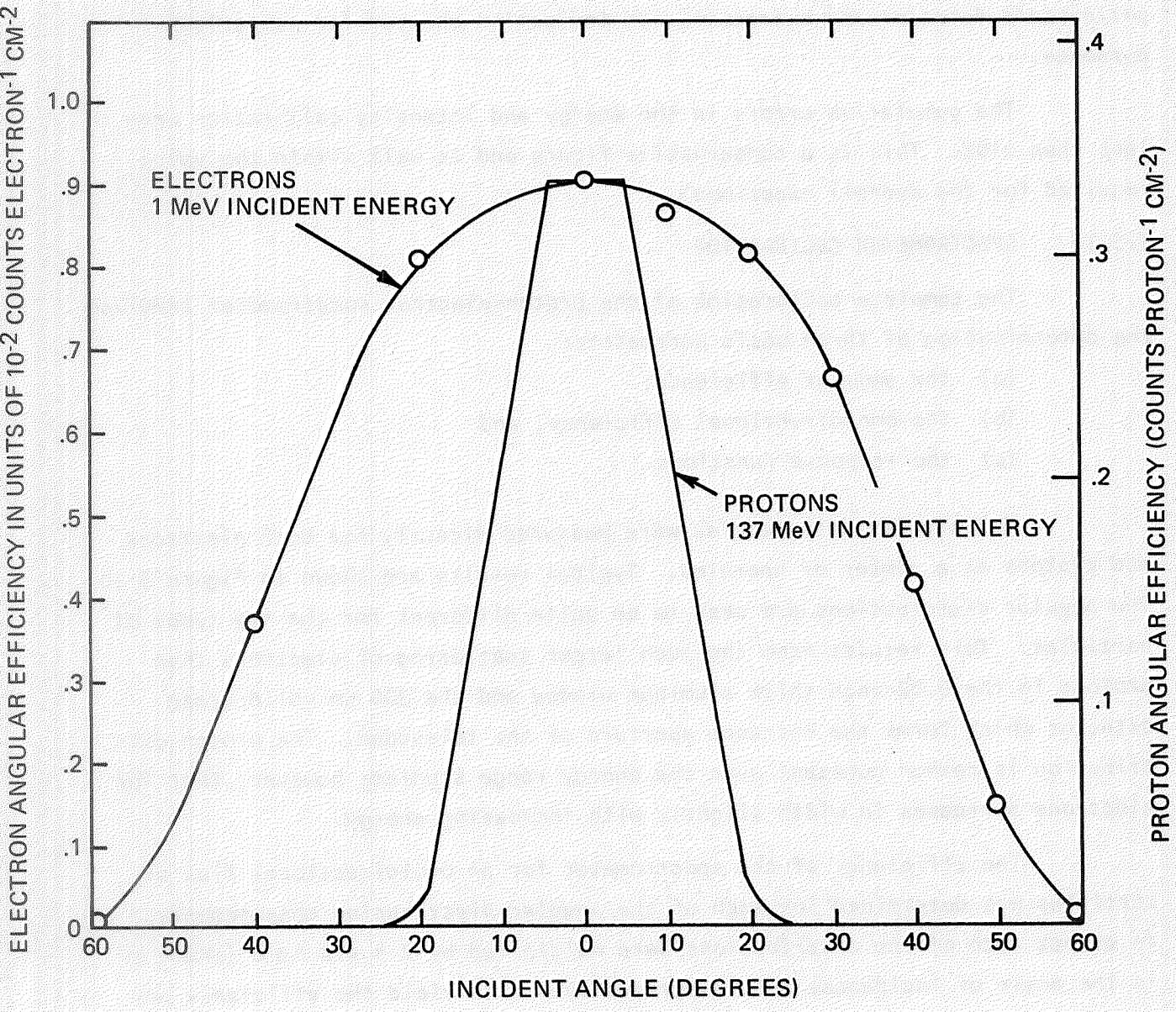


FIGURE 5-10 TYPICAL ANGULAR EFFICIENCIES OF THE ELECTRON-PROTON SPECTROMETER

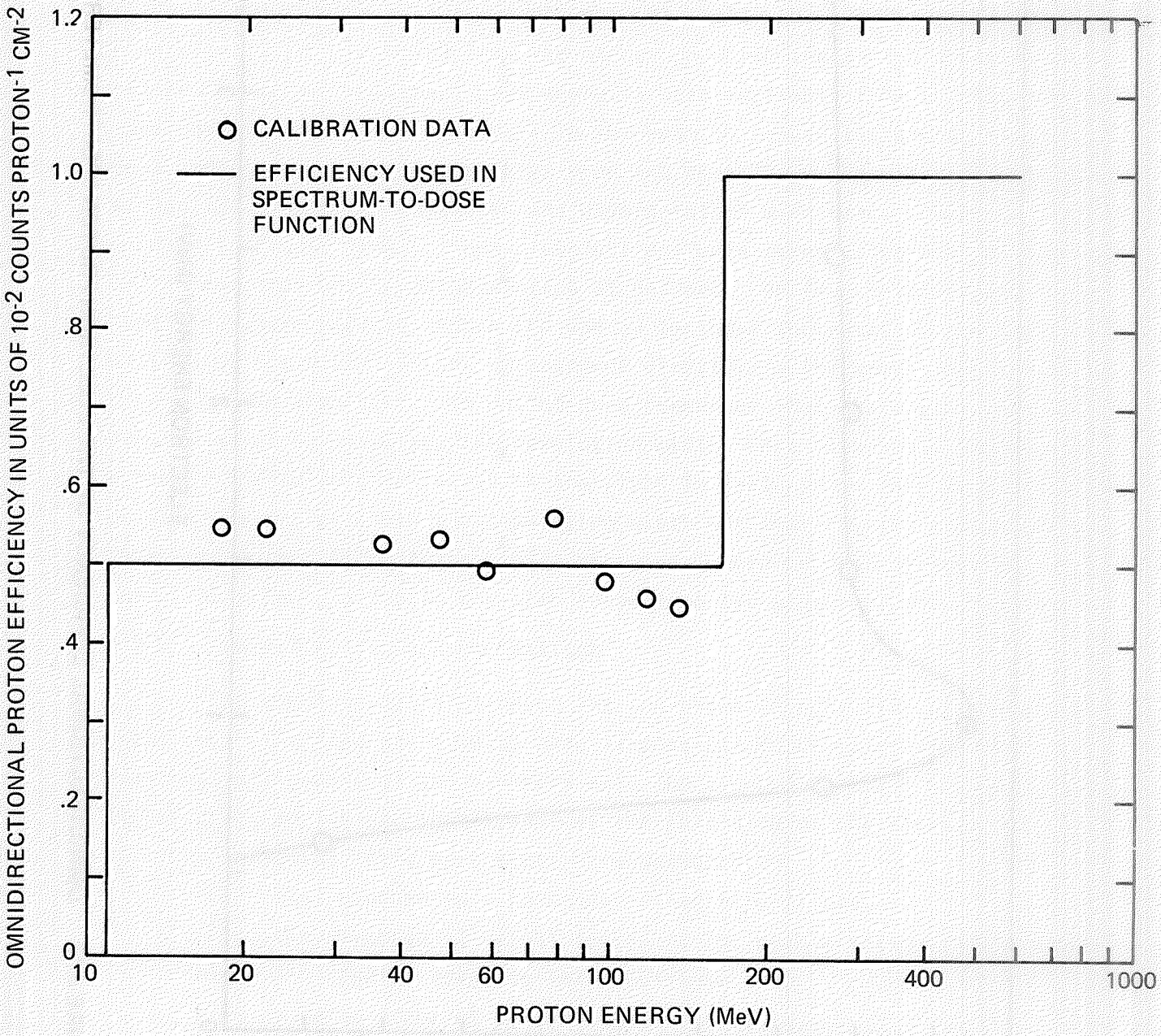


FIGURE 5-11 OMNIDIRECTIONAL EFFICIENCY OF THE ELECTRON-PROTON SPECTROMETER FOR PROTONS

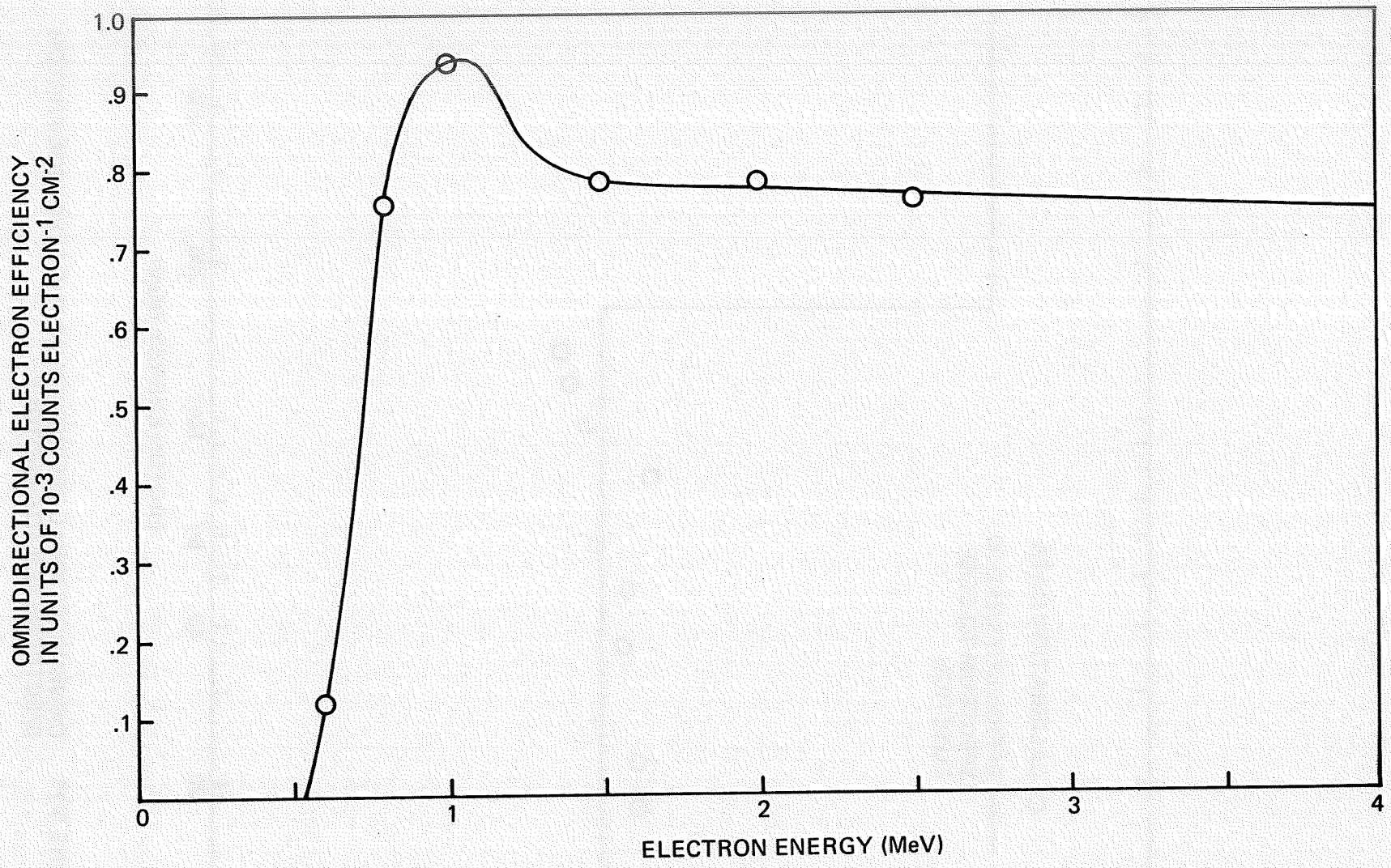


FIGURE 5-12 OMNIDIRECTIONAL EFFICIENCY OF THE ELECTRON-PROTON SPECTROMETER FOR ELECTRONS

is shown in Figure 5-13. This response function is characteristic of the detector in that the resolution width (full width at half maximum) is approximately 200 keV, which was the measured noise resolution of the total energy detector stack. Also, the tail on the distribution, which results from electrons being scattered out of the sensitive region, is as would be expected. The response functions of the protons were generally not characteristic of the detector. This resulted from the manner in which the proton energies were obtained. Only a few primary beam energies were available from the accelerators. It was necessary to place absorbers in the beam to reduce the energy and produce a homogeneous flux of particles over the detector. The materials caused a straggling of particle energies and gave a rather wide peak. Examples of this are shown in Figure 5-14. These distributions were taken using the 165 MeV primary beam from the synchrocyclotron at Harvard. Various thicknesses of polyethylene were used to reduce the energy to those indicated on the figure. The width of the distributions corresponds directly to the amount of straggling produced by the absorbers. It was of no consequence that these functions were not measured directly, since the resolution widths were very small compared to the energy channel boundaries which are given in Table 5-1. This is especially true at low energies where the resolution width was that resulting from noise in the detectors. Even at the higher energies, where Landeau straggling is larger, the effect is negligible with respect to the widths of the channels.

5.5.2 IONIZATION CHAMBER CALIBRATION

The complete calibration of the ion chambers consisted of measuring parameters in the laboratory which made it possible to calculate the omnidirectional efficiency of the chambers as a function of particle energy. This efficiency had to include the effects of the shielding of the satellite structure. The following basic parameters were measured:

(a) the response to a known gamma-radiation field,

(b) the response at normal incidence for both electrons and protons,

(c) the angular response for electrons, and

(d) a gamma probe of the satellite structure.

The absolute dose calibration and the response as a function of dose rate were obtained by placing the chambers, with no shields, in known radiation fields produced by the gamma-rays from accurately calibrated sources of Cs-137

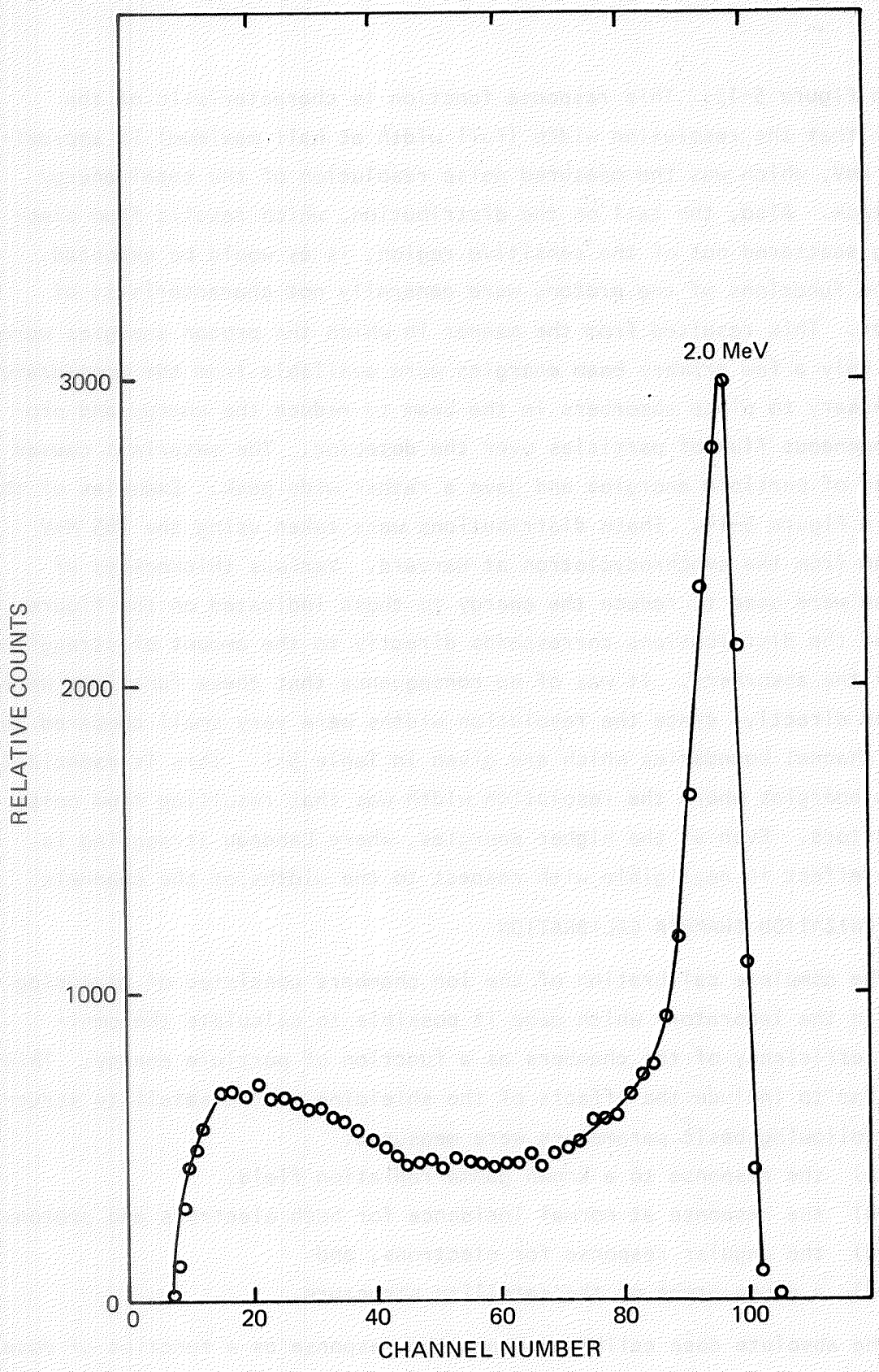


FIGURE 5-13 RESPONSE OF THE ELECTRON-PROTON SPECTROMETER TO 2-MeV ELECTRONS WITH NORMAL INCIDENCE

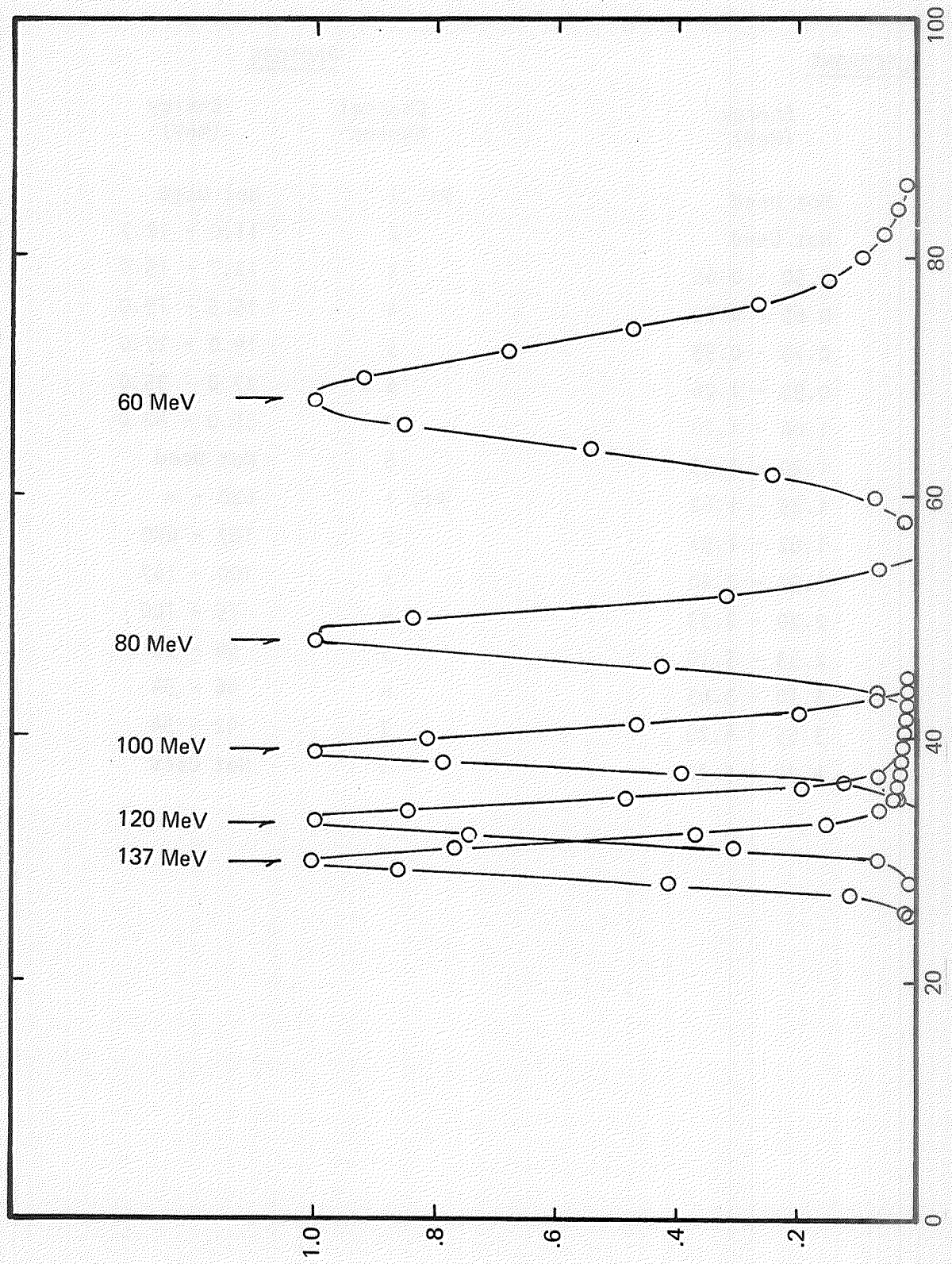


FIGURE 5-14 RESPONSE OF ELECTRON-PROTON SPECTROMETER TO PROTONS IN THE PROTON II REGION

TABLE 5-1 ENERGY CHANNEL BOUNDARIES FOR THE ELECTRON-PROTON SPECTROMETER

ELECTRONS		PROTONS		
Channel Number	Energy (MeV)		Channel Number	Energy (MeV)
1	Not Used	PI	1	Not Used
2	Not Used		2	11.0 - 12.7
3	0.50 - 0.65		3	12.7 - 15.5
4	0.65 - 0.79		4	15.5 - 19.0
5	0.79 - 0.93		5	19.0 - 27.0
6	0.93 - 1.06		6	27.0 - 35.0
7	1.06 - 1.20		7	35.0 - 42.0
8	1.20 - 1.35		8	Not Used
9	1.35 - 1.62	PII	1	620 - ∞
10	1.62 - 1.91		2	167 - 620
11	1.91 - 2.20		3	100 - 167
12	2.20 - 2.53		4	75 - 100
13	2.53 - 3.10		5	54 - 75
14	3.10 - 3.65		6	46 - 54
15	3.65 - 4.20		7	42 - 54
16	4.20 - 5.20		8	Not Used

and Co-60. These measurements were carried out by NASA MSC and the results are shown in Figure 5-15.

For electrons it was necessary to make measurements only for the unshielded ionization chamber, since the dose produced by the electrons in space would produce only a negligible dose in the other two chambers. The response was measured in air with a homogeneous electron beam which was monitored with a collimated solid-state detector. A typical angular efficiency is shown in Figure 5-16. The omnidirectional efficiency for electrons was obtained by integrating the angular responses over angle as was done for the proton-electron spectrometer discussed earlier. The resulting responses are shown as a function of energy in Figure 5-17.

The response to protons was obtained by first measuring the response as a function of energy with protons incident normally to the chambers. These responses are given in Figures 5-18 through 5-20. Then, with the chambers mounted on the satellite in orbital configuration, the responses of the three chambers were measured with a Cs-137 gamma source. Points were taken at 236 angular locations for each chamber. The attenuation of the gamma rays was transformed to an equivalent shield thickness for protons as a function of angle. For these data the omnidirectional responses shown in Figures 5-18 through 5-20 were computed. These computations were carried out by Radiation Research Associates, Inc. and are described in detail in reference 5.

5.5.3 DETERMINATION OF PULSE-HEIGHT SPECTRUM-TO-DOSE CONVERSION FUNCTIONS

The primary objective of this program as stated in paragraph 2.0 was to demonstrate the feasibility and accuracy of the spectrum-to-dose concept. The approval taken to accomplish this objective was to compare the reading of the ionization chambers with the values obtained from the electron-proton spectrometer using the spectrum-to-dose conversion concept. The spectrum-to-dose functions F were obtained using the ionization chamber response functions as the energy-to-dose conversion functions C.

Since electrons could penetrate only the unshielded chamber, only one function that related to the unshielded ion chamber was required for electrons. The technique used to generate this function (Figure 5-21) involved the use of a matrix iterative process and is discussed in detail in references (6) and (7).

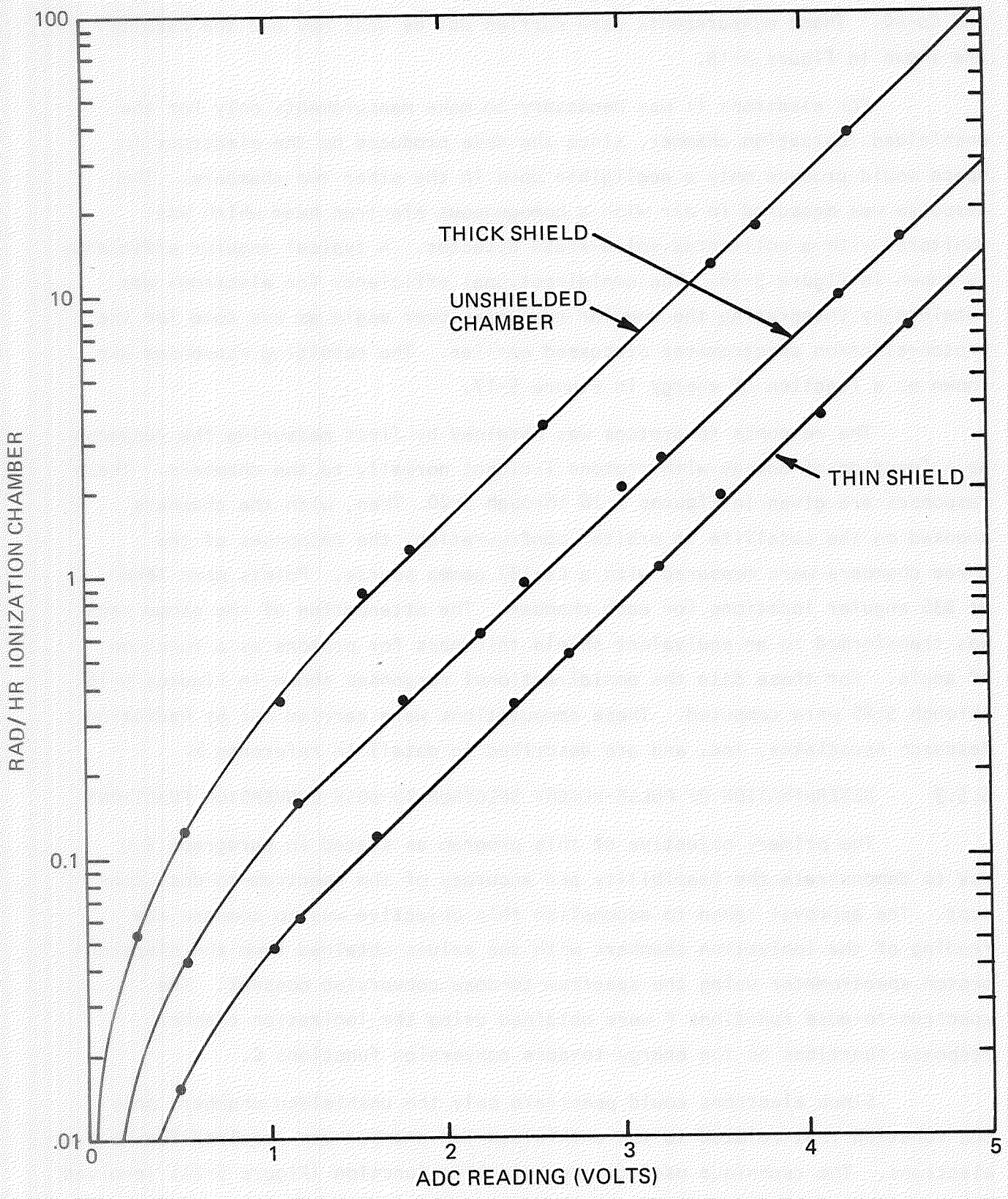


FIGURE 5-15 IONIZATION CHAMBER CALIBRATION CURVES

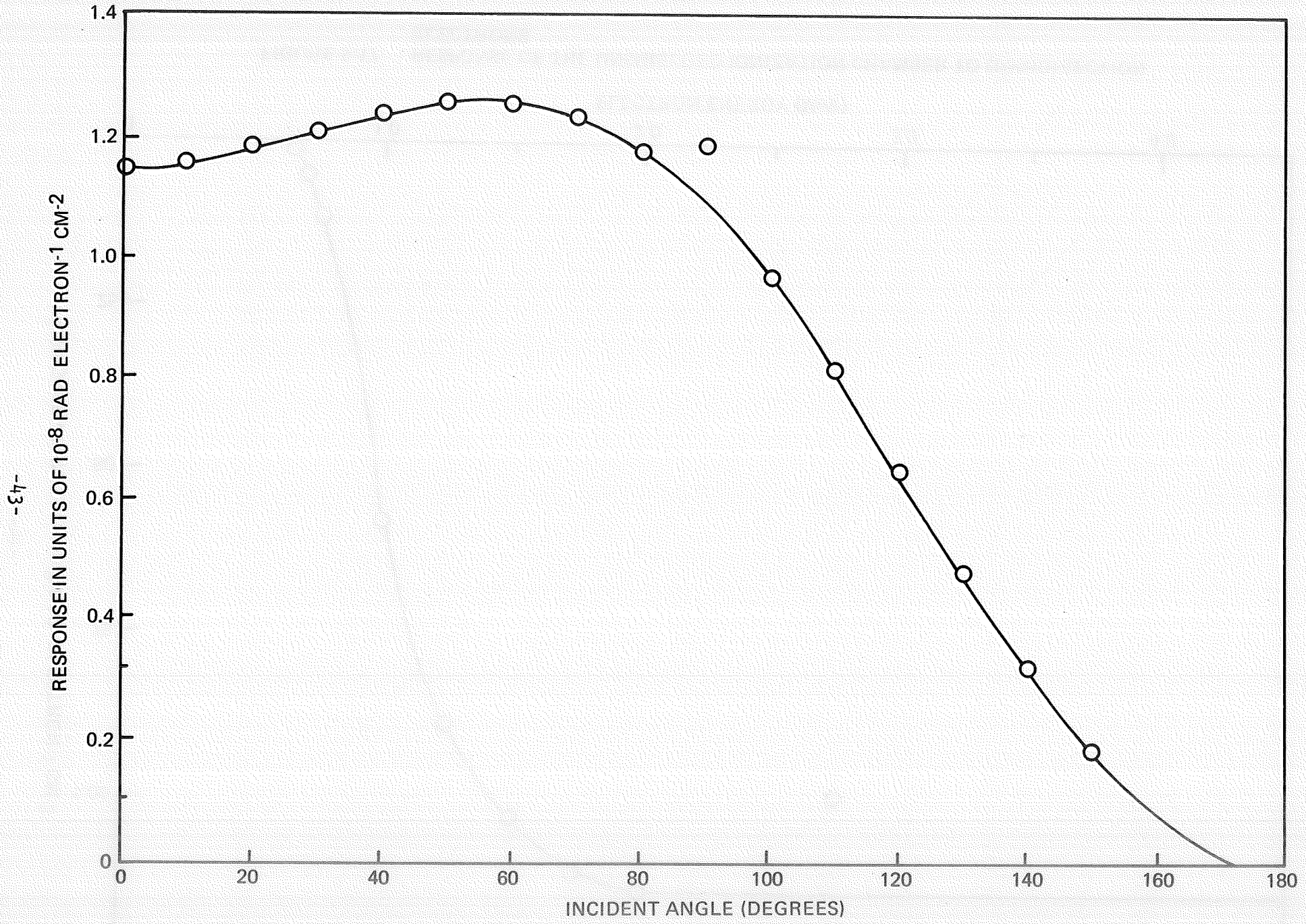


FIGURE 5-16 ANGULAR RESPONSE OF UNSHIELDED IONIZATION CHAMBER FOR 1 MeV ELECTRONS

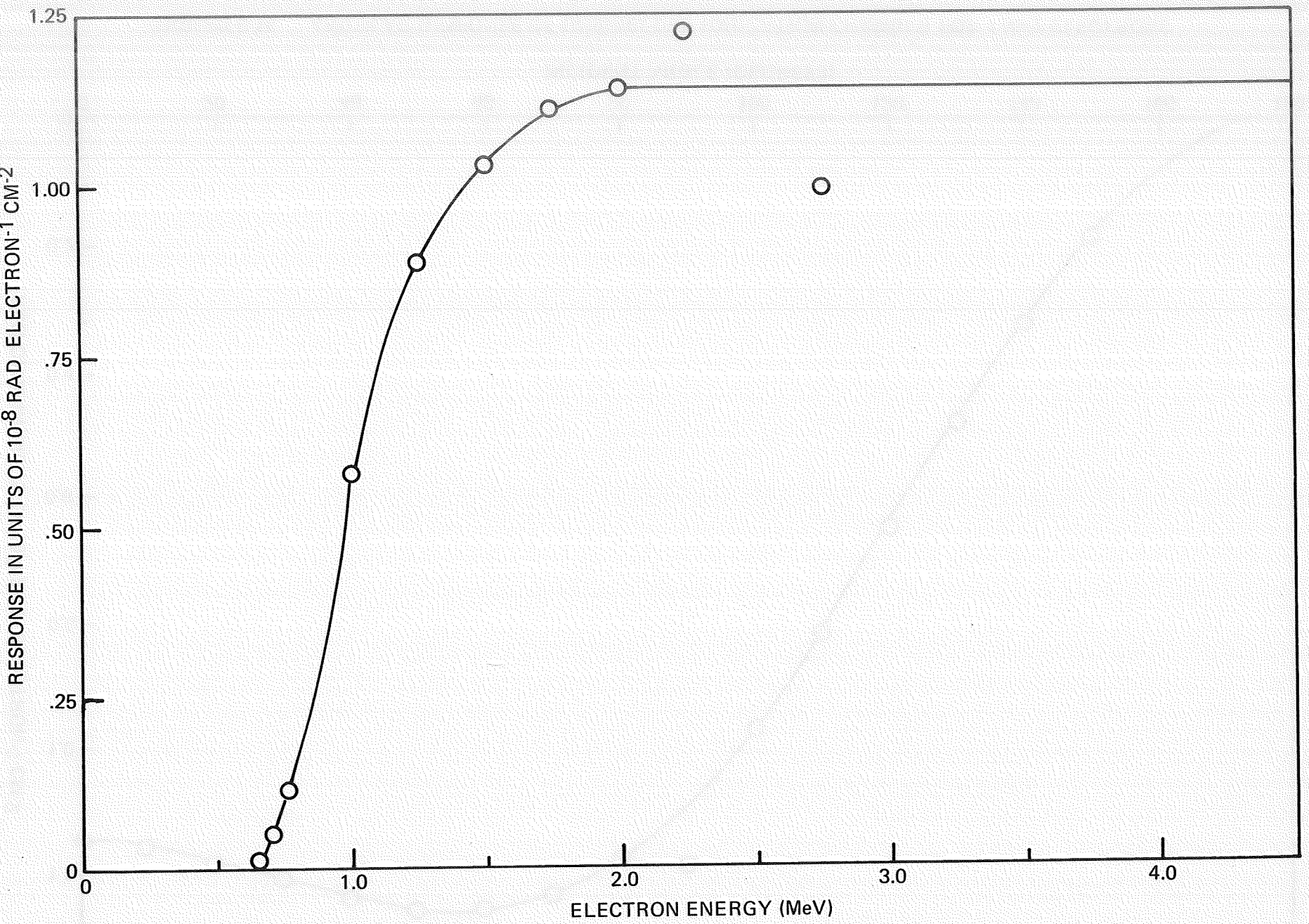


FIGURE 5-17 RESPONSE OF THE UNSHIELDED IONIZATION CHAMBER TO OMNIDIRECTION ELECTRONS

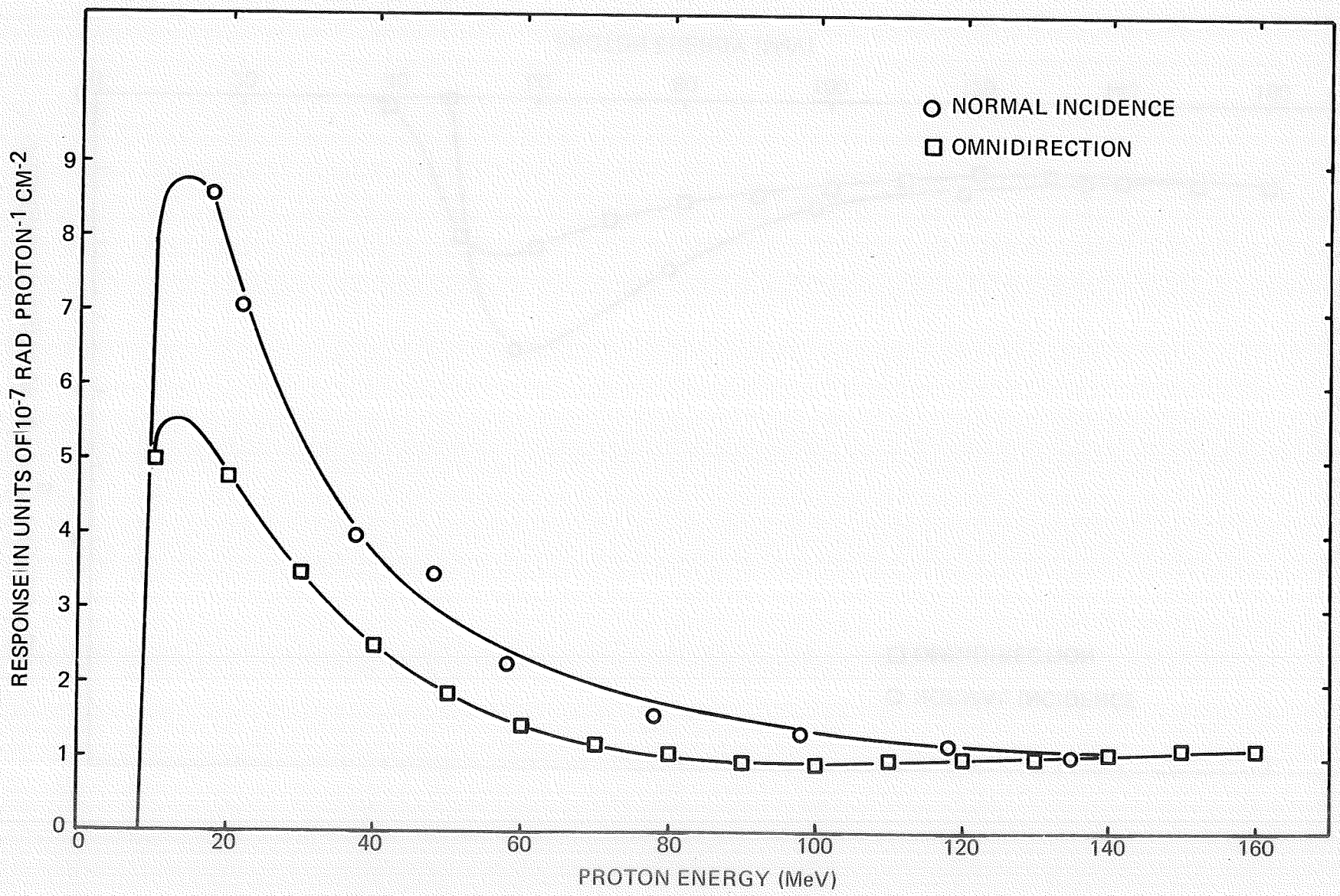


FIGURE 5-18 RESPONSE OF UNSHIELDED IONIZATION CHAMBER TO PROTONS AT NORMAL INCIDENCE AND OMNIDIRECTION

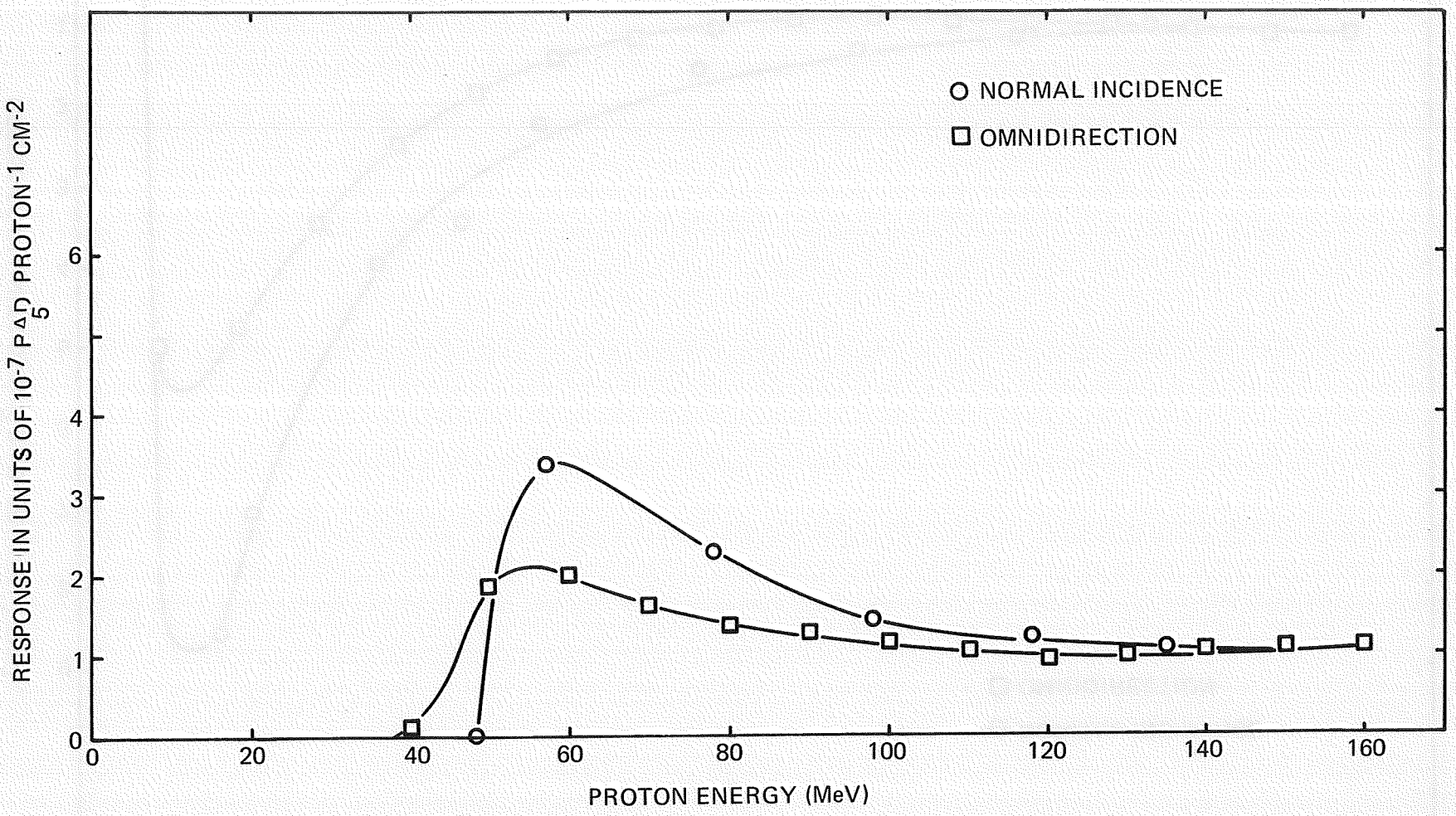


FIGURE 5-19 RESPONSE OF THIN-SHIELDED IONIZATION CHAMBER TO PROTONS AT NORMAL INCIDENCE AND OMNIDIRECTION

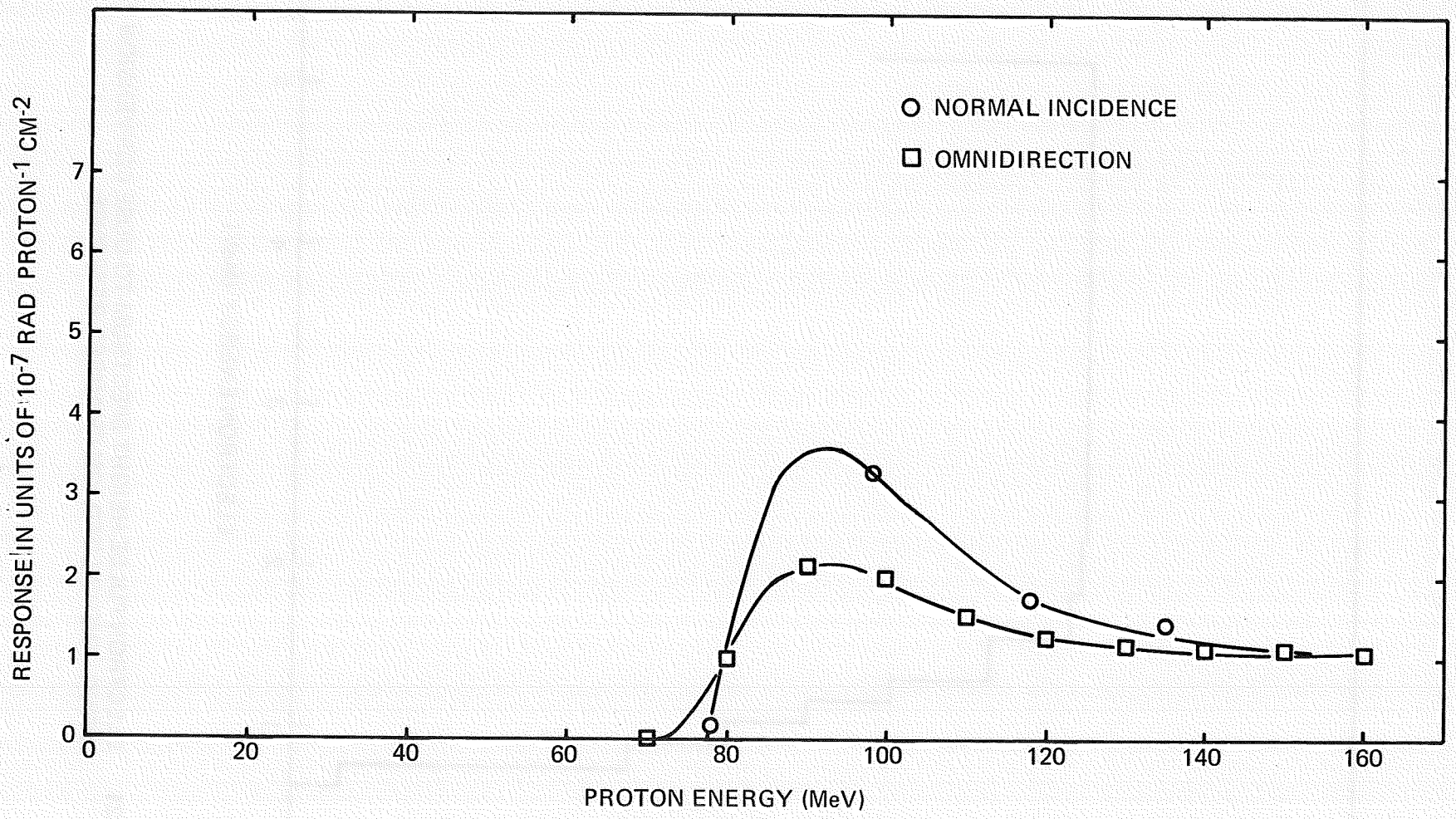


FIGURE 5-20 RESPONSE OF THICK SHIELDED IONIZATION CHAMBER TO PROTONS AT NORMAL INCIDENCE AND OMNIDIRECTION

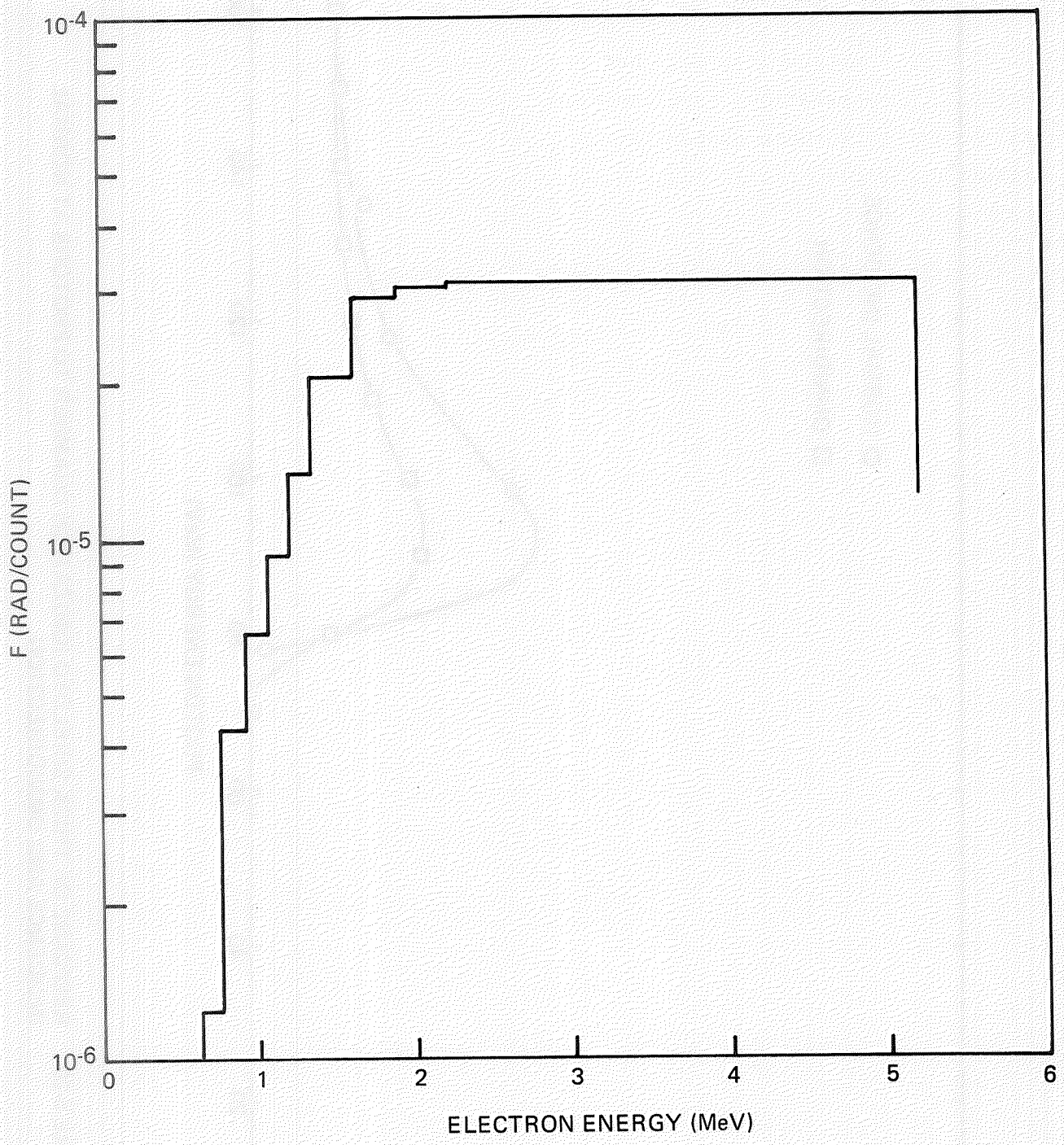


FIGURE 5-21 **ELECTRON PULSE-HEIGHT SPECTRUM-TO-DOSE CONVERSION FUNCTION USING UNSHIELDED ION CHAMBER RESPONSE**

Three functions for protons were generated which corresponded to the three ionization chambers shield thicknesses. The complexity of the matrix operations was less than for the electrons, since the proton resolution functions of the spectrometer had widths which were much less then the channel widths. The operations involved primarily the application of the efficiency to the energy-to-dose conversion functions of the ionization chambers. The resulting functions are shown in Figures 5-22 through 5-24. These functions were then entered into the spectrum-to-dose conversion unit of the satellite. A pulser was used to strobe a given address in the analog-to-digital converter and the potentiometer corresponding to that energy channel was adjusted until the dose output as read by the PDP 81 ground support computer corresponded to the correct value of the pulse-height spectrum-to-dose conversion functions F.

5.5.4 GSFC DATA REDUCTION

To facilitate the early comparisons of the dose readings from the ionization chambers and the spectrum-to-dose system the GSFC Control Center Operations group prepared a computer program which converted the raw satellite data into a useful format. The basic elements of the program are outlined in reference (8). It was written primarily to reduce the numbers to engineering and scientific units and arranged in a format that allowed easy comparisons. The electron-proton spectrometer spectra were arranged in order of channel number; however, only the raw data was presented and no attempt was made to include the efficiency, channel width, and resolution effects. A run summary was presented which was the sum of the thirty individual spectra divided by the channel width. This value could be compared roughly with the Vette spectra. The program also calculated the spectrum-to-dose values and presented them with the corresponding ionization chamber readings.

5.6 PRELIMINARY DATA ANALYSIS

The first orbital data was taken with all three heads of the electron-proton spectrometer enabled. The memory dumps from the first few passes through the South Atlantic magnetic anomaly indicated a problem with the proton pulse-height spectra. Also the dose readings from the two shielded ionization chambers did not agree with those from the corresponding spectrum-to-dose outputs. A series of runs were made for which only one head was enabled at a time. Comparisons of the data from the individual heads showed marked

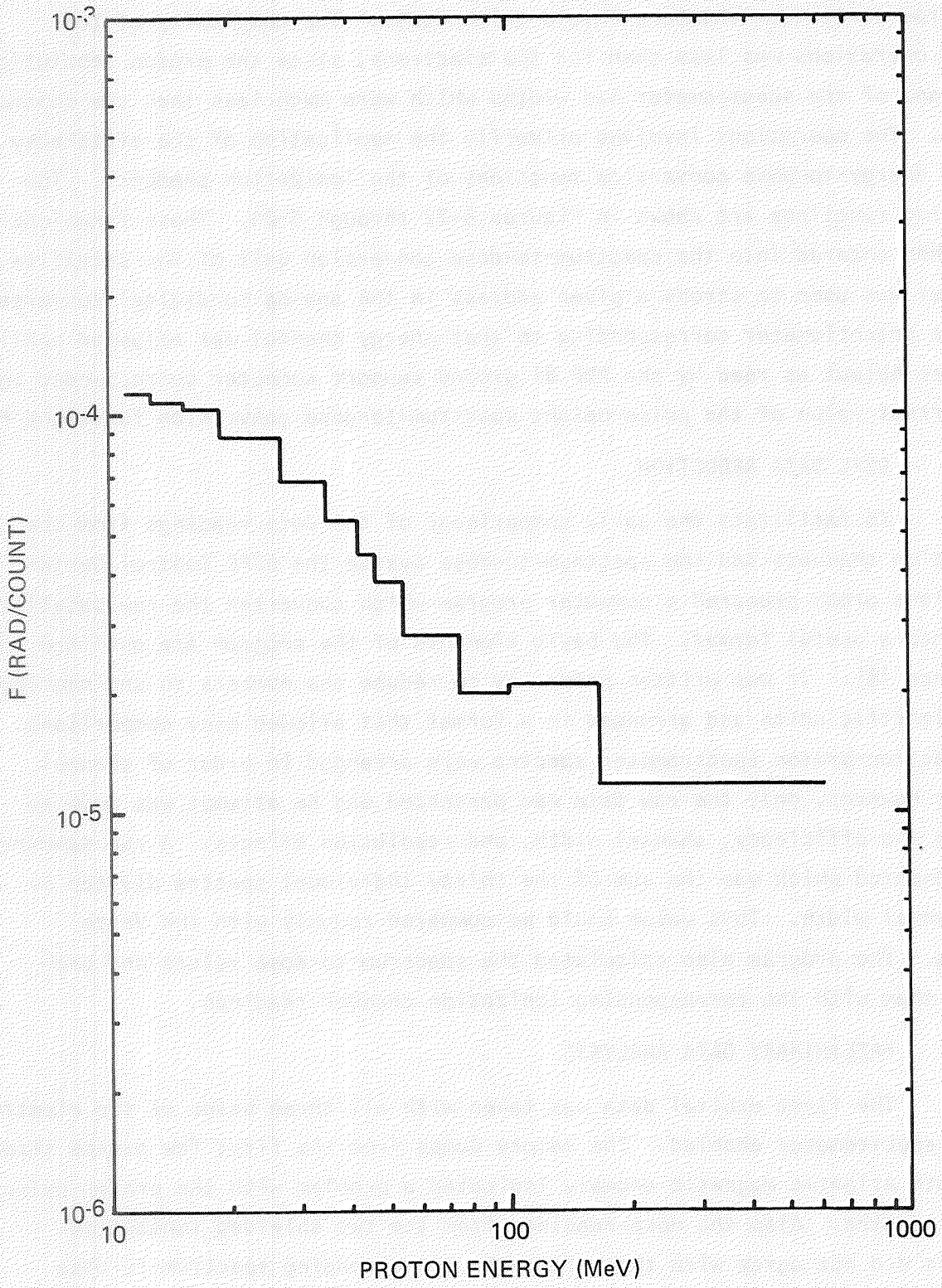


FIGURE 5-22 PROTON PULSE-HEIGHT SPECTRUM-TO-DOSE FUNCTION USING UNSHIELDED ION CHAMBER RESPONSE

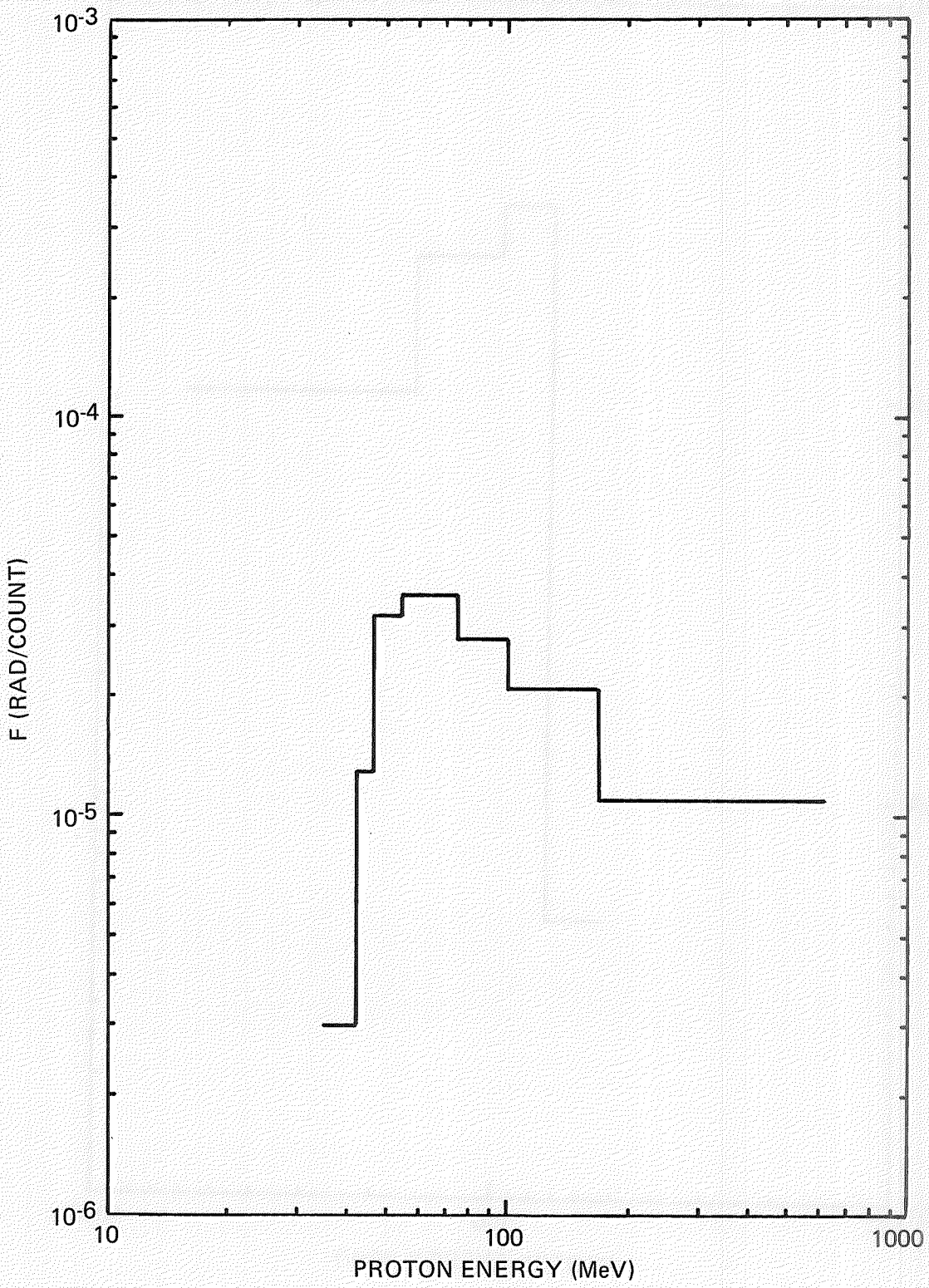


FIGURE 5-23 PROTON PULSE-HEIGHT-SPECTRUM-TO-DOSE FUNCTION USING THIN SHIELDED ION CHAMBER RESPONSE

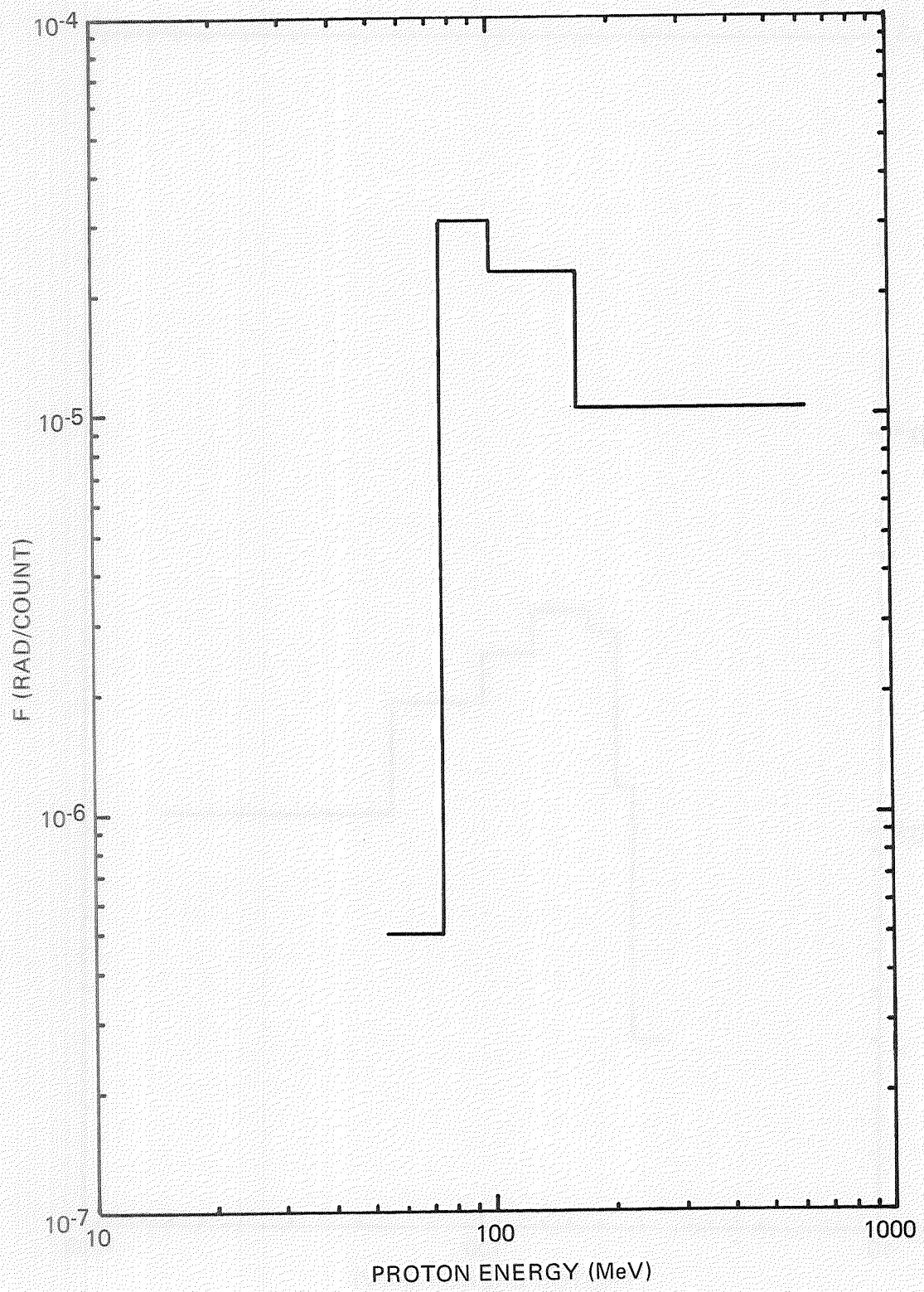


FIGURE 5-24 PROTON PULSE-HEIGHT-SPECTRUM-TO-DOSE FUNCTION USING THICK SHIELDED ION CHAMBER RESPONSE

differences in the proton spectra. Head number 2 displayed reasonable electron data; yet, no proton data were recorded, except in the first channels of both proton I and proton II. This head was excluded from further use, since it appeared that the total energy stack of solid-state detectors was not producing a signal. This could have resulted from a broken lead between the amplifier and the head or a malfunction in the amplifier itself. An examination of the spectra from heads 1 and 3 indicated good electron data when compared to the Vette spectra; however, the indicated proton fluxes were not only different in the two heads, but both were higher than the Vette model would predict. Also, the spectral shapes did not agree with the Vette models. Since the lower fluxes were obtained from head 1, it was used for the majority of the radiation runs.

Although no integration of spectra through the exact RMS orbits were available at the time of this report, rough comparisons with calculations for a similar orbit are given for electrons and protons in Figures 5-25 and 5-26 respectively. The RMS data were taken during orbit 52. The spectra have been summed through the anomaly and an allowance made for the 25% duty factor. The calculated values were obtained by the Manned Spacecraft Center and were taken from the Vette AE 2-68 electron model and the AP 1, 7, 6 proton model. No normalization factors have been applied to the spectra. The RMS electron spectrum is somewhat higher than that calculated, while the reverse is true for the proton data.

The integrated electron spectra in Figure 5-25 are seen to agree very well. The RMS data show not only the natural radiation (below 1.5 MeV) but also the high energy component resulting from the high altitude nuclear explosion, called Starfish, which was set off over the South Pacific in 1962.

Agreement of the proton spectra is good only below approximately 40 MeV. This corresponds to the protons in the proton I region. The RMS spectrum in the proton II region is seen in Figure 5-26 to be much higher than that predicted by the Vette model. It is believed that this anomaly in the RMS proton spectrum results from damage to the electron-proton spectrometer heads or harness leading to the heads, which occurred during the OFO/RMS separation. The problem was discussed earlier in this report in paragraph 4.2. It is possible that the two spacecraft collided due to a malfunction in the Scout fourth stage timer.

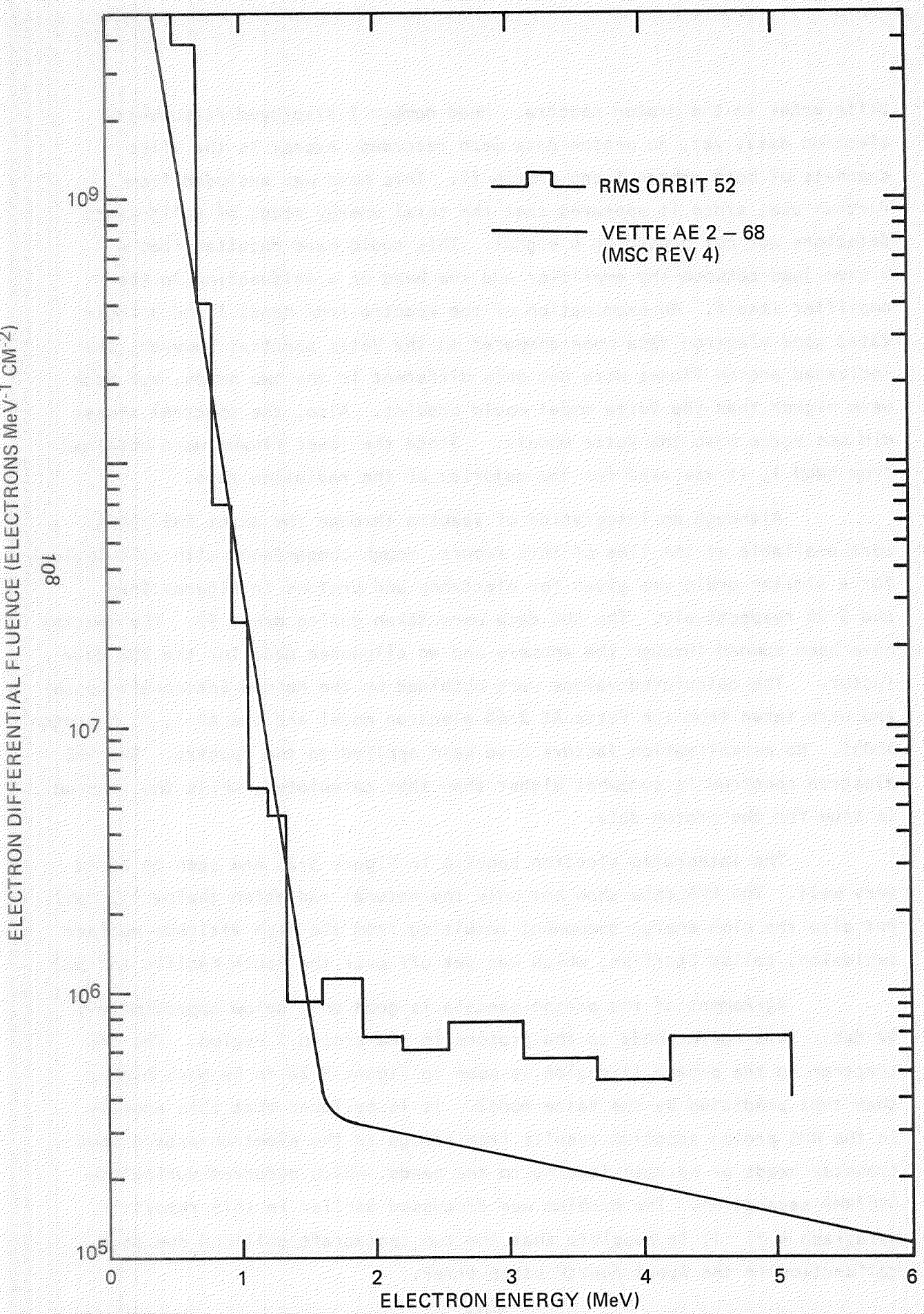


FIGURE 5-25 COMPARISON OF RMS ELECTRON AND VETTE MODEL FOR SIMILIAR ANAMOLY PASSES

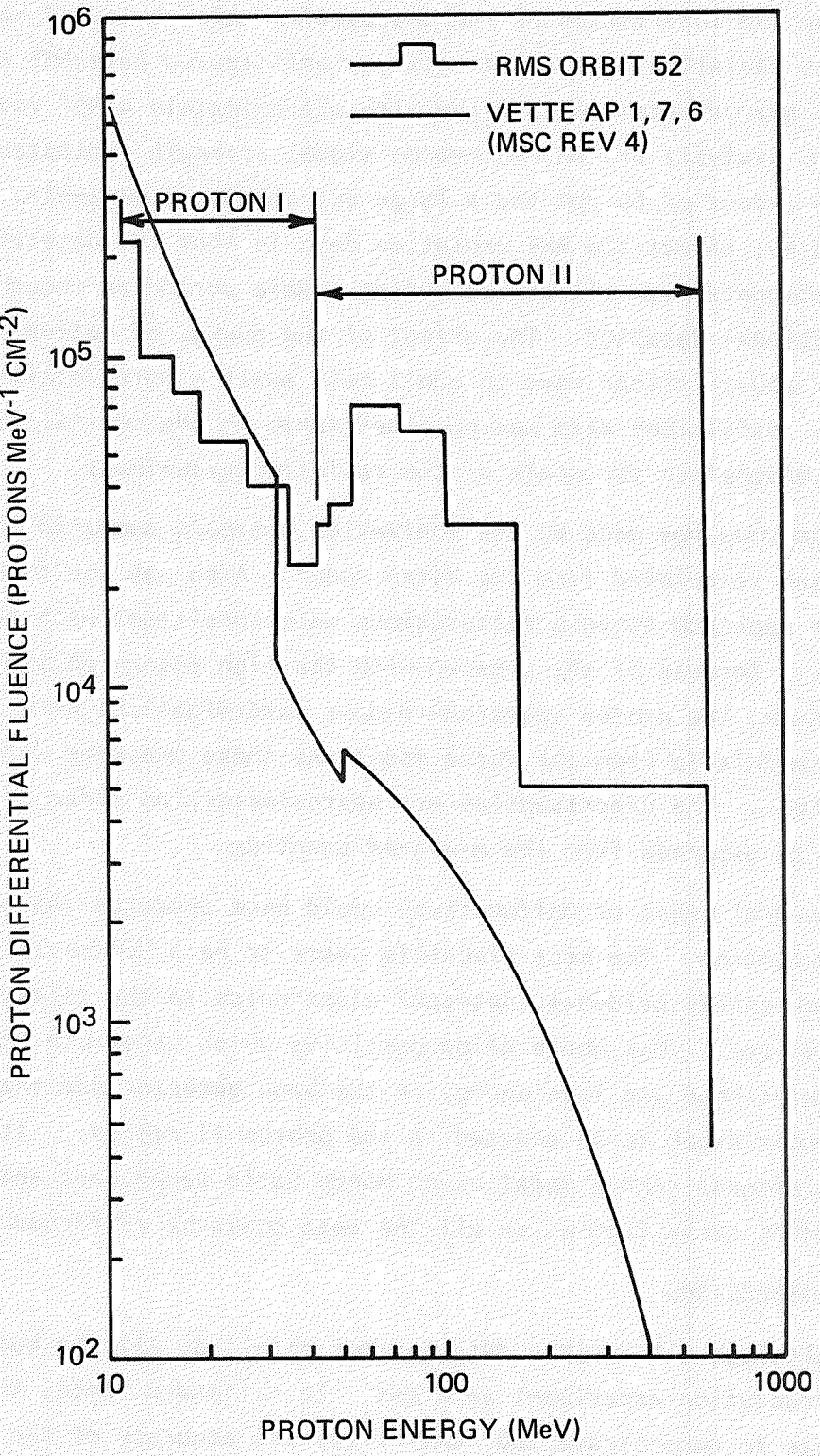


FIGURE 5-26 COMPARISON OF RMS PROTON SPECTRUM AND VETTE MODEL FOR SIMILAR ANOMALY PASSES

Although a significant change in the dynamics of the RMS spacecraft resulted from the interaction of the spacecraft, this in itself had no serious effect on the radiation experiment. It was anticipated that RMS would have a spin rate of approximately 6 to 8 rpm with approximately a 45° cone angle. A preliminary analysis of the RMS beacon signal strength indicated an initial spin rate in excess of 60 rpm and a large but unknown cone angle. Such a motion would not affect the RMS radiation data in that the detector would basically integrate over all angles during a data period as though it were an omnidirectional detector. The effect of the change of motion into a pure tumble after about fifteen days in orbit must await a more detailed analysis of the data. Sufficient data was obtained early in the orbital lifetime, however, to accomplish the goals of the radiation experiment.

The readings made by the ionization chambers compared favorably with the doses calculated from the Vette model. Also, as would be expected, the electron spectrum-to-dose calculations were consistent with the spectral measurements. Because of the problem with the high energy portion of the proton spectrum, the proton spectrum-to-dose determinations were much higher than those calculated from the Vette model and those measured with the ionization chambers. The discrepancies are approximately an order of magnitude, which would be expected from the measured spectrum.

Several types of malfunctions could have produced the observed spectral distortion. The most plausible seems to be a "cross-talk" effect from the back,anticoincidence, detector electronics to the telescope coincidence circuitry. This would allow particles which penetrate the walls of the detector head and lose energy in the back detector and the total energy detector stack to be counted in the proton II region. It would be feasible to program such a model using Monte Carlo techniques and obtain a new calibration curve from which all the data could be retrieved.

5.7 CONCLUSIONS

Although all desired data was not obtained, all the basic objectives of the RMS radiation experiment were met. To reiterate these, the primary objective was to demonstrate the feasibility and accuracy of the spectrum-to-dose conversion concept and instrumentation in a real-time mode in an actual space environment. The application of the spectrum-to-dose function

F was made to both the electron and proton spectra. The dose values thus obtained were consistent with the spectra obtained with the spectrometer. Because of the problem with the proton spectra, the comparison to the ion chamber readings could be made only with the electron dose values. Using the Vette models to calculate the electron and proton doses, a consistent and accurate relationship was established.

As a secondary objective, the experiment was to provide data to develop maps of the radiation belts in the South Atlantic magnetic anomaly. Readings yielding dose values behind various shield thicknesses were obtained with the ion chambers for approximately 70 passes through the anomaly. This corresponds to over four thousand data points per chamber. These data will provide a very closely spaced grid map of the high intensity radiation zone. In addition, approximately 30 good spectrometer passes were obtained. These will provide nearly a thousand spectral distributions of the electrons and protons. The electron spectra will be useful to update the Vette model and study the further decay of the "Starfish" electrons. The proton spectra below 40 MeV will add further information to the structure of the radiation belts and if an accurate model of the malfunction in the spectrometer can be formulated, the high energy data can be retrieved.

6.0 METEOROID EXPERIMENT

6.1 INTRODUCTION

Early meteoroid measurements were obtained from observations of meteoroids in the atmosphere of the earth. The meteor velocity was determined by recording the meteor trails on photographic plates with a rotating shutter which measures the deceleration by the atmosphere.

The early flight instruments measured impact momentum only with a piezoelectric device and the velocity was assumed to be the meteor velocity distribution previously measured from earth. The first flight instruments to directly measure velocity were velocity "telescopes" consisting of cylinders, 2.5 cm. in diameter and 10 cm. long. A thin-film plasma sensor was at the entrance and a thin-film capacitor on a glass substrate was the second station. Signals resulting from a meteoroid perforation of the films were used to measure time-of-flight in the cylinder. This type instrument was used on OGO-I, II, and III. Only four velocity measurements were obtained with the OGO-I instrument, possibly two with the OGO-II, and three with the OGO-III.

A more sophisticated instrument is used on the Pioneer VII and IX probes. The instrument is designed to measure the velocity (speed and direction) and momentum of meteoroids in interplanetary space. It consists of two, four square inch planes, 5 cm. apart. The sensor in each plane is the plasma type with biased collection screens on both sides of the thin film. The sensors and logic are constructed such that the perforation point in each plane is located within 1 square inch for trajectory determination. The meteoroid time-of-flight (TOF) between planes is also measured.

The meteoroid experiment on the Radiation and Meteoroid Satellite was an extension of the earlier flight experiments to larger sensor areas for measuring the intercept velocity of impacting meteoroids. The earth-orbital impact-velocity data should be very useful for interpreting existing meteoroid penetration data (Explorer and Pegasus) in terms of flux-mass for scientific purposes.

To resolve some of the basic questions concerning meteoroids, experiments of a much larger scale than previous experiments must be designed. Of particular interest is the measurement of velocity and mass of meteoroids in

the region from the sun to Mars. As a result, the meteoroid experiment of the Radiation and Meteoroid Satellite was used to flight qualify some of the meteoroid sensors and electronic instrumentation proposed for use on larger area experiments. The primary objective of the RMS meteoroid experiment was to space qualify materials and instrumentation to be used on large area, long duration meteoroid experiments for future deep-space missions. The meteoroid detection system was designed to measure the flux and intercept velocities of 10^{-12} gram meteoroids and larger and to count impacting meteoroids of 10^{-14} grams and larger. The RMS meteoroid experiment uses a velocity measuring technique similar to that used on the OGO series; however, it was expanded to an area of approximately one square foot.

Two meteoroid velocity measurements were made during the RMS's lifetime with each occurring during or shortly after a meteor shower. The first velocity measurement that occurred on 17 December 1970 might be associated with the Geminids meteor shower and the second that occurred on 24 December 1970 might be associated with the Ursids meteor shower. It was also observed that between December 23 and December 24 there was an extremely abnormal increase in the number of shorted outer-plane sensors. It is probably that these seven shorts were caused by impacting micrometeoroids having insufficient mass to pass through the sensor but which damaged the sensor sufficiently to produce a short.

Although the number of spurious RMS sensor discharges was higher than was anticipated, one should be able to place a reasonably accurate upper limit on the meteoroid flux. This would be accomplished by examining the statistical relationship between counts from inner and outer plane sensors and the rate at which sensors were observed to short.

6.2 METEOROID DETECTION INSTRUMENT

In general, the meteoroid experiment consisted of two detector packages (9 in. x 9 in. x 4 1/2 in.) having power conditioning, signal conditioning and encoding, temporary data storage and telemetry interface. Either or both of the two detectors could be independently turned on or off. Two detectors were required to efficiently utilize the space available around the Scout "E" section. The two flight packages are shown in Figure 6-1

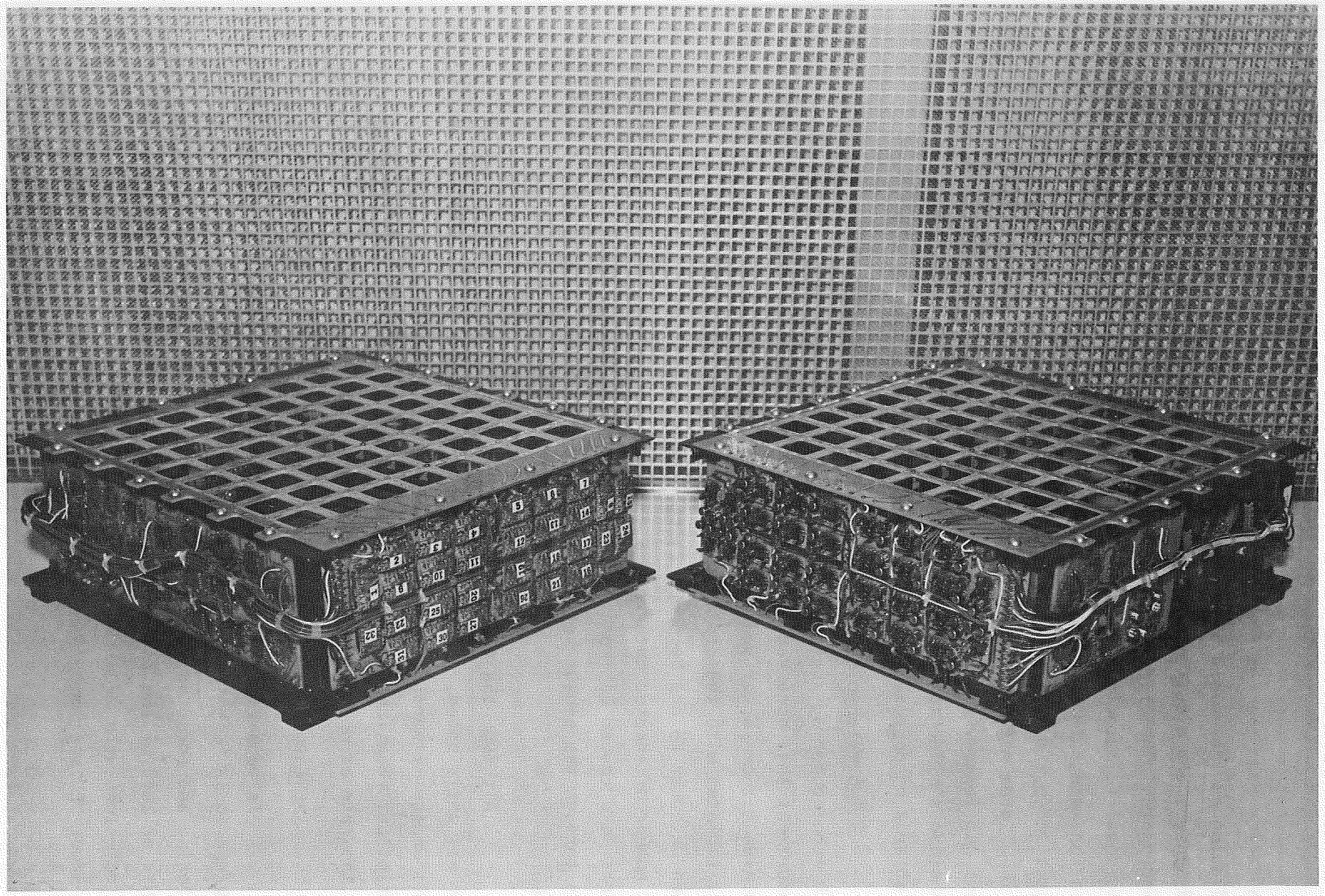


FIGURE 6-1 METEOROID DETECTORS

The thin-film capacitor sensors had not been installed at the time the photograph was taken.

The sensitive area of each detector package consisted of two 8 in x 8 in thin-film sensor planes about 3.16 in. apart. Each sensor plane consisted of a mosaic of 1 inch square, thin-film capacitors with each sensor element mechanically independent of the other sensors in the mosaic but electrically connected as a matrix of 1 in. by 8 in. rows and columns. Approximately 65% of the area was sensitive to meteoroids and the remainder was support structure. The total effective sensor area for two such detectors was approximately 80 square inches.

When meteoroids having velocities and masses greater than approximately 3 km/sec and 10^{-14} grams perforate the thin-film capacitor sensors a current pulse is produced that is used to identify the perforated sensor and to generate a timing pulse to be used in the measurement of the time-of-flight between the two sensor planes. If an inner plane signal does not occur within 80 μs of an outer plane signal, the pulse is considered to be either spurious or to have been produced by a meteoroid having a mass less than 10^{-12} grams. There were 256 memory locations corresponding to each of the 256 sensors where the number of all non-coincident events were stored. For coincident events the location of the two perforated sensors and the time-of-flight were stored with the velocity calculation being made on the ground.

Since previous experience has shown that the highest probability of of thin-film capacitor failure is due to shorting, the sensor leakage currents were monitored to allow determination of the approximate sensitive area.

6.2.1 THIN-FILM METEOROID SENSORS

The meteoroid sensor elements were thin-film capacitors similar to those developed for the Engineering Model Sensor for a Meteoroid Experiment under NASA Contract NAS9-8758. The basic capacitor consisted of two vapor-deposited metal plates separated by a plastic thin-film dielectric. One of the capacitor plates was approximately 300 Å of gold and the other 1000 Å aluminum and the dielectric was 4000 Å of polysulfone giving a total thickness of approximately 5000 Å and a surface density of 130 $\mu g/cm^2$. Meteoroid impact was on the aluminum plate of the capacitor.

Due to excessive capacitor heating caused by direct solar irradiation it was necessary to provide a means of thermal protection for the capacitors. There were two techniques by which this was accomplished. One of the techniques involved vapor depositing a layer of silicon oxide, approximately 6000 Å thick, directly onto the aluminum capacitor plate. The resultant increase in thermal emissivity lowered the maximum capacitor temperature to an acceptable level. However, due to a combination of a wrinkling effect caused by the silicon oxide and the manner in which the sensor elements were attached to the detector matrix, the capacitors were susceptible to development of small tears around the edge of the capacitor. A second technique that was also successfully used required the placement of a thin-film reflector 1/16 inch in front of the capacitor. This reflector consisted of a vapor deposited aluminum film 1000 Å thick on a laminated 4-layer polycarbonate film 4000 Å thick. For thermal control a silicon oxide film 6000 Å thick was vapor deposited onto the aluminum film resulting in a reduction of α/ε from 3.2 to approximately 1.2. This reduced the maximum temperature of the oxide-coated film to approximately 100°C. A drawing of a thin-film sensor element is shown in Figure 6-2.

Of the 128 outer-plane sensors flown on RMS, 104 consisted of the type having an oxide-coated solar reflector. One column of 8 sensors had silicon oxide deposited directly onto the capacitor. Another column of 8 sensors had solar reflectors consisting of a vapor deposited aluminum film on an 8000 Å single-layer polycarbonate film. The other column of 8 sensors consisted of control sensors. Four of these control sensors had a metal cover to repel meteoroid impacts and allow counting of spurious breakdowns only. The other 4 control sensors were intentionally shorted. These shorted sensors were designed in such a way that any significant damage would result in an open circuit which would be detected as a decrease in the measured leakage current for the column containing the damaged control sensor.

All 128 of the inner-plane sensors were of the same type. Each inner-plane capacitor was given minimal protection from direct solar irradiation that might be allowed through by damaged outer-plane sensors. This protection was provided by a reflector consisting of 1000 Å of aluminum, vapor deposited onto a 4000 Å laminated polycarbonate film. The surface density of each reflector was approximately 75 $\mu g/cm^2$.

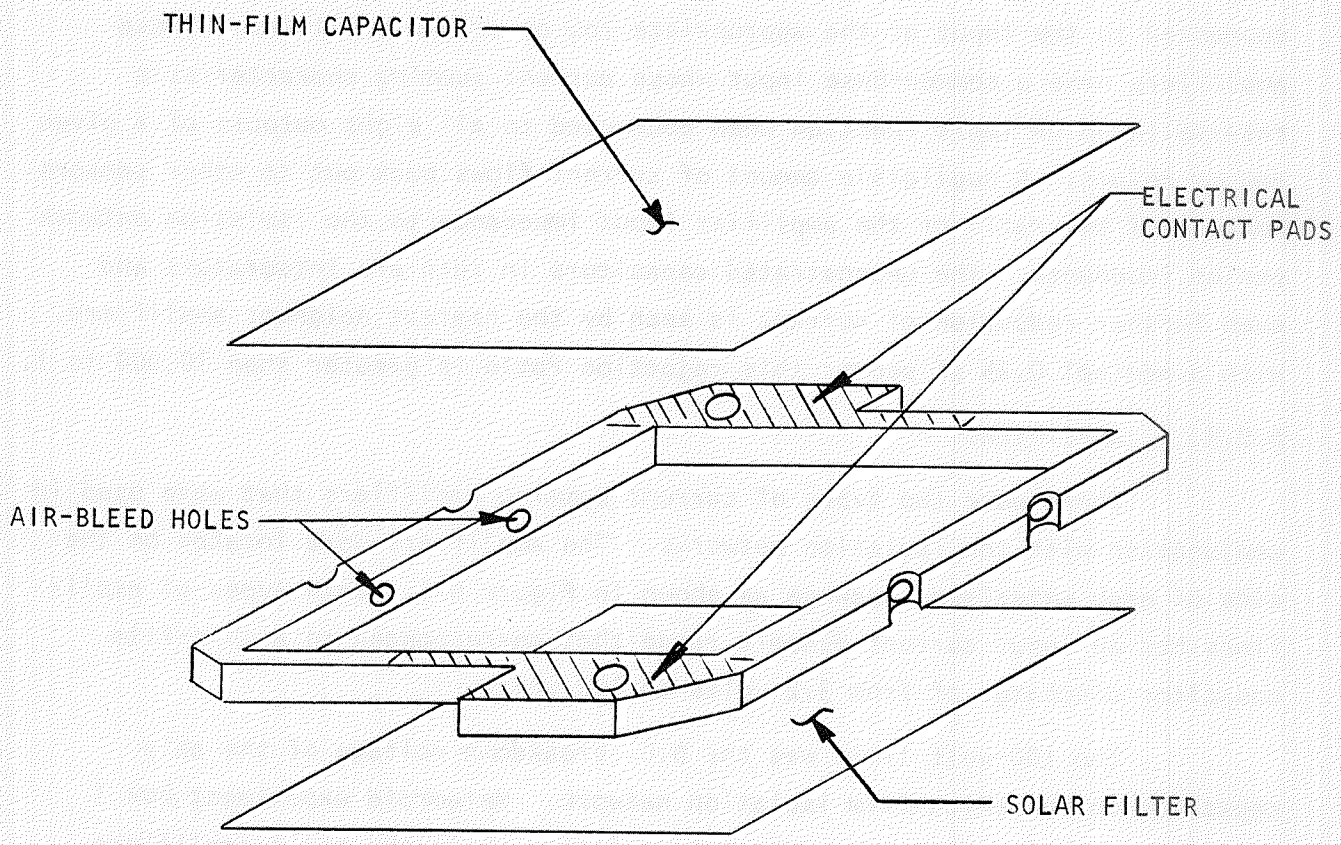


FIGURE 6-2 - THIN-FILM METEOROID SENSOR HAVING A SOLAR FILTER

6.2.2 ROW AND COLUMN ISOLATION

When a sensor is perforated by a micrometeoroid, the thin-film capacitor temporarily becomes a short circuit. The duration of the short is determined primarily by the amount of energy available to sustain the plasma conduction path between the two capacitor plates. Since the capacitor charging current is insufficient to sustain the plasma arc, the capacitor energy $1/2\ CV^2$ is the primary energy source. The current pulse that occurs after a micrometeoroid impact enters a thick-film isolation network that has two outputs that define the row and column, thus giving the X-Y location of the impacted sensor. Each row and column output of each isolation network is connected to the input of the appropriate row or column amplifier. These amplifiers have a common-base input whose current summing characteristic results in an OR logic function when connected to all eight outputs of a given row or column. A negligible amount of current flows back out to other sensors because of the ratio of the amplifier input impedance to the isolation network series impedance. The unpenetrated capacitors in turn are integrators and even further reduction of current is seen by the nearest neighbor amplifiers. With a nominal 0.25 μf sensor this rejection ratio is greater than 10,000 to 1.

6.2.3 AMPLIFIERS

There were two types of current summing amplifiers that were used in conjunction with the isolation networks. The amplifiers were located on the side of each experiment package as shown in Figure 6-1. Both types of amplifiers had an input-current dynamic range that corresponded to a thin-film capacitor discharge of from 3.2 volts to 100 volts.

The 100-volt limit was the D.C. breakdown voltage of the chip capacitor on the thick-film isolation network. Meteoroid experiment box 1 utilized a modular discrete-component amplifier while the box 2 amplifiers were thick-film hybrid microcircuits. Both amplifier types required ± 5 volts and the power dissipation was approximately 1.8 mw and 2.0 mw for each discrete component and each thick-film amplifier, respectively. Output characteristics were compatible with TTL logic.

6.2.4 DATA FORMATION AND ENCODING

A block diagram of the meteoroid experiment electronics is shown in Figure 6-3. The row, column, plane, and box identification of each capacitor

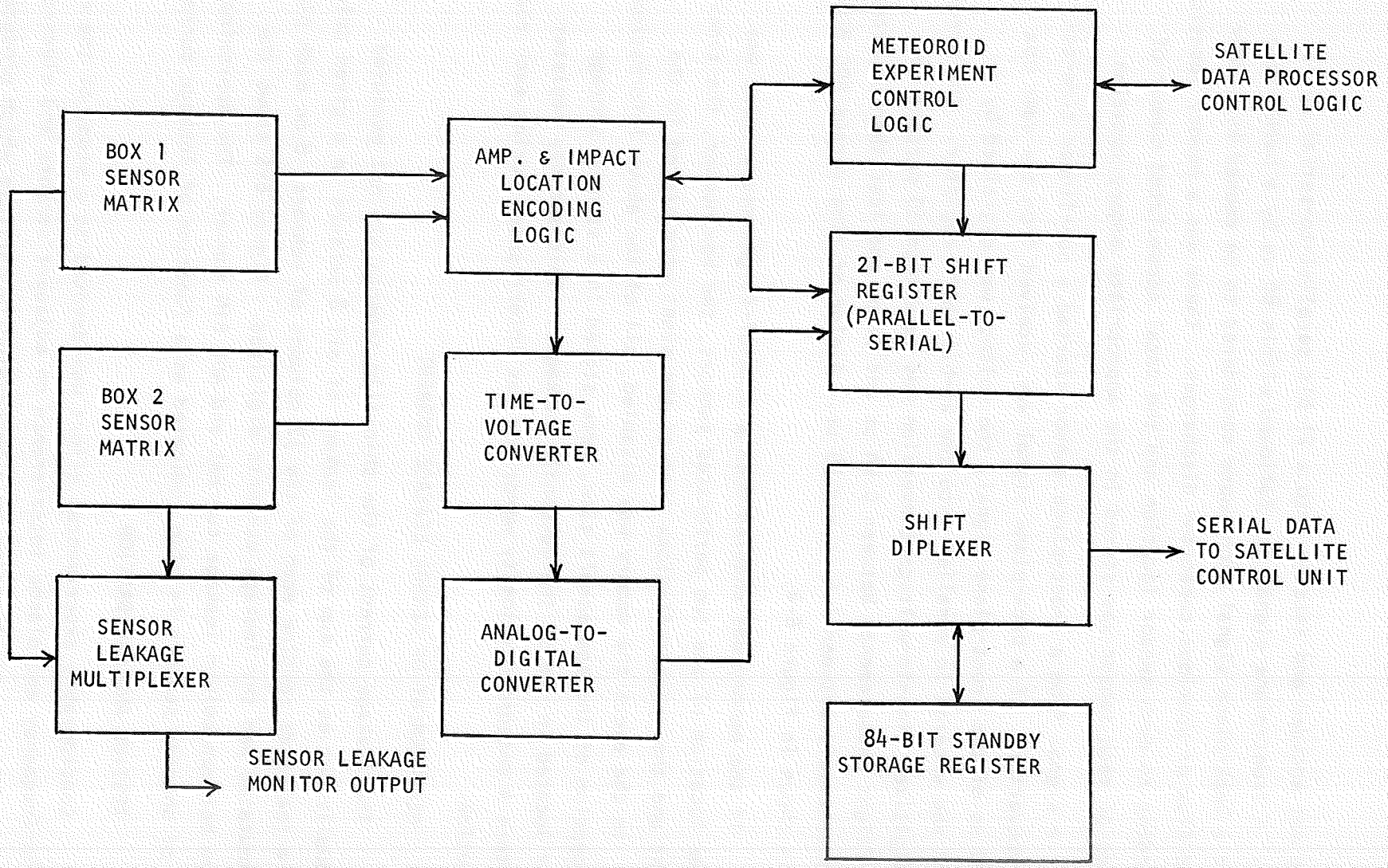


FIGURE 6-3 METEOROID EXPERIMENT ELECTRONICS

discharge was encoded and entered into a 21-bit parallel-to-serial shift register. A front-plane signal not followed within 80 μs by a back-plane signal or a back-plane signal alone were considered to be caused by either meteoroid flux or spurious capacitor discharges. There was a memory location corresponding to each sensor location and the total accumulated number of discharges of each sensor was stored in the appropriate memory location.

A signal from a front-plane sensor started a non-linear time-to-voltage converter. If a back-plane signal was received from the same box within 80 μs of the front-plane signal, the voltage was digitized by an 8-bit ADC and entered in parallel into the 21-bit shift register. The error in the digitized time-to-voltage conversion was less than 10 percent for time-of-flight measurements between 0.64 μs and 72 μs and less than 5 percent for time intervals between 1.6 μs and 59 μs. A plot of time versus ADC BIN number is shown in Figure 6-4.

If the memory was enabled when a time-of-flight measurement was made, the location of the two perforated sensors, the box number, the time-of-flight and the spacecraft-clock time of the event were stored in the memory. In the event the memory was disabled, all of the above information, with exception of the spacecraft time, were stored in a standby storage register located in one of the meteoroid packages. This standby register could store 4 meteoroid velocity words and was interrogated during each real-time routine.

6.2.5 MEASUREMENT OF SENSOR LEAKAGE CURRENT

The leakage current of the thin-film sensors was not measured individually but as the sum of the leakage of all 8 sensors in a given column. During a real-time routine each of the 32 columns of sensors, 8 on each plane, was commutated and the leakage currents digitized. Figure 6-5 shows the relation between column leakage current and ADC BIN number. The approximate number of shorted sensors is also indicated as a function of leakage current.

6.3 TESTING AND CALIBRATION

Considerable experimental effort was devoted to a study of the effects of radio-frequency and plasma interference on adjacent sensors and electronics when a given sensor was impacted by a hypervelocity particle which produced a

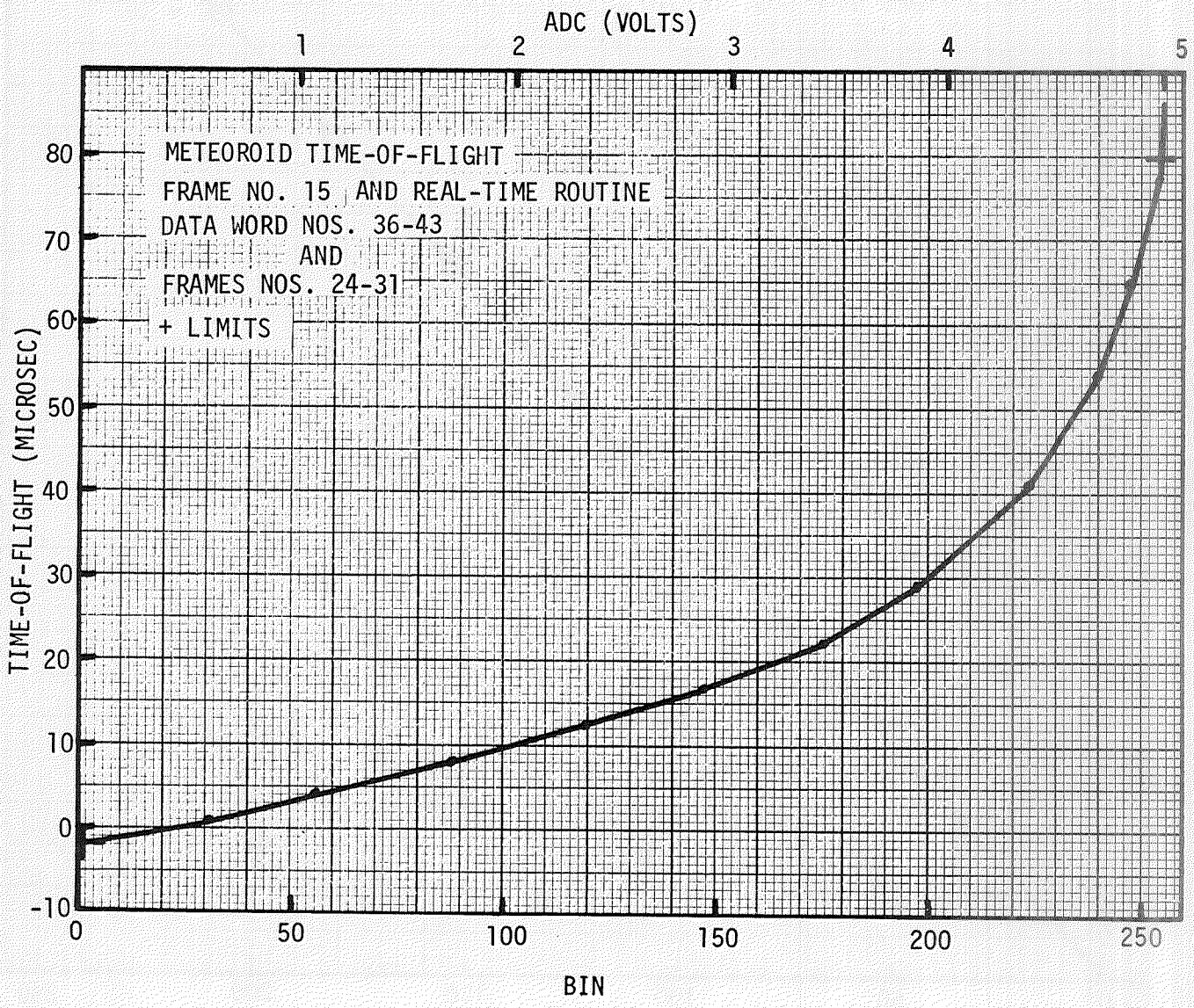


FIGURE 6-4 METEOROID TIME TO VOLTAGE CONVERSION

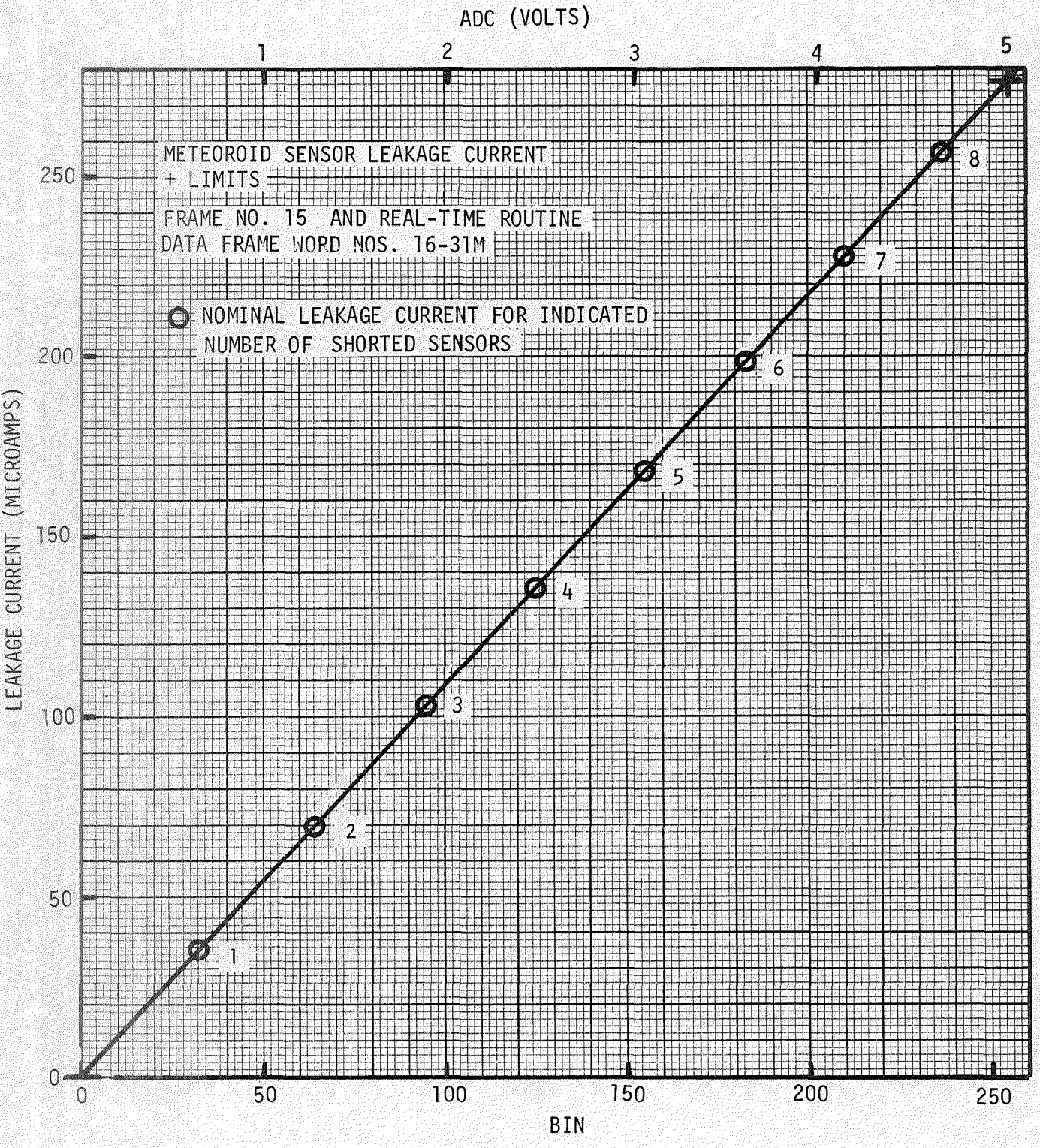


FIGURE 6-5 CONVERSION OF COLUMN LEAKAGE CURRENT TO ADC BIN NUMBER

breakdown in that sensor. Tests were conducted using a 2 x 2 sensor matrix to investigate the problem between nearest neighbors on a sensor plane and, with one sensor in front of the 2 x 2 matrix, to investigate the problem between one sensor plane and the other. Since impact breakdown may be simulated by raising the voltage on a sensor until its electrical breakdown potential is exceeded, early tests were made using this technique to acquire a large amount of data in a short time. These tests and subsequent tests involving hypervelocity particles indicated that with proper shielding the crosstalk and pick up would be insignificant.

In May and June of 1970 meteoroid impact testing of the RMS flight packages was performed at the Advanced Technology Center's Van de Graaff facility (data available in RMS Acceptance Data Package). Measurements were made using simulated meteoroids consisting of iron particles approximately 1 to 2 μm in diameter traveling at velocities of 3 to 6 km/sec. Data were taken for meteoroid impact angles of 90° (normal to the sensor), 47° and 32°. For particles of the size and velocity range given above, the velocity slow down caused by perforation of the outer sensor ranged from approximately 15 to 20% with an average of 17% for normal incidence. For an impacting angle of 47° from the normal the velocity decrease varied from 20 to 32% with an average of 25%. For an angle of 32° from the normal the velocity slow down was from 24 to 47% with an average of 36%. All of the above tests were conducted with sensors having solar reflectors without a coating of silicon oxide.

While the meteoroid impact acceptance tests were being conducted on the RMS flight packages it was found that on four of sixty-eight impacts the location of one of the two perforated sensors was stored incorrectly. This was found to be due to the fact that during the initial impact testing, sensors were not placed at all matrix locations. The uncovered sensor contact pads acted as pickup points for the plasma produced by a meteoroid impact, resulting in an occasional erroneous impact location. Additional testing in which all contact pads were covered by either a sensor or by a sensor frame produced no erroneous locations.

During the spacecraft solar/vacuum tests conducted in June 1970 at NASA MSC it became apparent that the probability of survival of the thin-film solar reflectors during a deep-space mission was at best marginal.

A subsequent testing program[9] carried out in the Radiometry Research Simulator Laboratory at the Goddard Space Flight Center in July 1970 showed that a coating of silicon oxide deposited on either the capacitor (without reflector) or on the reflector reduced thin-film heating to an acceptable level. For this reason all outer-plane sensors, with the exception of 8 sensors, were coated with a layer of vapor deposited silicon oxide. It was felt that due to the spinning motion of the spacecraft any direct solar illumination of inner-plane sensors through holes or tears in damaged outer-plane sensors would be of a duration too short to damage the inner-plane sensors.

Simulated meteoroid impact testing at Advanced Technology Center on sensors having silicon oxide on either the reflector or on the capacitor proved sensors having this thermal control coating to be acceptable for the RMS mission. Although the additional mass of the silicon oxide resulted in a several percent increase in the meteoroid velocity decrease, the sensors still detected simulated meteoroids and were usable for measuring velocities of simulated meteoroids of the size and velocity range, given above, that are available from the LTV Van de Graaff. It was anticipated that the particle slowdown would decrease as the meteoroid mass increased.

With the exception of the simulated-meteoroid impact testing on the individual flight packages, all electronic checkout and calibration were carried out with electronic pulses applied at the sensor inputs on the sensor matrix. This allowed a thorough checkout of each package and the interface with the main satellite data processor. These tests demonstrated that the meteoroid detector electronics were capable of accurately measuring meteoroid velocities extending over a range of 2 km/s to above 100 km/s. The lower limit of 2 km/s is believed to be the low-velocity limit for meteoroid detectability by the thin-film sensors.

6.4 PRELAUNCH OPERATIONS

The RMS flight meteoroid packages were delivered along with the rest of the spacecraft to Wallops Island in early July 1970. A complete set of thin-film capacitor sensors were installed 28 July 1970 prior to spin balance. Of the thin-film sensors that were installed approximately one-half of the outer-plane sensors were of the type that had silicon oxide deposited directly

onto the thin-film capacitor. All remaining outer-plane sensors with exception of the eight control sensors had a thin-film solar reflector that had a coating of vapor-deposited silicon oxide. During spin balance approximately one-third of the outer-plane sensors suffered some damage that varied from small tears in the capacitor or in the reflector to very severe damage for a few cases. Most of the damaged sensors were of the type having silicon oxide deposited directly onto the capacitor.

Although a large number of the sensors were broken due to handling, the precise reason for many losses is not known. It is possible that the losses were due to air turbulence caused by the spinning spacecraft during spin balance. However, previous tests at Vought Missiles and Space Company in which sensors were installed on the RMS mass model had resulted in no damage to the sensors during spin up. It should be pointed out that during the LTV MSD tests the RMS spacecraft was attached to neither the Scout fourth stage nor the OFO spacecraft.

Prior to each launch attempt the meteoroid packages were examined and all defective sensors were replaced. After each aborted launch attempt the packages were removed from the spacecraft and stored at either Wallops Island or Advanced Technology Center, depending on the time interval before the next scheduled launch. Due to the fragility of the sensors and the high humidity at Wallops Island it was felt that the sensors should be left there as little as possible. It was observed that there was a significantly higher loss rate of sensors, due to shorting, while at Wallops Island than while at Advanced Technology Center. The loss rate for sensors stored at Advanced Technology Center was essentially zero with only an occasional sensor failure being observed.

A final check of the meteoroid packages was made on 7 November 1970 and the packages were then installed on the spacecraft. All shorted or broken sensors were replaced. The following variety of sensor types were mounted. The front-plane sensors on box 1 consisted of only one type, capacitors with an oxide-coated aluminized sun shield. The front plane sensors of box 2 consisted of one column of 8 oxide-coated capacitors, one column of 8 capacitors having an aluminized single-film sun shield, five columns of 40 capacitors having an oxide-coated aluminized laminated sun shield and one column of 4 each of 2 types of control sensors. Four of the control sensors were capacitors having

a 5-mil metal covering that were for the purpose of measuring spurious capacitor discharges. The other four control sensors simulated thin-film meteoroid sensors in all ways with the exception that they were shorted. These sensors were so designed that if they were broken during launch or by the near-earth space environment the probability was high that the shorts would open which would cause a decrease in the measured leakage current. Since the electrical contacts for the shorted sensors were identical to those for the meteoroid sensors it was felt that these control sensors would also give additional information relating to the reliability of the contact techniques used in the assembly and installation of the thin-film sensors.

The leakage current of the sensor columns and spurious sensor discharges were monitored during the launch countdown that began on 8 November 1970. Final pre-launch measurements were made at T-50 minutes. At this time there was one short indicated on the front plane, column 3 of box 1 and one short on the back plane, column 3 of box 2 in addition to the 4 control shorts on the front plane, column 6 of box 2. There were no sensor discharges stored in the memory. The meteoroid packages were then turned off and the memory cleared.

6.5 ORBITAL OPERATIONS AND DATA ACQUISITION

The meteoroid packages were not turned on until the fifteenth orbit. The first sensor-plane temperature measurements were made during orbit 3. At the time of this measurement the spacecraft, during this orbit,had been in the sun for approximately 41 minutes. The outer-plane temperature was 67°F and the inner-plane temperature was 68°F. During the first 8 to 10 days in orbit, the measured outer-plane temperatures fluctuated fairly consistently between approximately -2°F and 60°F and the inner-plane temperature fluctuated between 22°F and 55°F. After approximately two weeks the spacecraft rotation resolved into a tumble about an axis perpendicular to the long axis of the spacecraft. The RMS spacecraft stayed in this rotational configuration for the remainder of its lifetime. During the time in which RMS was in this flat spin only one side of the spacecraft was illuminated by the sun. Temperature measurements indicated that meteoroid detector box 1 was on the dark side of the spacecraft and box 2 was on the side that faced the sun. During this period the temperature of the outer-plane of box 1 varied between -21°F and 27°F and the inner plane of box 2 varied between 28°F and 75°F.

The first meteoroid sensor leakage current measurements were made when the detectors were turned on during the fifteenth orbit. The leakage currents measured at this time indicated that there were 7 sensors on the front plane and 2 on the back plane of box 1 that were shorted. There were 14 sensors that indicated shorts on the front plane and none on the back plane of box 2. Of the 14 shorts, 3 were in the column where the four control shorts were located indicating that one of the control sensors had been severely damaged. Also the pre-launch short of the back plane of box 2 had opened.

The meteoroid boxes were left on and the leakage currents were measured on almost every orbit. There was a gradual increase in the number of shorted sensors on each of the front planes and one additional sensor shorted on the back plane of box 2. During orbit 23, the memory was turned on so that the number of sensor discharges could be stored. The memory dump during orbit 24 indicated that two front-plane sensors on box 2 were very noisy, one having over 7000 discharges and the other over 500. The remainder of the front plane sensors were fairly quiet with a total of 29 discharges from 10 sensors. The back planes had a total of 11 discharges from 3 sensors. The number of front-plane shorts increased to 12 and 18 for box 1 and box 2, respectively. No additional back plane sensors were observed to be shorted.

A memory dump during orbit 33 contained capacitor-count data for four orbits. The back planes of both packages showed a total increase of two counts since the memory dump during orbit 24. Five sensors on the front plane of box 2 and four on the front plane of box 1 had more than ten counts. Eighteen of the 128 front-plane sensors had at least one count. There was an increase of two shorts on each of the two front planes with no change in the number of back-plane shorts.

Meteoroid box 2 was turned off during orbit 32 because of excessive power drain caused by repeated memory cycling by one very noisy sensor. Both box 1 and the memory were left on.

During orbit 90, box 2 was turned on. Since orbit 31 the number of front-plane shorts on box 1 had increased by 7 to 21 and for box 2 by 4 to 24. The number of back-plane shorts remained at three with two on box 1 and one on box 2. Although the number of shorted sensors seemed to still be increasing, the loss rate seemed to be decreasing.

The memory dump for orbit 91 on 15 November 1970 showed that more than ten pulses had been stored for each of 24 front-plane sensors and 43 sensors had produced at least one signal. Only one back-plane sensor had recorded more than ten pulses and 23 had produced at least one pulse during the periods that the memory was on.

The memory and box 1 were left on for most of the time until orbit 145 to allow storage of data from box 1. During orbit 145 the memory was turned off and box 2 turned on until Orbit 231 when both detectors were turned off to allow radiation runs to be made. Both box 1 and box 2 were on for orbits 261 through 443. Since the sensor bias voltage was beginning to drop due to current limiting by the sensor bias voltage regulator, the decision was made to turn off box 2 during orbit 443. For orbits 444 through 931 box 1 was on for all but a few orbits. The memory was also on for approximately 15 orbits during this period.

Due to the apparent failure of one cell in the battery pack the meteoroid packages could be operated only while the spacecraft was in the sun after orbit 931. As a result of this failure the only meaningful data that could be obtained from the meteoroid detectors wasinformation concerning the shorting of additional sensors. Since the primary objective of the experiment was to determine the lifetime characteristics of the thin film sensors in the space environment and since shorting of the sensors is the principal mode of failure, during the remainder of the satellite lifetime the meteoroid detectors were periodically turned on and the sensor leakage currents telemetered to the ground.

During each of two meteor showers a meteoroid velocity measurement was made. Since the memory was not on, the two velocity words were stored in the meteoroid experiment's standby-storage registers and transmitted to the ground during the next real-time data transmission. This real-time routine was run on a daily basis which means that the time at which the velocity measurement was made is known within a given one-day data taking period. After each velocity measurement the memory was turned on for one orbit to observe count-rate of the two perforated sensors. This was done to rule out the possibility that either velocity measurement was the result of a chance coincidence of pulses from two extremely noisy sensors. Each of the four

sensors involved in the two velocity measurements were found to be very quiet with no sensor discharges being stored during time in which the memory was on following each velocity measurement. An in orbit calibration check of the ability of the meteoroid time-of-flight measurement system to accurately digitize an essentially zero time interval was also performed after each time-of-flight measurement. In both instances this check showed the time-of-flight measurement system to be functioning properly.

6.6 PRELIMINARY DATA ANALYSIS

6.6.1 SENSOR LIFETIME

The meteoroid boxes were first turned on during orbit 15 and the sensor leakage currents were monitored periodically throughout the lifetime of the spacecraft. These measurements were made on an individual column basis for each of the 32 columns of eight sensors. Figures 6-6, 6-7, 6-8, and 6-9, show the time history of the total sensor-leakage current of each of the four sensor planes. The leakage current for each plane is arrived at by summing the leakage currents of the 8 columns of sensors on that plane. The approximate percentage of shorted sensors is also indicated on these figures.

The initial loss rate of outer plane sensors was very high; however, by orbit 200 the loss rate due to shorting had significantly decreased. By orbit 300 the number of shorted outer plane sensors had become relatively constant and remained so throughout the satellite's lifetime for box 2. The number of outer-plane shorts on box 1 also remained constant after orbit 300 with the exception of the sudden increase of seven shorts that occurred in the data period between orbits 694 and 710. It is probable that these shorts were caused by meteoroid impacts. The second of the two meteoroid velocity measurements was also made during this data period. This coincides with a period of known high meteoric activity due to the Ursids meteoroid stream.

It is believed that the initial high loss rate of outer-plane sensors was the result of damage to the sensors' solar reflectors due to the launch environment. Since the sensors had survived simulation of all launch phases with the exception of heat-shield ejection which could not be accurately simulated, it is possible that this damage occurred when the heat-shield was ejected.

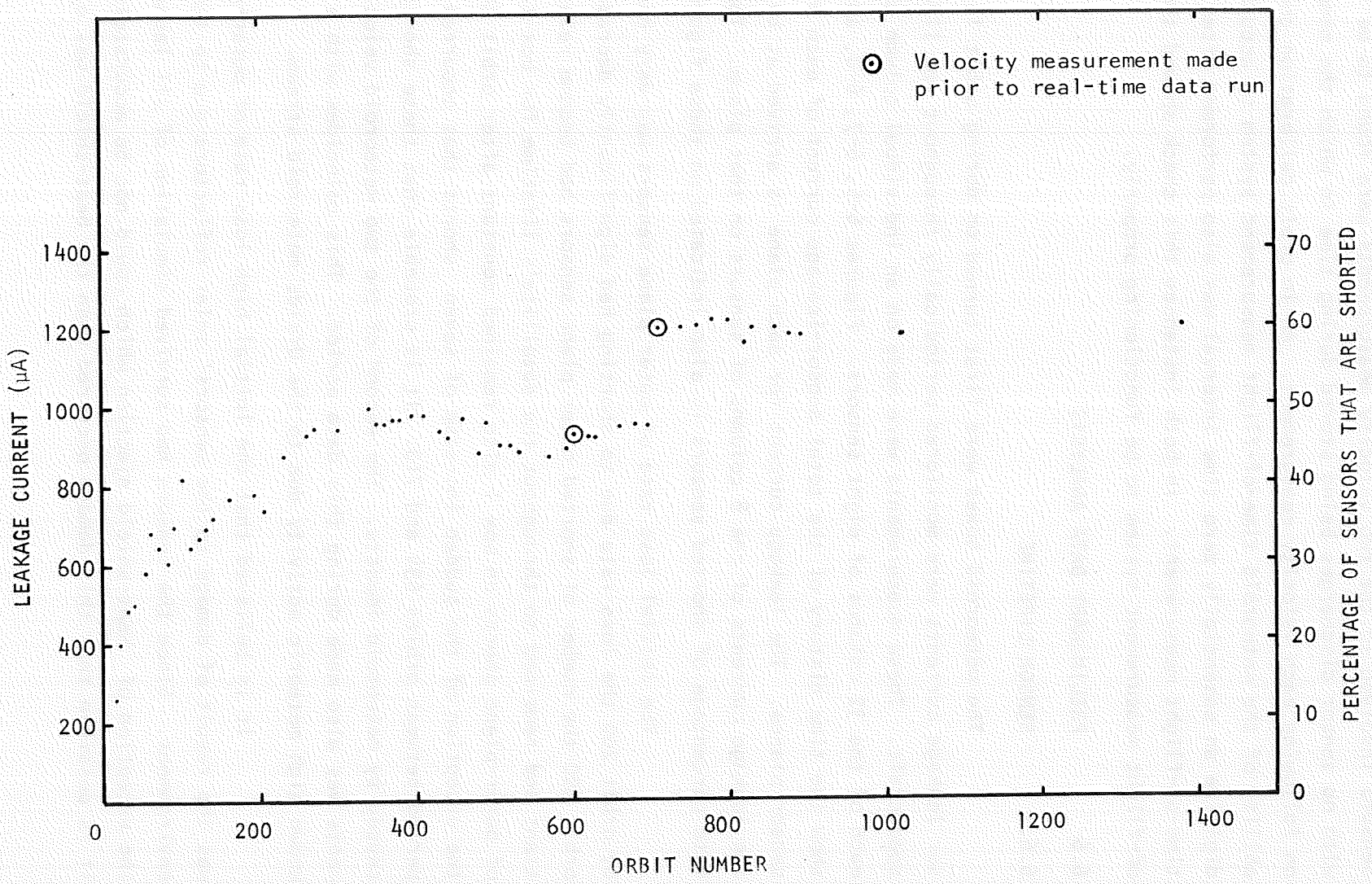


FIGURE 6-6- LEAKAGE CURRENT FOR THE OUTER PLANE OF METEOROID DETECTOR BOX 1

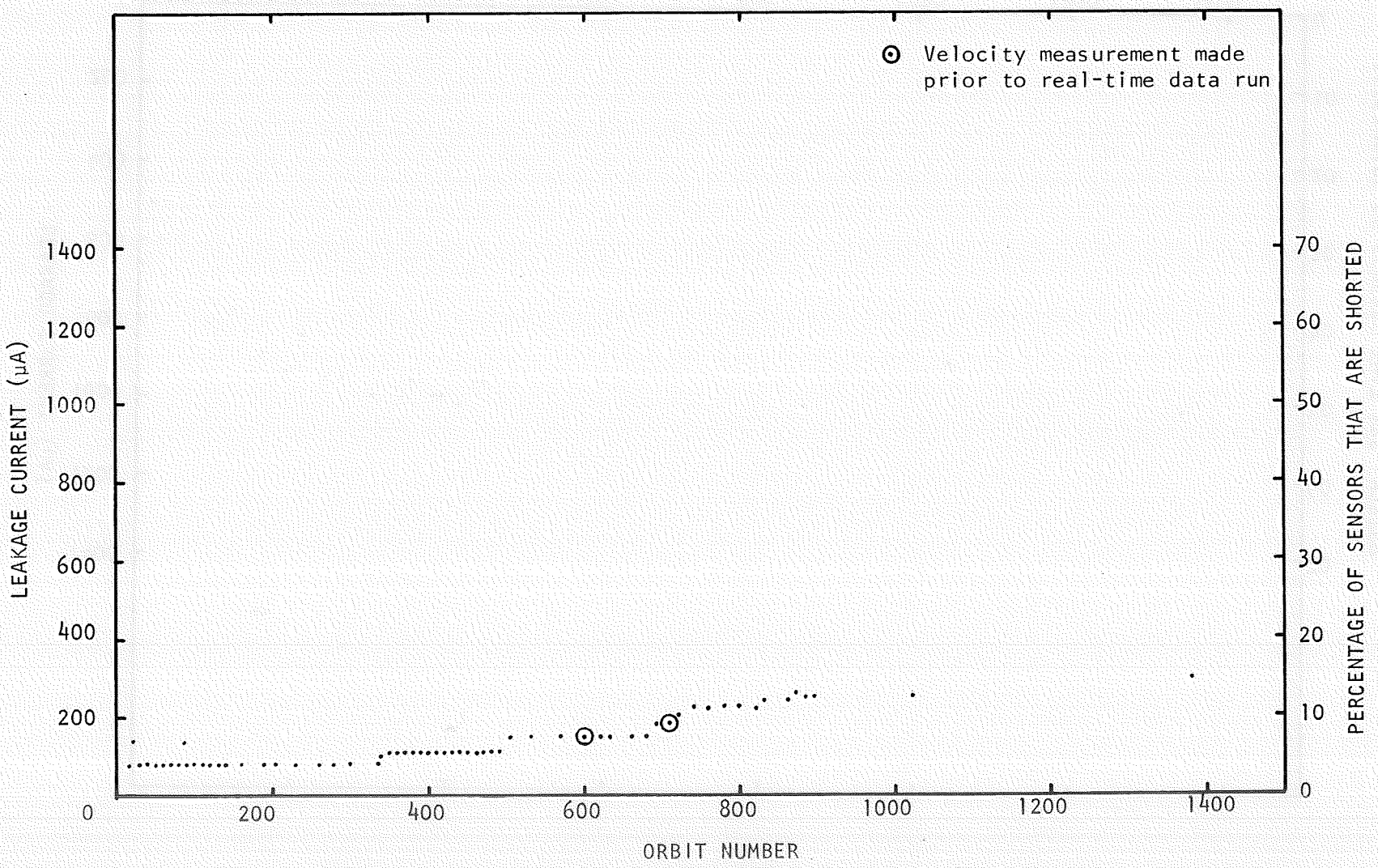


FIGURE 6-7 - LEAKAGE CURRENT FOR THE INNER PLANE OF METEOROID DETECTOR BOX 1

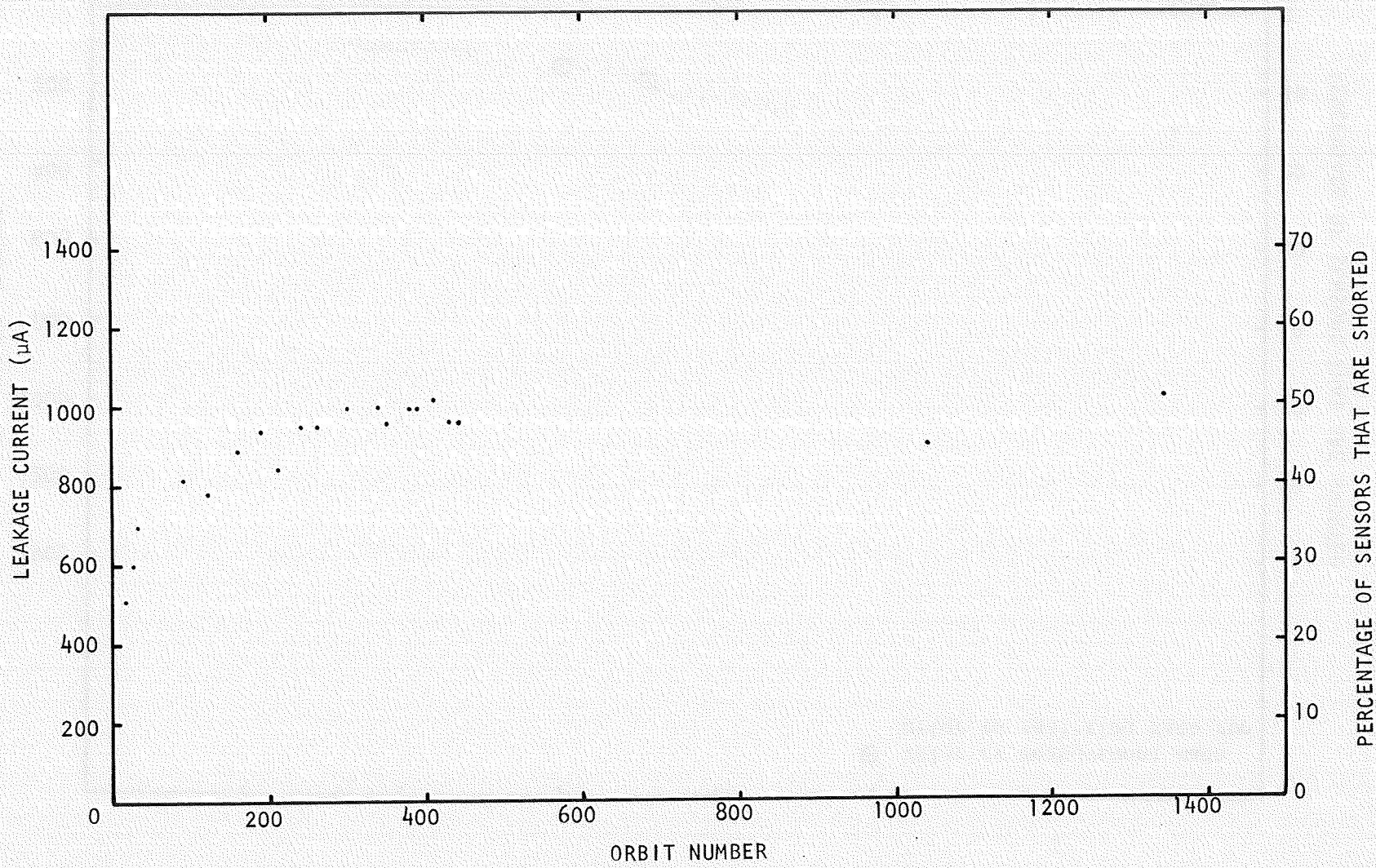


FIGURE 6-8 - LEAKAGE CURRENT FOR THE OUTER PLANE OF METEOROID DETECTOR BOX 2

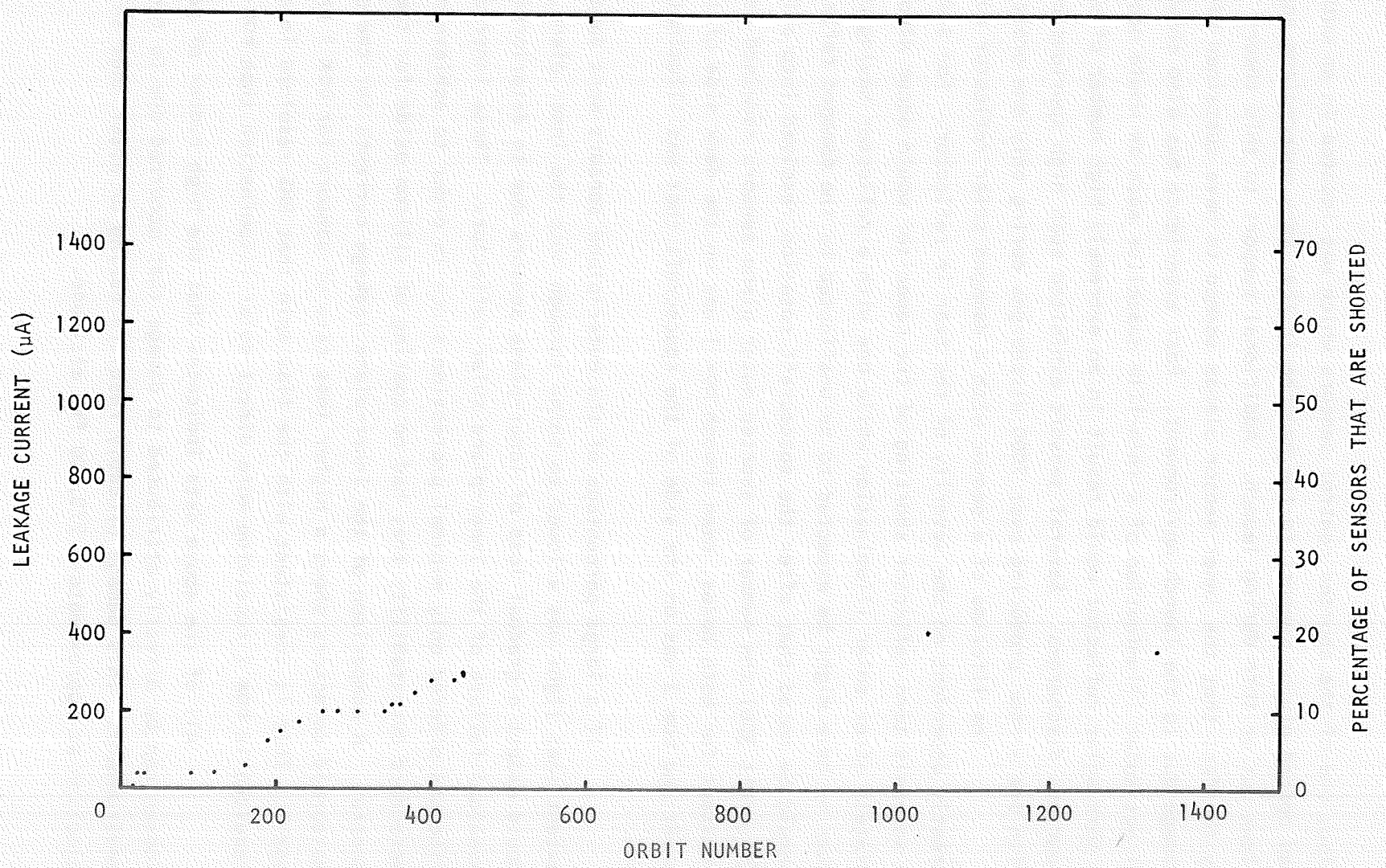


FIGURE 6-9 - LEAKAGE CURRENT FOR THE INNER PLANE OF METEOROID DETECTOR BOX 2

Also, one of the shorted control sensors which was located in an outer plane had opened giving support to the hypothesis that many outer-plane sensors were blown out or torn during launch. Additional support to this theory is given by the fact that the inner sensor planes seemed to have sustained minimal damage due to the launch environment. Past experience has also shown that direct solar illumination of a thin-film capacitor such as would occur through a torn solar reflector would result in an extremely high number of sensor spurious discharges. Several sensors exhibited such high spurious count rates with one sensor producing over 7000 discharges during only one orbit.

The lifetime of a sensor with a damaged solar reflector would be greatly dependent on the severity of the tear in reflector. For a sensor with a severely torn reflector shorting of the capacitor would occur almost immediately after solar illumination while one with a reflector having only a slight tear or hole might be expected to be unaffected by the damaged reflector. It should be noted that after the spacecraft rotation resolved into a flat spin (by orbit 300) the number of shorted outer plane sensors remained essentially constant for both boxes, even though box 1 was on the dark side of the spacecraft and box 2 was on the side of the spacecraft that was illuminated by the sun.

If a large percentage of the outer-plane sensors were damaged to the extent that light was allowed to shine through onto the inner plane, one would expect a gradual loss of inner-plane sensors due to deterioration and eventual failure of the inner-plane solar reflectors. These inner-plane reflectors offered only minimal protection since in order to achieve maximum meteoroid detectability they had no coating of silicon oxide for thermal control. A comparison of the inner-plane leakage currents for the two meteoroid detectors shows a higher loss rate of sensors for box 2 than for box 1. This is consistent with the flat spin that RMS resolved into which resulted in box 2 receiving more direct solar illumination than box 1.

All of the above data indicates that the high number of sensor losses can be directly attributed to damage that occurred due to the launch environment. This damage probably resulted during or after heat shield ejection at approximately 270,000 ft. altitude.

6.6.2 METEOROID VELOCITY MEASUREMENTS

Two meteoroid velocity measurements were made during the RMS's lifetime. The first measurement occurred during the data period that ended on 17 December 1970. This measurement may possibly be related to the Geminids meteoroid shower that peaked on 14 December 1970. The meteoroid time-of-flight between the two sensor planes of box 1 was measured to be 28.5μs which resulted in a velocity of 3.3 km/s if perforation is assumed to be through the centers of the two sensors involved. Due to the uncertainty in the exact perforation point on each sensor element the velocity may have been as low as 3.0 km/s or as high as 3.9 km/s. The two sensor elements involved were at location 5,1 on the outer plane and location 7,1 on the inner plane.

The second meteoroid velocity measurement was made during the data period that ended on 24 December 1970. The Ursids meteor shower occurred on 22 December 1970. A time-of-flight of 34.7μs was recorded as the meteoroid transit time between the two sensor planes. The two sensor elements that were perforated were located on box 1 at 0,4 on the outer plane and 2,3 on the inner plane. A velocity of 2.8 km/s results if one assumes the meteoroid trajectory to have been from sensor center to sensor center; however, due to geometrical uncertainty the velocity may have been as low as 2.5 km/s or as high as 3.3 km/s.

The memory was not enabled which prevented storage of the exact event time when either of the meteoroid velocity measurements were made. The velocity words were stored in the meteoroid standby-storage register.

There are at least two plausible explanations as to why the two meteoroid velocities were as low as they were. The first possibility is that the meteoroid velocity measurements were due to detection of lunar ejecta caused by the primary meteoroid shower. If one assumes the particles to have initial velocities slightly greater than lunar-escape velocities then the particles would be expected to arrive in the near-earth vicinity at velocities that are very close to 11 km/s. The orbital velocity of the Radiation and Meteoroid Satellite was approximately 8 km/s. Therefore, it is possible that the particles caught up with RMS which would result in a relative measured velocity of approximately 3 km/s. Additional support is given to this theory

by the fact that in both instances the velocity measurements were made approximately two days after the peak of the primary meteoroid shower. This two day delay agrees well with the expected transit time of a particle traversing the distance between the moon and earth.

A second possibility is that the detected meteoroids were very small primary meteoroids (10^{-14} g or less) having initial velocities of approximately 35 km/s that were slowed down by the outer plane sensors. Such a possibility has very interesting implications in that such very small primary meteoroids would have to be of fairly recent origin. Therefore if it can indeed be shown that these detected meteoroids were very small primaries, additional information will be gained that can be related to theories concerning the generation of such particles.

On 31 December 1970 in orbit 812 the satellite memory was enabled to allow storage of the event time for any velocity measurements that might be made during the Quadrantids meteoroid shower that was anticipated to be active from the first through the fourth of January. On January 2, the satellite power system automatically turned off all experiments and switched to a minimum-power condition. This was due to low battery voltage that apparently resulted from the failure of a battery cell. During this period no velocity measurements were made. Meteoroid detector box 1 was again enabled on January 3 and remained on through January 5 until another power shutdown occurred.

6.6.3 MEASUREMENT OF METEOROID FLUX

Upon consideration of the time periods in which the meteoroid detectors were turned on and the approximate number of good sensors one arrives at a time-area product of approximately 10 to 15 ft^2-days for the outer sensor planes and 20 to 25 ft^2-days for the inner planes. Sixty-two percent of the outer-plane sensors and 28 percent of the inner plane sensors had produced at least one discharge signal. However, most of these discharges occurred in the first two weeks of satellite operation. During this initial two week period the percentage of sensors showing counts were essentially the same for box 1 and box 2 even though the time data were taken with box 1 was approximately ten times that for box 2. Therefore, it can probably be assumed that

most of these early counts were due to spurious breakdowns. By removing these early counts and then examining statistically the rate at which counts occurred one should be able to detect periods of high meteoroid flux and even set a reasonably accurate upper limit on the observed meteoroid flux. The ratio between counts on outer-plane and inner-plane sensors will also be of importance in the determination of this flux and the percentage of meteoroids that are less than 10^{-12} grams.

The sudden increase in leakage current on the outer plane of box 1, as can be seen in Figure 6-6, can with a high degree of confidence be attributed directly to meteoroid flux. There were seven additional shorts observed in the data period prior to orbit 710 after a long period in which very few new shorts were observed. Laboratory testing of thin-film sensors with simulated meteoroids has shown that a short often forms due to perforation by extremely small meteoroids that are either completely or almost stopped by the impact with the sensor. The fact that such an increase was not seen on box 2 may be due to a meteoroid stream trajectory that had a velocity component in the direction of the sun. Due to the RMS rotational motion, box 1 looked away from the sun and box 2 toward the sun.

6.7 CONCLUSIONS

In spite of an early loss of a sizeable number of individual sensors due to the effects of wind blast at heat shield ejection, all the objectives of the meteoroid experiment were met. The measurements on RMS successfully demonstrated that thin film capacitor type meteoroid sensors can be flown in the space environment, survive the launch and measure meteoroid flux and velocity.

7.0 SPACECRAFT

7.1 STRUCTURE

The RMS payload consisted of two assemblies which were electrically connected but structurally independent of each other. The upper assembly was a multiple bracket system supported from the Scout "E" Section. The bottom member of this structure was a ring which slipped over "E" Section and was bolted down on top of the "E" Section lower flange using longer versions of the bolts that normally hold down "E" Section. The top member of this same assembly was another ring that fastened to conical angles riveted to "E" Section. The basic structural concept is illustrated in Figure 7-1. All components either fastened ring-to-ring or to longerons that fastened ring-to-ring. Figure 7-1 also illustrates the lower assembly, which supports the cylindrical solar cell array from the upper flange of the FW-4S Scout fourth stage motor. Sheet metal clips (not illustrated) were bolted to the captive nuts in the FW-4S and riveted to the solar cell support ring. These clips held the ring down on the FW-4S shoulder and prevented the ring from rotating. Figures 7-2 and 7-3 illustrate the structural modifications that were required to the Scout "E" Section to add the RMS auxiliary payload. Figure 7-4 illustrates the arrangement of RMS components around "E" Section. This arrangement was dictated by several constraints related to Scout launch vehicle needs and by "field-of-view" requirements for the experiments. First, the payload was required to stay within the 30" dia. envelope dictated by Scout Heat Shield clearance requirements. Second, access had to be provided for "E" Section motor ignition and payload separation system servicing. Specifically, it had to be possible to remove either ignition battery with the RMS payload installed, to remove the squib access door, and to insert fourth-stage motor squibs or to replace timers or relays. Also clearance had to be provided for the departing umbilical connectors during launch. In addition, the Scout Heat Shield bumper, which in this case rested on the solar cell support ring, had to have clearance during separation.

It is evident from Figure 7-4 that all components were within the 30" clearance envelope. The ignition battery on the lower left hand side could be removed up through the RMS upper ring, however, the RMS electronic memory had to be temporarily removed to gain access to the tie down screws. The ignition

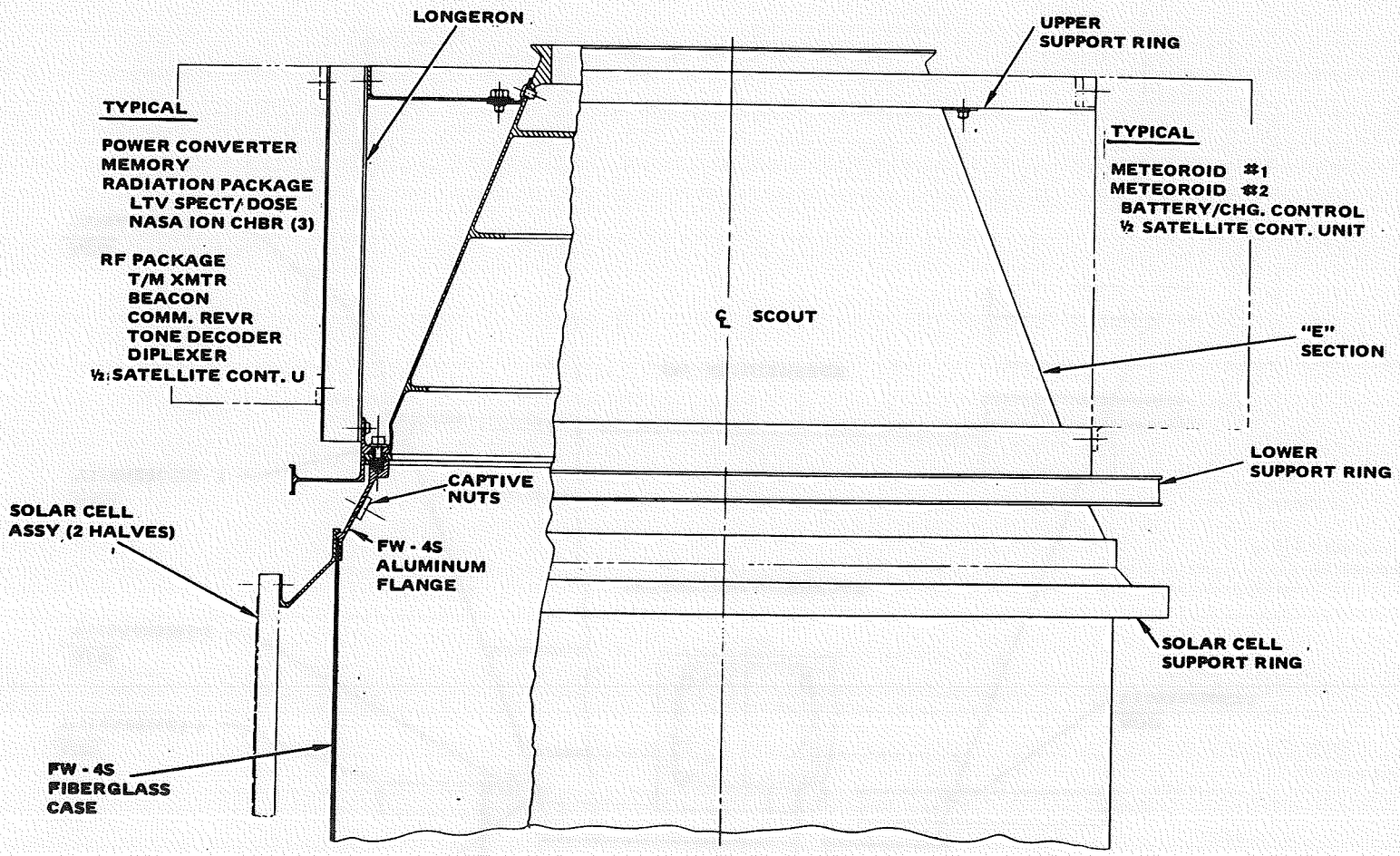


FIGURE 7-1 FW - 4S SCOUT INTERFACE

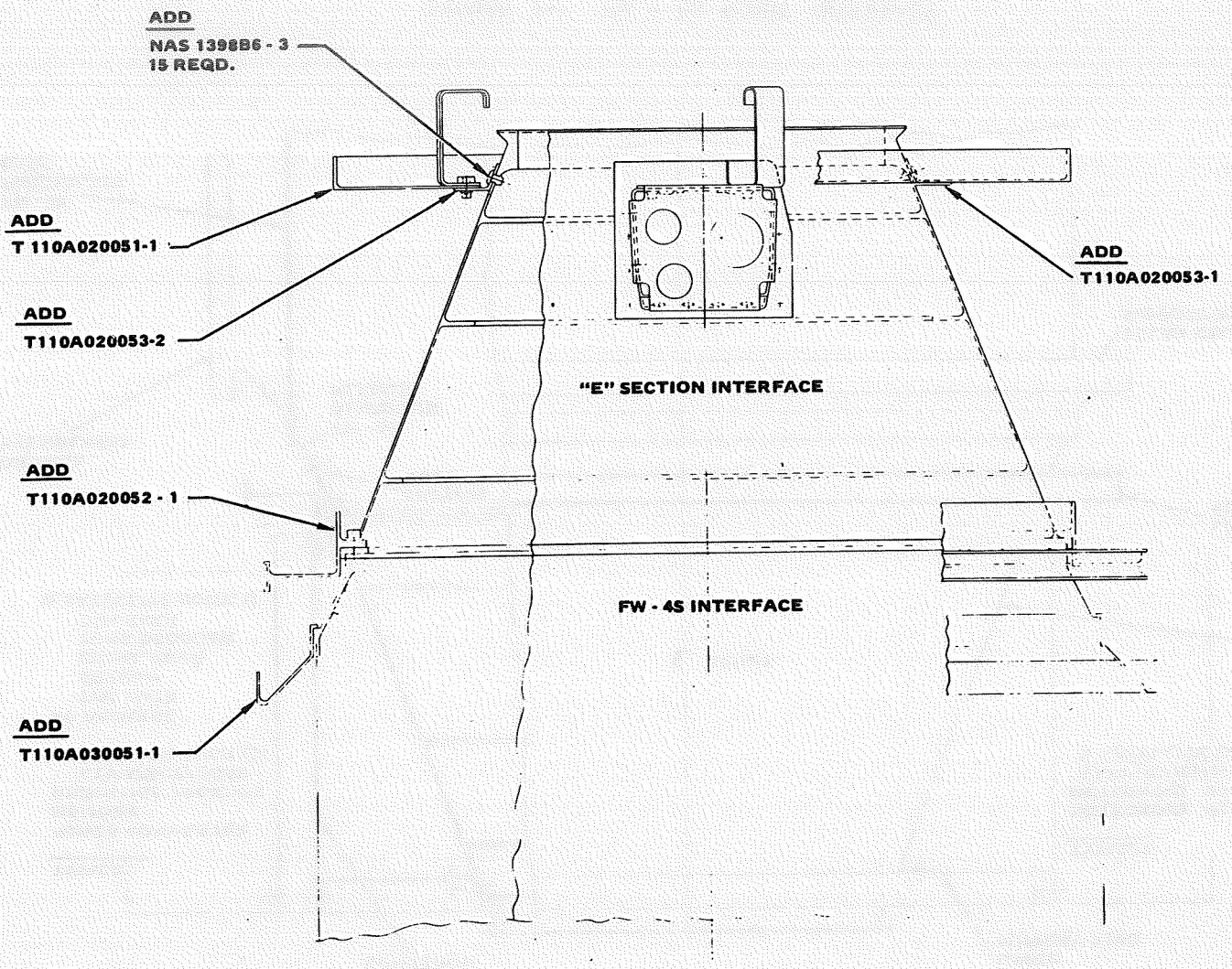


FIGURE 7-2 RMS STRUCTURAL ARRANGEMENT

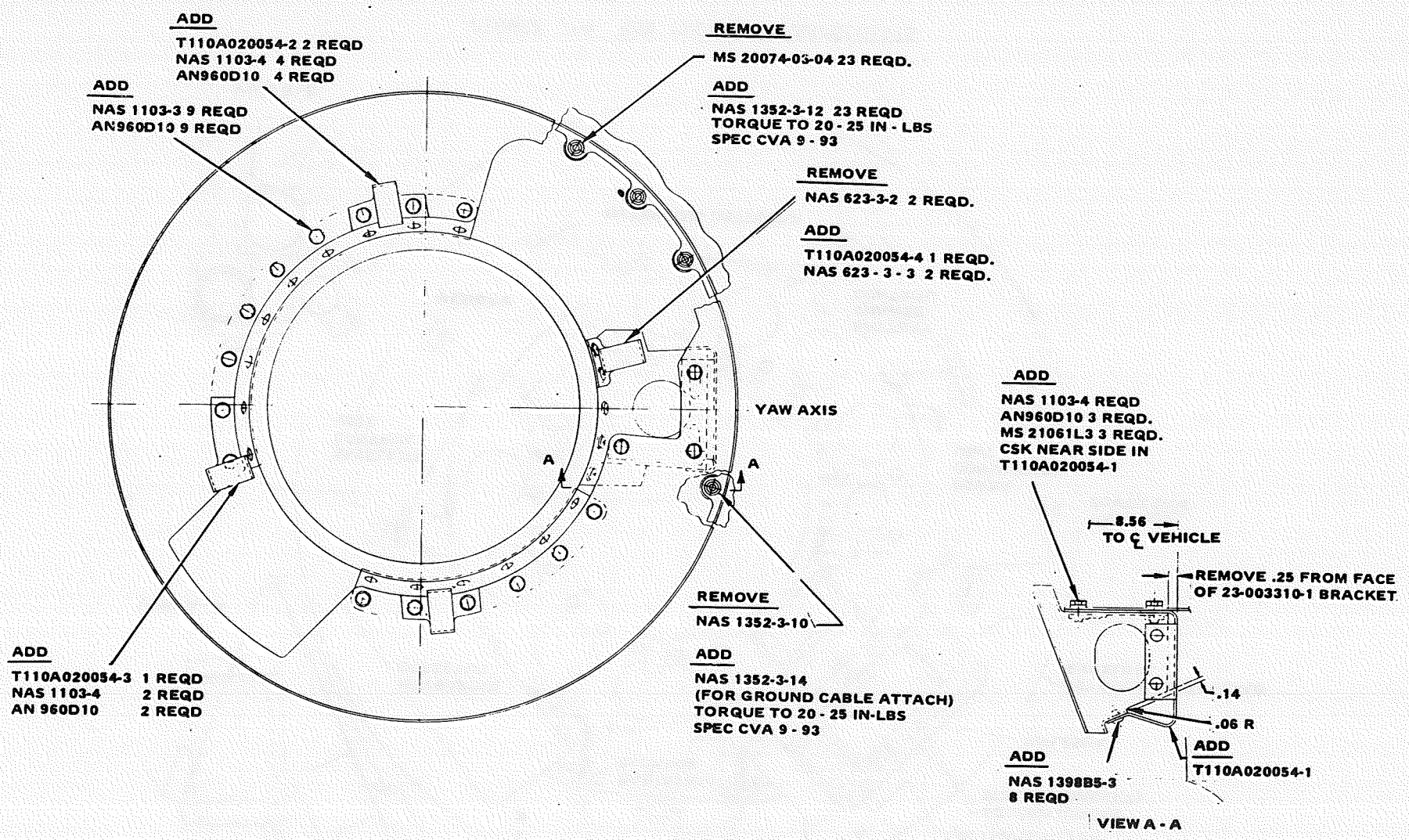


FIGURE 7-3 "E" SECTION MODIFICATIONS

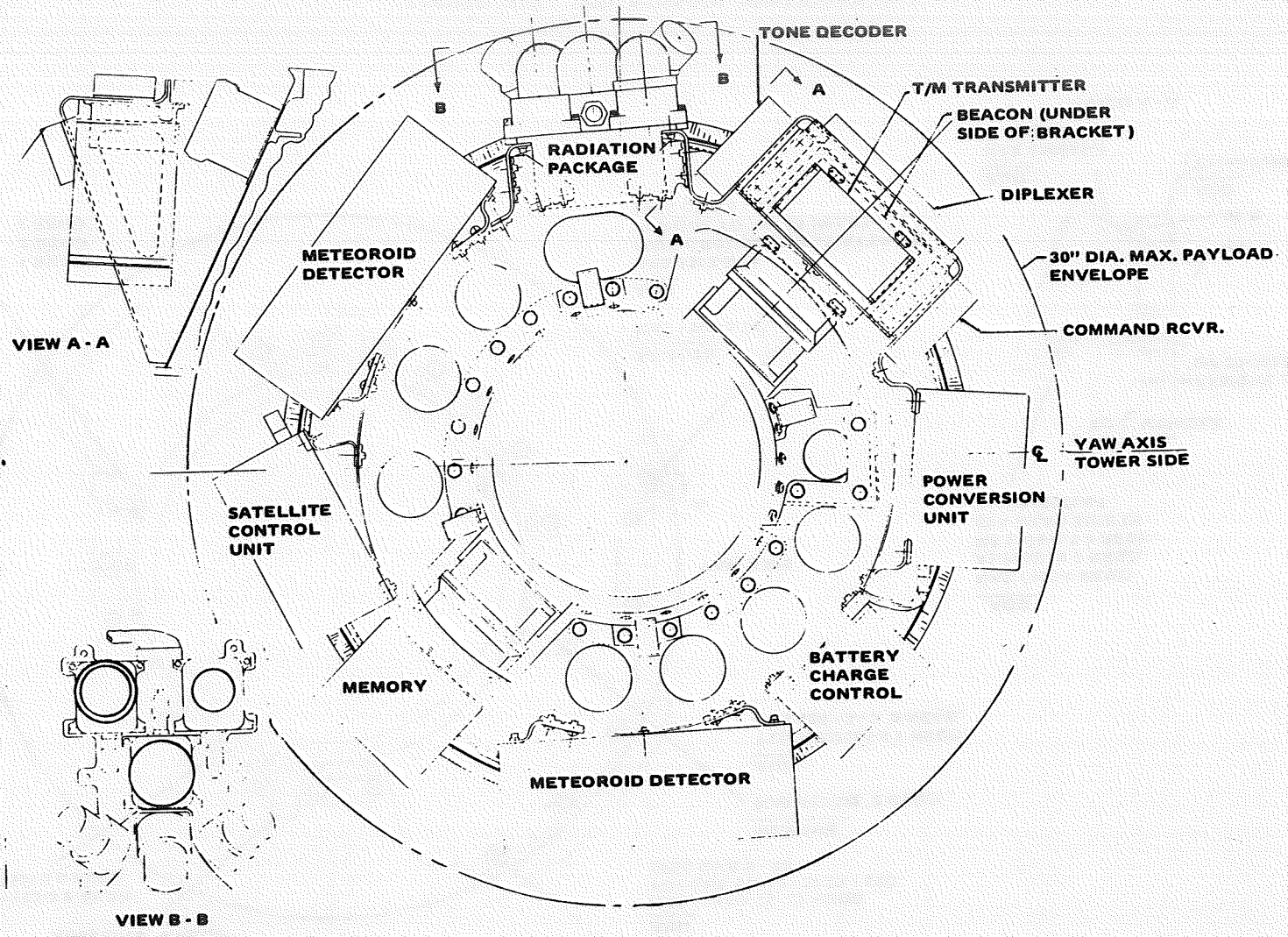


FIGURE 7-4 RMS PACKAGE ARRANGEMENTS

battery on the upper right hand side could be removed up through the RMS upper ring Hold down screws for the battery could be removed through the arch-like structure supporting the five RF components. The squib access door could be reached through the same arch. The heat shield bumper rested on the upper cylindrical surface of the solar cell support ring at four discrete points, as illustrated in Figure 7-1. The bumper was clear of the "yo" (a device for despinning RMS) cable drum by 3/4 inches and it cleared the upper part of the solar cells by 1/3 inch. The four sheet metal hold down clips for the solar cell support ring and the two RMS antennas, which extend downward from the web of the "yo" cable drum, were located between the bumper contact points. The guide tunnel for Scout and RMS umbilical connectors was located over the RMS power conversion unit and was scarfed off to provide clearance with the command receiver.

The basic dimensions of the spacecraft are shown in Figure 7-5 and a weight breakdown by major components is given in Table 7-1. Figure 7-6 is a photograph of the completed RMS, mated to the fourth-stage motor and OFO, as it appeared on the spin-balance machine at Wallops Island just prior to launch. The cylindrical solar cell arrangement is seen around the fourth-stage motor and immediately above this can be seen one RMS meteoroid experiment package on the left, the battery and power conversion unit in the center, and the RF group on the right. OFO is the large domed structure on top. Figure 7-7 shows the RMS/OFO with the Scout heat shield partially in place. The umbilical connections are supplying external power and the radiation experiment package with its domed ion chambers and cylindrical telescopes is the central item in the picture.

7.2 DYNAMICS

The RMS was attached to the Scout "E" Section, so that independent moments of inertia for the spacecraft were never determined. The spacecraft was a relatively simple dynamic structure with no onboard fluids, nutation or precession dampers, experiment booms, or gyroscopic devices. Solar cells were arranged as depicted earlier, on a fixed cylindrical array which did not deploy in orbit. RMS did have two whip-type antennas approximately 1/16 inch diameter by 20 inches long arranged 154° apart, retained by the Scout Heat Shield, which deployed at approximately 50° from Scout centerline after heat shield ejection.

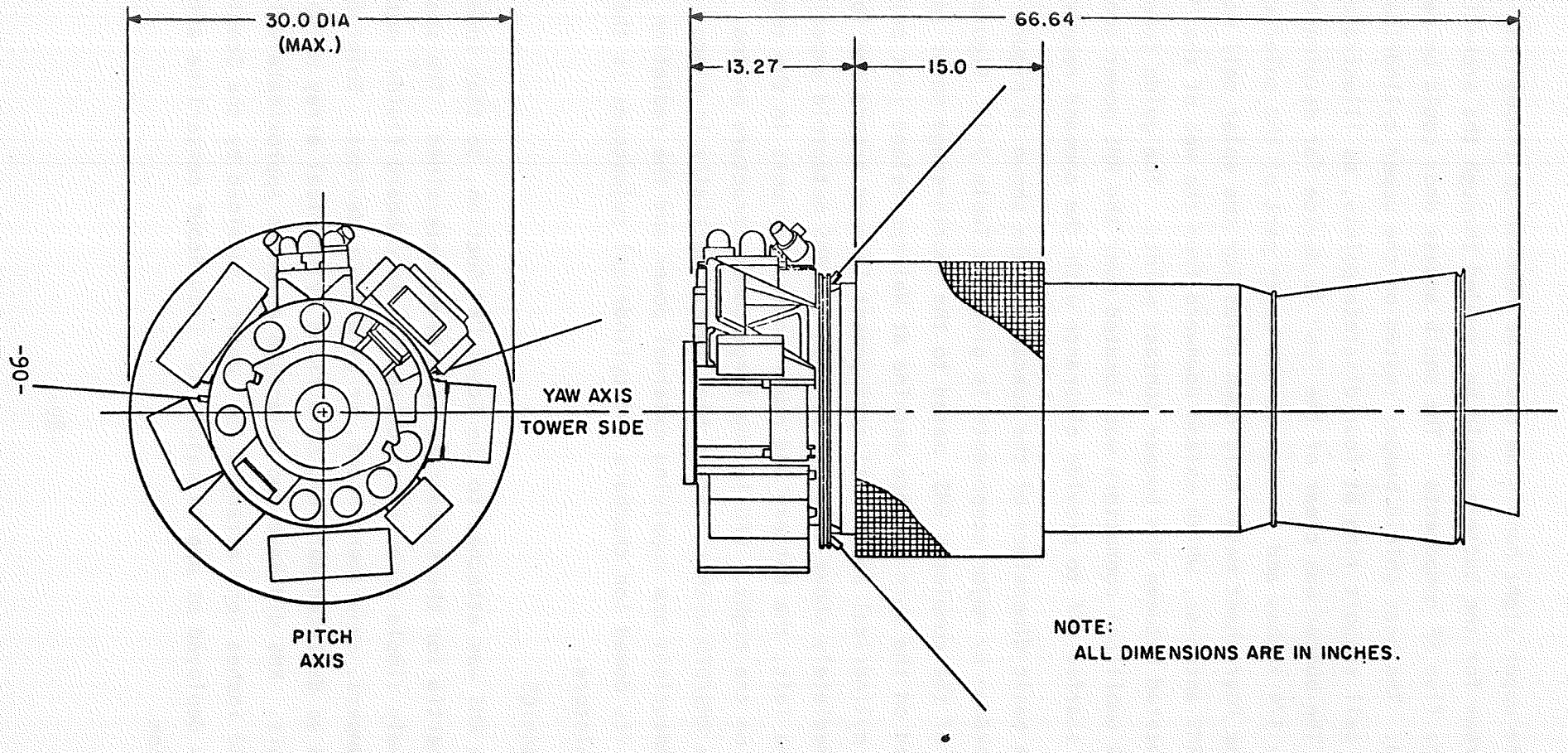


FIGURE 7-5 RADIATION AND METEOROID SATELLITE



FIGURE 7-6 RMS/OFO AT SPIN BALANCE

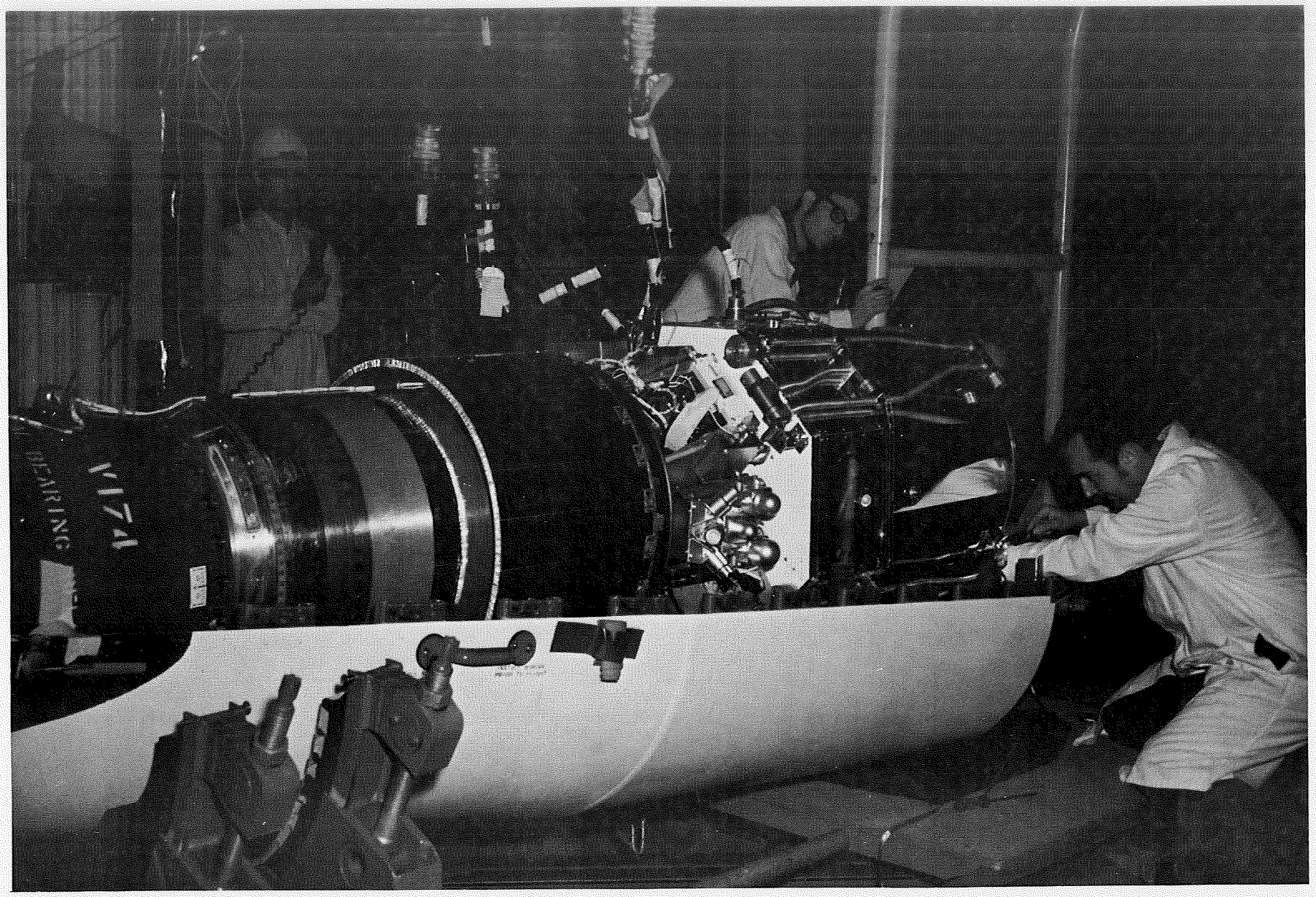


FIGURE 7-7 RMS/OFO WITH SCOUT HEAT SHIELD PARTIALLY IN PLACE

TABLE 7-1

RMS WEIGHT SUMMARY

	Weight (lbs)	Weight (lbs)
Scientific Units		11.85
Radiation Experiment Unit	4.48	
NASA Dosimeter I (no shield)	0.45	
NASA Dosimeter II (thin shield)	0.93	
NASA Dosimeter III(thick shield)	1.54	
Meteoroid Experiment Unit I	2.07	
Meteoroid Experiment Unit II	2.38	
Satellite Data Units		9.58
Satellite Control Unit	4.40	
Memory Unit	4.32	
Tone Decoder	0.86	
Electrical Power System		12.37
Power Conversion Unit	1.85	
Battery Pack & Charge Control Unit	5.36	
Solar Panels	5.16	
RF System		2.68
Command Receiver	0.86	
T/M Transmitter	0.37	
Beacon	0.79	
Diplexer	0.49	
Antennas	0.17	
Structural Components (Structure, Wiring and Yo)		9.76
Scout "E" Section Weight Increase due to RMS		0.06
Total RMS Weight		46.3

The Scout fourth stage spin rate of 120 RPM was dictated by the biological specimens in the OFO payload. This value was satisfactory for RMS and was used as the initial condition in the RMS "yo" analysis. The OFO/RMS mission plan called for the OFO, RMS, the FW-4S motor, and the "E" and upper "D" interstages, to be injected into orbit tangent to the orbital track. One hundred seconds after ignition of the FW-4S motor, the OFO was to separate at a relative velocity of 2.77 ft/sec. At that time the system spin axis was to be about 20° above the orbit track, as illustrated in Figure 7-8. The OFO would then move ahead of and above the spinning RMS. At a point 10 seconds after separation the RMS single "yo" was to deploy. This sequence, just as the separation sequence, was initiated by the Scout fourth stage timer. The resulting RMS motion was to have a spin rate of 6-7 RPM around its long spin axis with a half-cone angle of approximately 45°. The spacecraft configuration remaining in orbit was then to be the spent FW-4S motor case, Scout "E" section, upper "D" section, RMS structure and components around the "E" section, and the cylindrical solar cell array surrounding the FW-4S. Within five minutes the OFO was to be approximately 800 feet ahead of RMS and almost on the original system spin axis. Due to a malfunction in the Scout timing sequence the actual resultant motion of the RMS in orbit configuration is uncertain, but the inferred spin rate of approximately 60 RPM from telemetry transmission data indicates that the OFO, RMS system was still coupled with the RMS "yo" deployed. The rate at which the RMS system went into a complete tumble, an end-over-end motion with one side always to the sun, also indicates that a half-cone angle considerably greater than 45° was achieved. A discussion of other consequences of the separation mishap will be found in other sections of this document.

7.3 ELECTRONICS

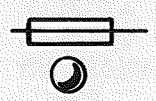
7.3.1 COMMAND SYSTEM

In order to command the spacecraft to perform various routines, a command system consisting of a beacon, receiver, antenna diplexer, and command decoder was used. The system is shown in Figure 7-9.

The receiver and beacon antenna was a single canted monopole at approximately 180° from the telemetry transmitter antenna radial to the centerline of the thrust axis of the spacecraft. A diplexer was used to

- **RELATIVE POSITION AND RMS ORIENTATION**

RMS
OFO



- **FINAL RMS MOTION**

  ≈ 7 RPM AROUND LONG AXIS
  ≈ 45° HALF CONE ANGLE

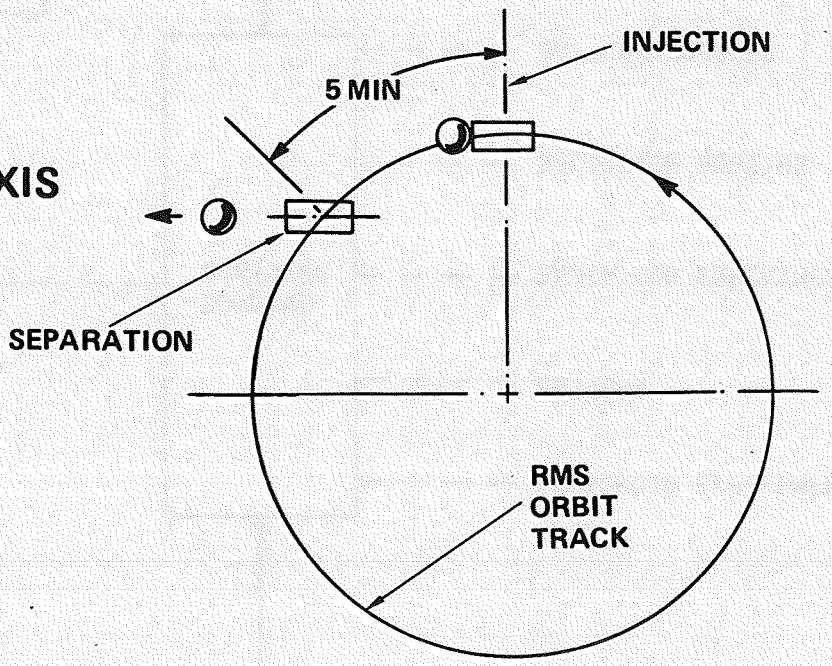


FIGURE 7-8 RMS/OFO DYNAMICS

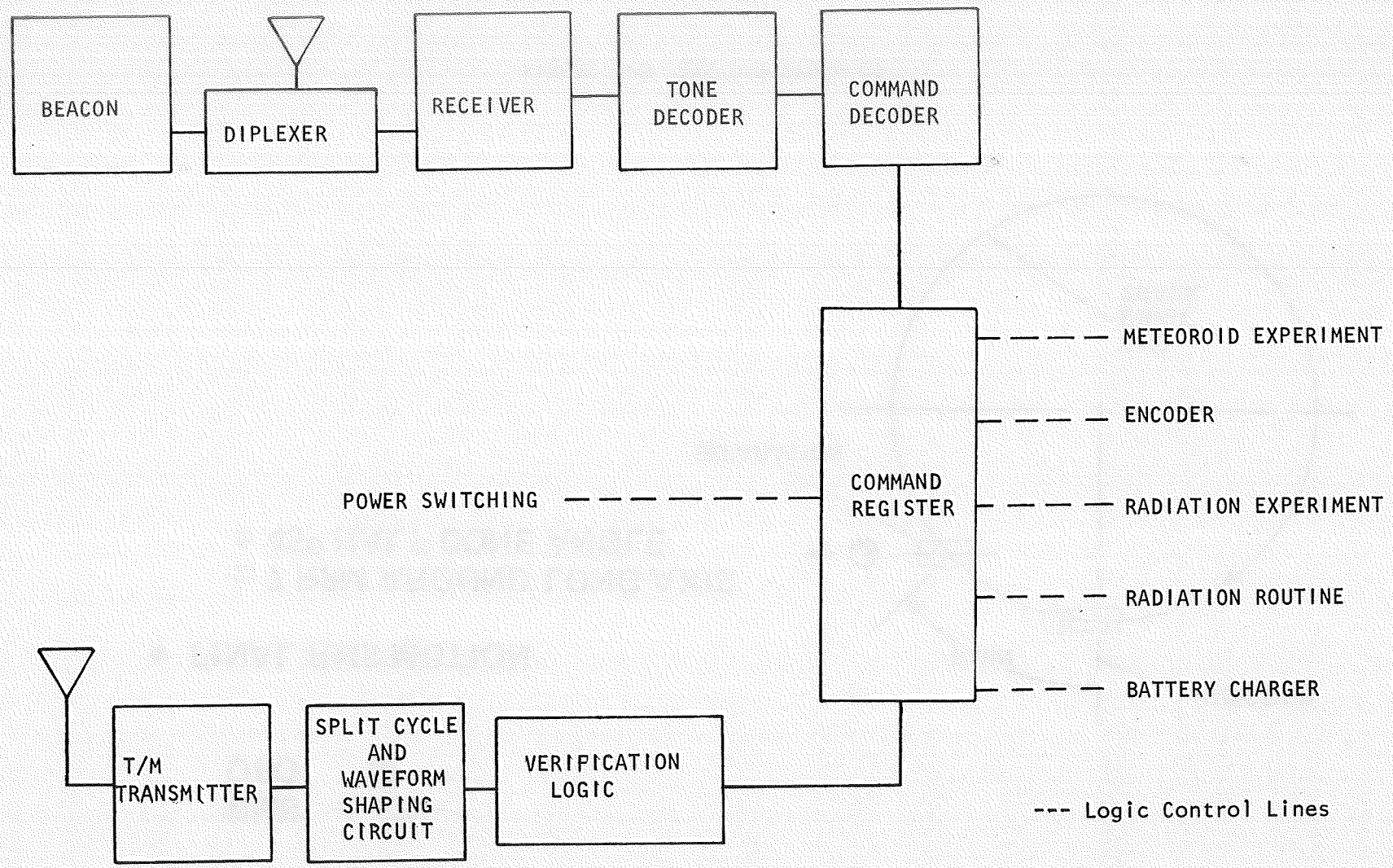


FIGURE 7-9 COMMAND SYSTEM

isolate the receiver input from the output of the beacon and to allow the operation of both from a common antenna. The beacon was a 50 mw unmodulated transmitter with a 136.38 MHz carrier frequency. The beacon was to remain on for the lifetime of the satellite for accurate tracking and definitive orbits but could be turned off if required by ground command.

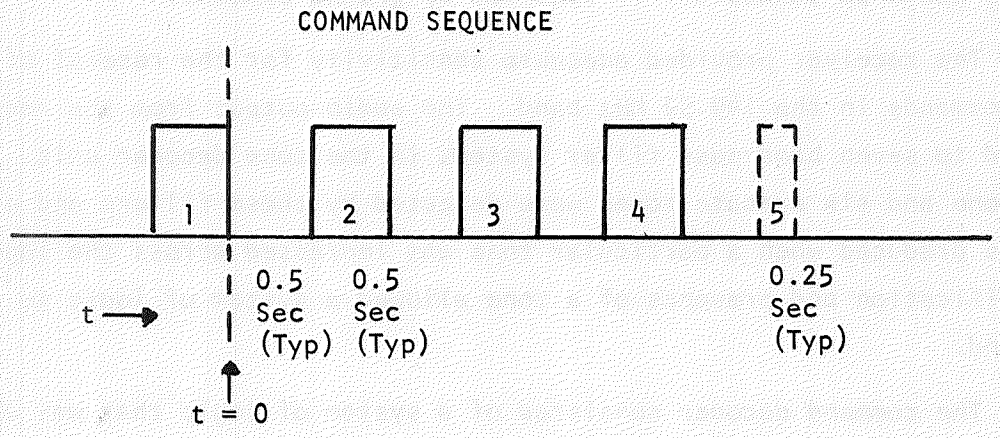
The receiver provided adequate sensitivity for the receipt of ground station commands in the 149.52 MHz band. The audio output from the receiver was routed to seven band-pass filter systems in the tone decoder unit. The address tone and six execute tones were detected by these filters and a "0" output was produced when a particular tone was impressed across the input. The identification and presence of a tone allowed a system of logic to interpret the command.

The command decoder consisted of a system of logic that was able to accept a particular command only if the sequence of tones and the time spacing of the tone bursts were correct. A command was accepted only if the address plus three execute tones sent in each command were sent properly and no additional tones were received during the tone acceptance windows shown in Figure 7-10. A multiple-tone-reject circuit that rejected commands if two or more tones were received at the same time could be eliminated by ground command if the spacecraft experienced command difficulties. These decoded commands were entered into a command register to produce changes in power switching or automatic sequence conditions and to start various automatic routines on the spacecraft. The command register could be displayed in real time by the real-time routine for ground interrogation. When the real time routine was not in progress, each command that was entered into the command register or did not produce an otherwise recognizable response, produced a verification tone burst after the acceptance window. Although 216 different commands could be realized by taking six tones three at a time, only 33 commands were used.

7.3.2 TELEMETRY SYSTEM

To secure the data acquired by the spacecraft a telemetry system consisting of an antenna, transmitter, and encoder was used. The system is shown in Figure 7-11.

The telemetry transmitter antenna was similar to the receiver and beacon antenna except it was approximately on the opposite side of the



1. Address Tone - Timing Sequence Begins at End of Address Tone
2. Execute Tone
3. Execute Tone
4. Execute Tone
5. Acceptance Modulation of T/M Transmitter

(Not a command tone - The time relation of the 1/4 sec modulation of the 137.89 MHz down-link for command verification; Note 1 page 360.2)

Address Tone - 5155 Hz
Tone A - 2270Hz Execute Tone Reserved for Time Entry Only
Tone B - 2650Hz Execute Tone Reserved for Time Entry and Command
Tone C - 3000Hz Execute Tone Reserved for Time Entry and Command
Tone D - 3305Hz Execute Tone Reserved for Command Only
Tone E - 3621Hz Execute Tone Reserved for Command Only
Tone F - 3850Hz Execute Tone Reserved for Command Only

FIGURE 7-10 TONE ACCEPTANCE WINDOWS

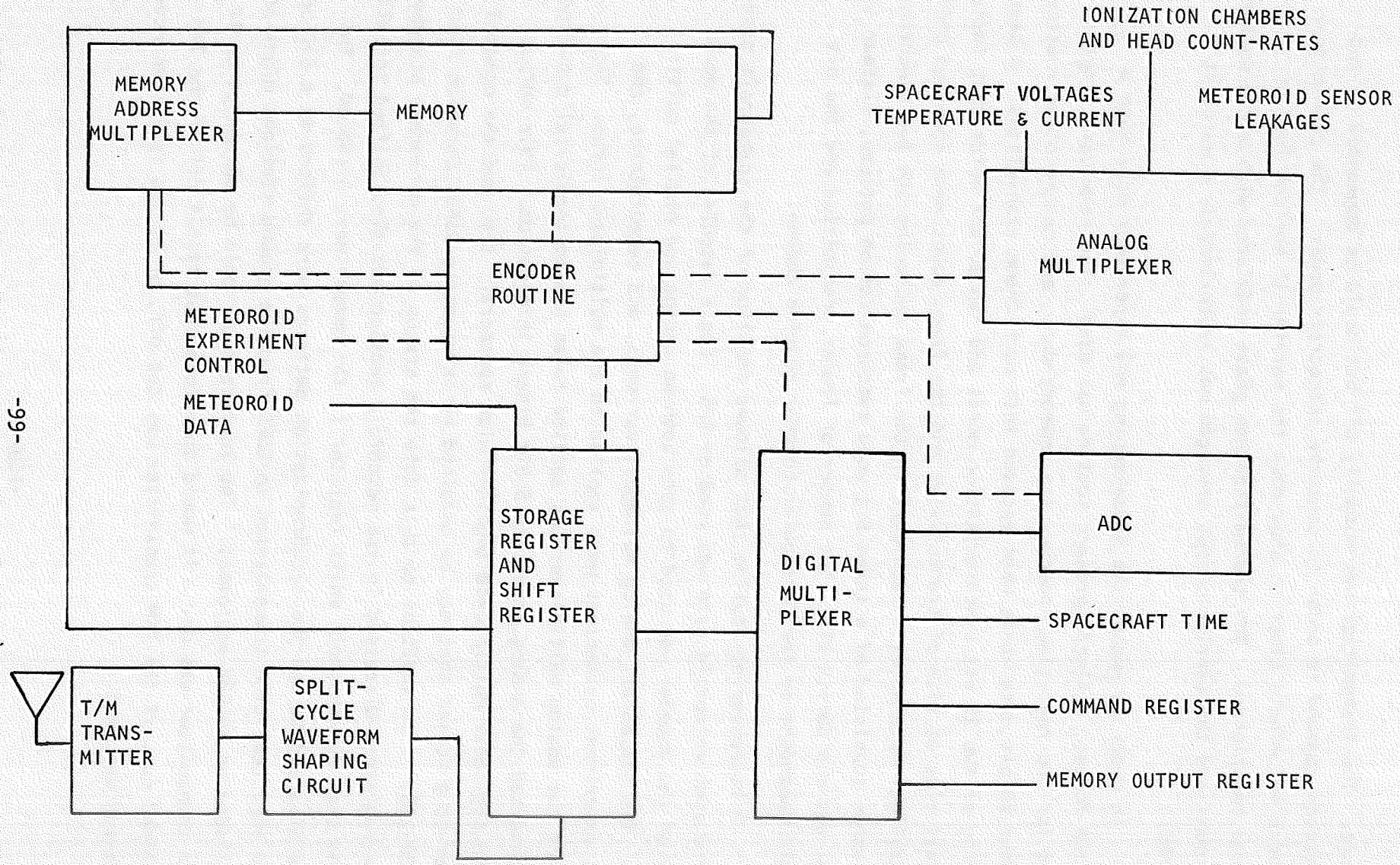


FIGURE7-11 TELEMETRY SYSTEM

spacecraft. The transmitter was normally off but could be commanded on and off by ground command in order to conserve spacecraft power. The transmitter also used a 4.2 minute timer to shut down the carrier if horizon loss of signal was experienced. The transmitter was phase modulated with a PCM split-phase format and the carrier output strength was approximately 2 watts at 137.89 MHz.

In order to encode the housekeeping and experiment data into a usable PCM format, a fixed hardware routine was used. The same basic logic was used for the real-time housekeeping, memory-dump, and memory-clear routines. Sixty-four 20 bit data words were encoded into each frame transmitted. A header consisting of two 20 bit synchronization words and two 20 bit words that included spacecraft time at time of transmission and the frame count were inserted before the sixty-four data words. Each word in the frame excluding the two synchronization words consisted of a three bit word synchronization pattern, sixteen bits of data, and one parity bit. The number of frames transmitted and the bit rate were dependent on the particular encoder routine chosen.

A housekeeping routine that allowed sampling of the spacecraft conditions and some meteoroid data was used on RMS. Logic decoding of the word counter of the encoder was used to gate both an analog and digital multiplexer. The spacecraft analog voltages, currents, and temperatures, and various experiment parameters were applied to the multiplexer input. The output of the analog multiplexer was applied to an analog-to-digital converter that converted the analog inputs to 8 bit binary information. This output was then digitally multiplexed together with spacecraft time and the command register to a format that may be obtained by referencing GSFC Operation Plan X-513-70-218. In addition to this data the status of the meteoroid standby-storage registers discussed in the meteoroid section was also shifted serially into and then out the main shift register if the memory were disabled. The shifted binary data and the synchronization patterns were shifted at a 512 bps rate so that real-time transmission to GSFC from the ground stations might be accomplished on NASCOM equipment. The routine could only be commanded on if the T/M transmitter was on. It would therefore shut itself off if the T/M timer timed out, if the T/M transmitter was cut off, or if the real-time routine off command was sent.

The basic encoder routine was also used for the memory dump and both the half memory clear and full memory-clear commands. When the memory was dumped, the status of each 16 bit data word was read sequentially into the main shift register using the encoder frame and word counters as the address. The data was then shifted out serially in a manner identical to the real-time routine except that the bit rate was 2048 bps. Since RMS used a 2048 word memory and 64 data words were packed into each frame, 32 frames were required to completely sequence through the memory. The frame counter then sequenced over again until four redundant readings of the memory contents were transmitted. The total sequence lasted 85 seconds when the frame header, word synchronization and parity bits were included.

The memory-clear commands used identical bit rates but "0"s were written into the memory in place of the read cycle. During this sequence the main register was cleared in order to enter zeroes into the memory and thus were shifted out the telemetry link. Since data was not to be obtained during these periods only one sequence was required. The half-memory clear therefore runs only sixteen frames or approximately 10.5 seconds and the full memory clear runs all thirty-two frames or approximately 21 seconds. Since the telemetry transmitter might be on during these sequences, verification could be made easily.

7.3.3 DATA PROCESSING

A system that automatically stored the data produced by both the radiation and meteoroid experiments was used on the spacecraft. The system for the meteoroid experiment is shown in Figure 7-12 and the radiation experiment in Figure 7-13.

All meteoroid data processing was accomplished by serial-to-parallel conversion of the data loaded into the shift register in the experiment. As was previously discussed in the meteoroid experiment discussion, the data which consisted of location encoding, time of flight, and box identification bits was loaded into a 21 bit shift register at the time of the meteoroid event. The meteoroid routine was initiated by a signal from the experiment indicating that data was ready but the routine would not process it if the radiation experiment or a memory function was busy. When both of these were not busy, the routine

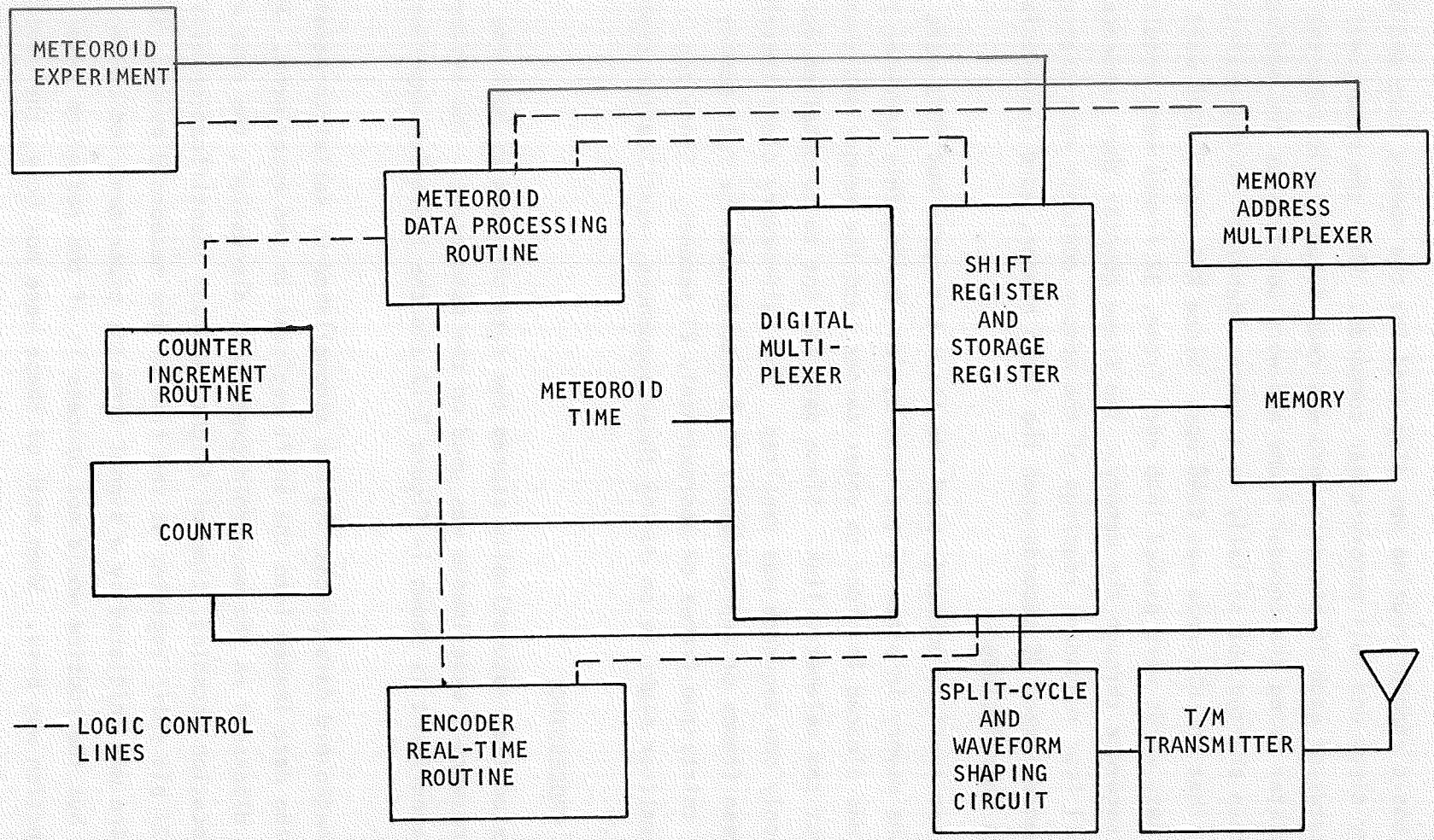


FIGURE 7-12 METEOROID EXPERIMENT DATA PROCESSING

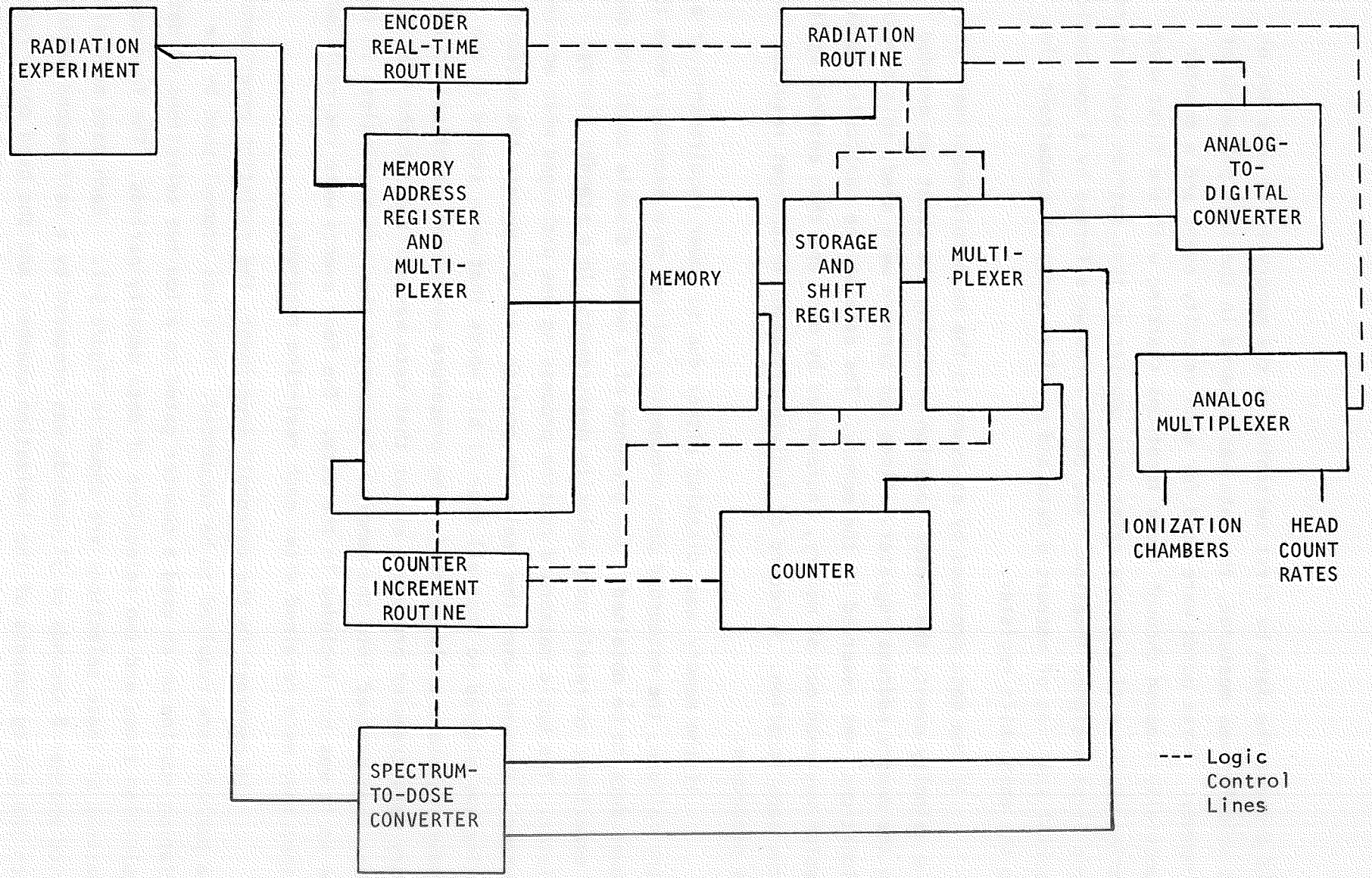


FIGURE 7-13 RADIATION EXPERIMENT DATA PROCESSING

would process the data by first switching on the memory if it were not on. If a velocity was measured, the data was entered in the last 512 words of the memory. Three words were used for each velocity event and a counter sequentially stepped through these locations starting with the first word. Clearing of the entire memory reset this counter so that entries would start at the first assigned location. The three words were formed by a combination of serial shifting of meteoroid data and parallel entry of spacecraft time into the main shift register.

If the data produced by an event in the meteoroid experiment was not a velocity event, the sensor location producing the event was encoded into the memory address register. Since 256 sensors were used, this number of locations was reserved in the memory. The data at the particular sensor location was read out of memory, incremented by one, and then entered again in the same location. A record of individual sensor discharges resulted from this procedure.

If the memory was disabled either due to power requirements or a memory failure, the meteoroid data processing shifted to a secondary mode that allowed data to be obtained. The presence of a memory disable condition caused the experiment to retain only velocity measurements in a standby storage register. The basic meteoroid routine processing was unchanged when an event occurred. However, when the real-time routine was in progress the meteoroid routine was altered so that all four 21 bit words that were stored in the standby registers could be read. The procedure was almost identical to the memory data transfer procedure except that data was shifted out the T/M link rather than entered into the memory. Spacecraft time was meaningless in this case so it was not included in the data. The four events were recirculated so that they were retained after each real-time read-out.

In contrast to the meteoroid experiment, the radiation experiment data periods were required to be sequenced. This was accomplished by the radiation routine which used a counter gated to allow two selections of data acquisition times and two selections of data density periods. The four combinations of these selections are shown in Figure 5-1. Each data acquisition period whether 8 seconds or 31 seconds was preceded by a half-second period in which the analog outputs of the ionization chambers and the head count-rate

indicator circuits were sampled by the ADC and the data stored in the first 256 word section of the second half of the memory. Following the data acquisition period another half-second interval was used to again sample the same parameters as before and additionally store the digital output of the proton and electron spectrum-to-dose converters. A data acquisition period consisted of simultaneous pulse-height spectra acquisition and spectrum-to-dose conversion. This was accomplished by using the address and the data-ready pulses produced by the radiation spectrometer to initiate a routine that removed the data stored in the particular address, incremented it by one, and then wrote it in the same address. This maintained a count of the number of events in each spectrometer address. The incrementing routine also initiated a hardware routine in the spectrum-to-dose converter that used the address to locate the weighting function.

Each data acquisition period was progressively stored in the first section of the memory. This was accomplished for each data period by incrementing a counter that was used as part of the address. This counter was incremented twenty-nine times to result in thirty separate data periods, each separately stored. After the completion of the last cycle, the real-time routine was initiated. It was identical to the telemetered real-time routine except that the data was written into the memory and the routine completed only one cycle. This completed the data entry into the first half of the memory and allowed the data that would not normally be cleared on entry to be erased from core by a memory half-clear command.

7.3.4 POWER SYSTEM

The system shown in Figure 7-14 used to supply electrical power to RMS consisted of solar panels, a battery and charger, and a power distribution system.

In order to supply adequate electrical power to RMS for various spacecraft attitudes a cylindrical solar cell array was attached around the four stage engine. This contained approximately 6.5 square feet of solar cells that supplied approximately 23 watts of power when incident solar energy was applied. The final expected orientation of a flat spin produced about 13 watts of power.

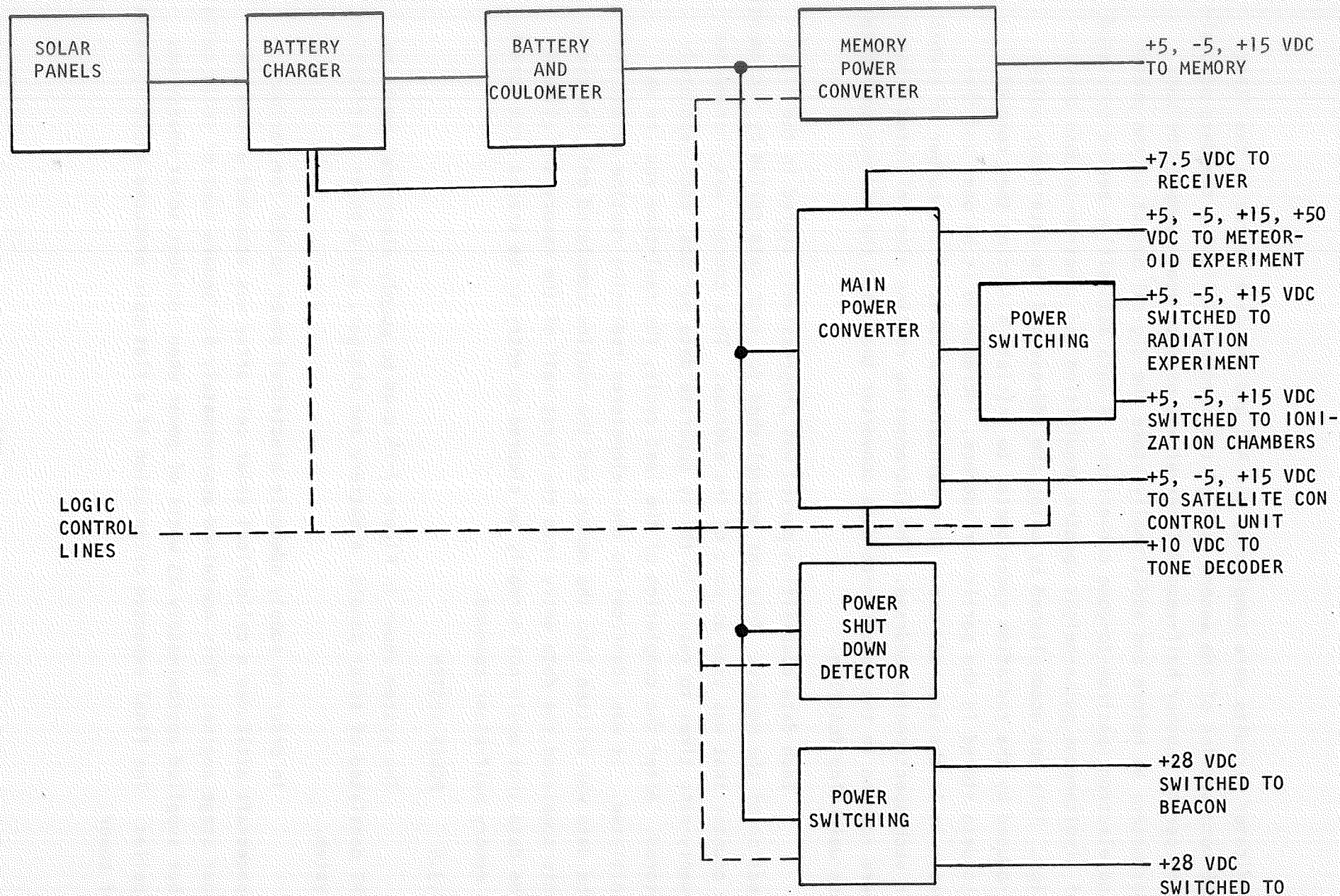


FIGURE 7-14 POWER SYSTEM

In order to supply power in dark periods a nickel-cadmium battery was used. It consisted of 21 series connected cells capable of 1.8 ampere-hours. This produced a nominal voltage of 28 volts which was supplied to the spacecraft. The current, both flowing out and flowing into the battery chain, was integrated by a coulometer. By sensing the voltage across this device the amount of charge was controlled by switching the full charge capability of the solar panels on or off depending on the coulometer state. To maintain equilibrium between cells a trickle charge was applied directly to the battery, bypassing the coulometer.

Since many units on the spacecraft use various voltages that were to be switched on or off by ground command, a power distribution system was incorporated. This unit produced all the voltages required by the experiments and controlling functions by use of dc-to-dc converters and integrated circuit regulators. All switching of the output voltages was accomplished by command register and programmed logic control of transistor switches. The main satellite converter supplied voltages continuously to the power switches, whereas the memory power converter was switched on when memory operation was required. A redundant voltage level circuit was used to detect when the battery buss fell below approximately 25 volts. When both circuits indicated low buss the power to all experiments and memory was shut off to conserve power and allow the battery to recharge.

7.4 GROUND SUPPORT EQUIPMENT

In order to adequately check out the spacecraft both during final acceptance and prelaunch activities, a ground support system consisting of the items shown in Figure 7-15 was used. To check the basic accuracy of all registers and routines in the spacecraft, a register display and command encoding unit was used. This unit was able to display the progress of each routine at each step by either interrupting and controlling the sequence or by displaying the binary information formed by the spacecraft at a given step. It was also able to command the spacecraft directly rather than going through the RF link. This unit was then able to verify the correct operation of all the digital equipment aboard the spacecraft.

Since testing of individual items prior to installation and testing of the RF link by NASA-GSFC after installation on the spacecraft was

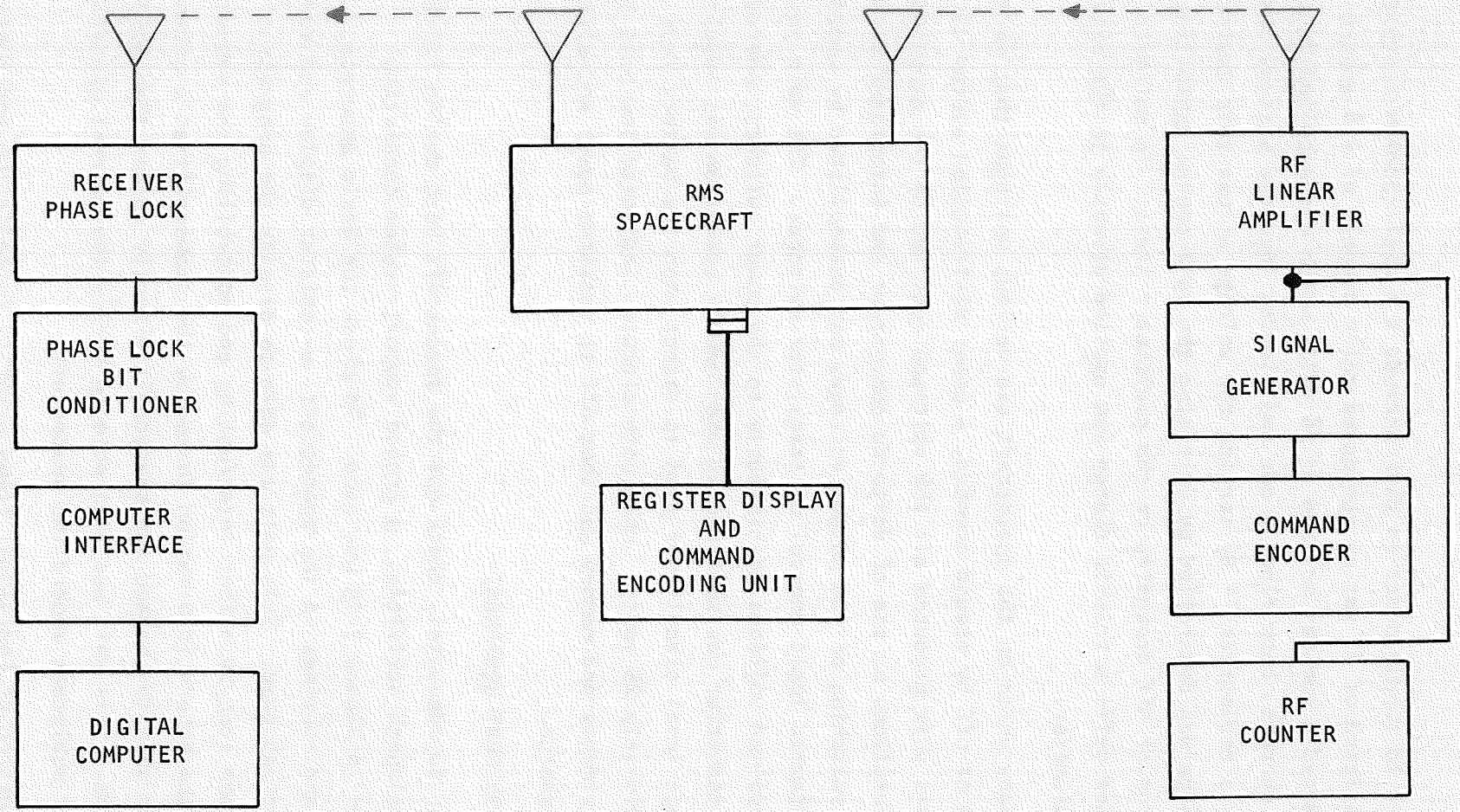


FIGURE 7-15 RMS GROUND SUPPORT

accomplished, additional testing was not performed through the RF link. The link allowed communication between the spacecraft and the operator without hard-wire connectors. Any major abnormal operation could be detected by this link. Commanding was accomplished in a manner similar to STADAN station procedures. The telemetry link used receivers and pulse code demodulation equipment similar to station and GSFC equipment. The computer reduced the data to a decimal character display of the binary information transmitted by the spacecraft. This permitted detection of any abnormal numbers as well as spacecraft conditions before launch.

7.5 THERMAL ANALYSIS

In order to determine approximate spacecraft temperatures in orbit a thermal analysis, LTV MSD release 00-DIR-228, of the spacecraft was performed. This analysis was coupled with a thermal vacuum test to check its validity for the spacecraft in a spinning condition. The results of the tests, LEC Document 14-D-70, proved that the analysis was valid and could be used for the orbiting spacecraft. All instruments were painted with an aluminum colored paint except the tone decoder and the beacon which were brown and black, respectively. The solar vacuum tests did not produce conditions that totally simulated the orbital parameters so corrections were made and results indicated that most instruments would be in the center of the temperature range specified.

An excellent method of comparing the calculated temperatures and the actual orbital temperatures is to observe the battery temperature. It is a high mass unit and as a result integrates the temperature excursions. Using the hot orbit calculations the average battery temperature was calculated to be 60°F and was approximately 54°F in the initial orbits. All other instruments were very close to the calculated values and were in satisfactory operation ranges.

After approximately orbit 160 the spacecraft seemed to have resolved all of its spin axis inertia to a long axis tumble and no spin. This caused one side to face the sun continuously during the sun cycle of the orbits. A heating effect was noticed starting at that orbit and continuing to before reentry, although stabilization was basically achieved by Orbit 330. This side consisting of the battery, power converter, and meteoroid box number 2 experienced a significant heat rise, whereas, the other side became much cooler. The spacecraft was operated in a lower-power condition to maintain power converter and battery temperatures within the design temperature range.

8.0 CONCLUSIONS

The Radiation and Meteoroid Satellite program demonstrated that a sophisticated, piggy-back satellite system composed of two complex experiments, a solar power supply, telemetry, an on-board memory, and a computer/controller could be conceived, designed, fabricated, and flown on a Scout launch vehicle in less than two and one-half years for a total expenditure of less than one million dollars. The success of the mission and the accumulation of the data required to meet all mission objectives is evidence of the fact that, although system redundancy was eliminated for economy, sufficient versatility was designed into the satellite to overcome a significant problem caused by a vehicle malfunction at separation. The suspected collision at separation compromised the high energy proton data, but all other portions of the radiation experiment were completed and the real-time spectrum to dose conversion system was successfully demonstrated in the space environment. The meteoroid experiment performed as designed and produced two meteoroid velocity measurements during its short lifetime. Data was also accumulated to determine meteoroid flux.

Based on the results of the mission it is judged that the original concept of an austere program, in which a single satellite was fabricated, flight qualified and flown, was completely justified.

9.0 REFERENCES

1. "Radiation and Meteoroid Satellite Preliminary Design Report," Report No. 0-71100/8R-15, Advanced Technology Center, Inc., Dallas, Texas, 12 November 1968.

2. "Interface Definition Document Orbiting RMS Spacecraft," Report No. 0-71100/8R-17, Advanced Technology Center, Inc., Dallas, Texas, 8 November 1968.

3. "Experiment Implementation Plan (Revision B), Radiation Meteoroid Satellite," Manned Spacecraft Center, Houston, Texas, 27 March 1970.

4. "OFO-A Mission Performance Report," Report No. 1333-032, Space General Company, El Monte, California, December 1970.

5. Leopard, F. O., "Calculations of the Response of the Proton Dosimeters on the Radiation and Meteoroid Satellite to Monoenergetic-Isotropic Proton Fluxes," Research Note RRA-N7013, Radiation Research Associates, Inc., Fort Worth, Texas, 23 July 1970.

6. Farmer, B. J., et al, "A Real-Time Spectrum-to-Dose Conversion System," Paper presented at the National Symposium on Natural and Manmade Radiation in Space, Las Vegas, Nevada, March, 1971.

7. Farmer, B. J., and Rainwater, W. J., "Study to Determine the Utility of Spectrum-to-Dose Conversion," Report No. 0-71100/9R-5, Advanced Technology Center, Inc., Dallas, Texas, 30 April 1968.

8. "NASA Support Plan," Goddard Space Flight Center, Greenbelt, Maryland, February, 1970.

9. "Solar/Vacuum Test Results for Thin-Film Meteoroid Sensors," LEC Document No. 0F2013, Lockheed Electronics Company, Houston, Texas, September, 1970.

10.0 BIBLIOGRAPHY

1. "Radiation and Meteoroid Satellite Critical Design Review," NASA Contract NAS9-9195, Advanced Technology Center, Inc., Dallas, Texas 31 July 1969.

2. "Scout S-174C Post Operation Report," Missiles and Space Division, LTV Aerospace Corporation, Wallops Island, Virginia, 9 November 1970.

3. "Vibration Tests of the Radiation Meteoroid Satellite (RMS) Payload with Dummy Components," Report No. ETL-081, Missiles and Space Division, LTV Aerospace Corporation, Dallas, Texas, 22 October 1969.

4. "Vibration Tests of Radiation Meteoroid Satellite (RMS) Payload Solar Cell Array (SCA)," Report No. ETL-079, Missiles and Space Division, LTV Aerospace Corporation, Dallas, Texas, 20 October 1969.

5. "Yo Despin System Test RMS Payload," Release No. T110-TIR-0003, Missiles and Space Division, LTV Aerospace Corporation, Dallas, Texas, 20 January 1970.

6. "NASA-GSFC Operations Plan 2-70, Radiation Meteoroid Satellite (RMS)," Report No. X-513-70-218, Goddard Space Flight Center, Greenbelt, Maryland, June, 1970.

7. "NASA-GSFC STADAN-Spacecraft Compatibility Test Procedures and Data Sheets," Report No. X-531-69-27(A), Goddard Space Flight Center, Greenbelt, Maryland, June, 1969.

8. "Compatibility Test Report Radiation Meteoroid Satellite (RMS) Flight Model," Goddard Space Flight Center, Greenbelt, Maryland, February,1970.

9. "Support Instrumentation Requirements Document," Goddard Space Flight Center, Greenbelt, Maryland, December,1969.

10. "Payload Description Document for Radiation Meteoroid Satellite Project," Manned Spacecraft Center, Houston, Texas, June, 1970.

11. "Derivation of Pulse-Height Spectrum-to-Dose Function for a 2" x 6" NaI Crystal Spectrometer, Report No. 0-71100/9R-5, Advanced Technology Center, Inc., Dallas, Texas, March, 1969.

12. "Radiation and Meteoroid Satellite, Monthly Progress Report", Advanced Technology Center, Inc., Dallas, Texas

	Report No.	Date
(a)	0-71100/9R-13	1 April 1969 - 30 April 1969
(b)	0-71100/9R-22	1 May 1969 - 20 May 1969
(c)	0-71100/9R-29	21 May 1969 - 15 June 1969
(d)	0-71100/9R-33	16 June 1969 - 15 July 1969

	Report No.	Date
(e)	0-71100/9R-37	16 July 1969 - 15 August 1969
(f)	0-71100/9R-45	15 August 1969 - 15 September 1969
(g)	0-71100/9R-49	16 September 1969 - 15 October 1969
(h)	0-71100/9R-55	16 October 1969 - 15 November 1969
(i)	0-71100/9R-59	16 November 1969 - 15 December 1969
(j)	0-71100/0R-2	16 December 1969 - 15 January 1970
(k)	0-71100/0R-8	16 January 1970 - 15 February 1970
(l)	0-71100/0R-12	16 February 1970 - 15 March 1970
(m)	0-71100/0R-13	16 March 1970 - 15 April 1970
(n)	0-71100/0R-21	16 April 1970 - 15 May 1970
(o)	0-71100/0R-27	16 May 1970 - 15 June 1970
(p)	0-71100/0R-29	16 June 1970 - 15 July 1970
(q)	0-71100/0R-35	16 July 1970 - 15 August 1970
(s)	0-71100/0R-37	16 August 1970 - 15 September 1970
(t)	0-71100/0R-40	16 September 1970 - 15 October 1970
(u)	0-71100/0R-51	16 October 1970 - 30 November 1970



ADVANCED TECHNOLOGY CENTER, INC.

P.O. BOX 6144 DALLAS, TEXAS 75222